Title
Application of Nanotechnology in Biological Research: Diagnostics and Physical Manipulation

Author
Eaimkhong, Sarayoot

Publication Date
2013

Peer reviewed|Thesis/dissertation

UNIVERSITY OF CALIFORNIA

Los Angeles

Application of Nanotechnology in Biological Research:

Diagnostics and Physical Manipulation

A dissertation submitted in partial satisfaction of the requirements for the degree

Doctor of Philosophy in Chemistry

By

Sarayoot Eaimkhong

2013

ABSTRACT OF THE DISSERTATION

Application of Nanotechnology in biological research:

diagnostics and physical manipulation

by

Sarayoot Eaimkhong

Doctor of Philosophy in Chemistry

University of California, Los Angeles, 2013

Professor James K Gimzewski, Chair

Nanotechnology has been around for several decades and been adopted by many researchers in biological science and medicine. It has transformed and changed the way many researchers perform experiments. This includes ability to visualize molecules, protein at smaller scale with high precision and cost-effective. In addition, nanofabrication, microelectromechanical systems (MEMS) and surface analysis techniques derived from nanotechnology enable innovative studies and allow researcher to design novel experiment that have not been done before. In this thesis, we focus on the application of nanotechnological techniques and instruments on biological research including gas sensing, biosensing and developmental study of pluripotent stem cells towards cardiomyocytes.

With many scientific and nanotechnological listed and explained in chapter 2, microtransducers such as quartz micro-resonators, aluminium nitrile micro-cantilevers and capacitive micromachined ultrasonic transducers (CMUT) were adapted and developed to detect carbon dioxide and volatile organic compounds (VOCs). Carbon dioxide and certain VOCs are required in the metabolism in our body. However, high concentration of these gases can become toxic to our body. Monitoring of carbon dioxide has gained much interest in the past since the greenhouse effect became evidential in many areas. The lack of affordable and reliable carbon dioxide sensors has created a demand in research to develop a device or a system to detect carbon dioxide effectively. We explored the potential of a new micro-transducer called CMUT, fabricated using nanofabrication techniques as a mass sensor for carbon dioxide at low concentration of around 1-4% v/v. This concentration range is critical because carbon dioxide will start to create many symptoms and become toxic. The results from CMUTs, in chapter 3, illustrate CMUTs to be capable of carbon dioxide detection over the critical range reliably. With further development, CMUTs can be used commercially to detect carbon dioxide and provide alternative solution to carbon dioxide monitoring.

In addition to gas sensing application, CMUTs were also capable of biological detection. We used them as biosensors to detect biomarkers for cardiovascular diseases in chapter 4. By functionalizing their surface with appropriate biomaterials, CMUT surface became biocompatible. For example, after functionalizing the surface with anti- C-reactive protein and anti- tumor necrosis factor alpha, CMUTs can detect the corresponding antigens: C-reactive protein (CRP) and tumor necrosis factor alpha (TNFα), which are the biomarkers for cardiovascular diseases. The device was calibrated and applied accordingly and was proven to have detection sensitivity of at least 10ng/ml in term of protein concentration. This sensitivity is

lower than the critical concentration for some cardiovascular protein markers including CRP; Hence this system will be useful to monitor CRP level for at risk patients. However, higher sensitivity is required to cover the critical range for TNFα. We believed that the limitation of the detection was derived by high noise level in the detection of pg/ml range. With further development in signal acquisition and processing, it is promising that this limit can be improved.

In chapter 5, cellular development of stem cells were visually enhanced with interferometric optical profiler using novel techniques called live-cell interferometry (LCI) and mechanical imaging interferometry (MII). In this study, physical stimuli such as mechanical motion, force and electrical pulse were introduced to stem cells to study the effect of these inducers on the differentiation of these cells as they to become cardiomyocytes. The effects of these stimuli were observed to induce the differentiation of stem cells. Motion and contact of neonatal cardiomyocytes were shown to induce newly differentiated stem cells to beat in synchrony with them. Electrical pulse was shown to increase the amount of cardiac gene expression in the stem cell colony after 4 days of pulsation with respect to the control.

The dissertation of Sarayoot Eaimkhong is approved by

Richard Kaner

Peter Felker

Dolores Bozovic

James K Gimzewski, Committee Chair

University of California, Los Angeles

2013

TABLE OF CONTENTS

LIST OF FIGURES

List OF TABLES

ACKNOWLEDGEMENTS

First and foremost, I would like to acknowledge and thank my advisor and mentor, James Gimzewski. His talent and ideas in science and nanotechnology inspired me to work on nanotechnology field and cutting edge research. James has been very open minded and welcome new ideas and collaboration. This made my research exciting with many promising directions beyond the frontier of my traditional training in physical chemistry. He gave me opportunities when I needed and shaped me into a good scientist. I would also like to thank our collaborators: Dr.Atsushi Nakano, Dr. April Pyre, Dr. Haruko Nakano, Dr. Sean Sherman and Armin Arshi. Without their efforts and willingness to share the knowledge in stem cells research, our projects would not be complete.

I would like to acknowledge the following people in Gimzewski's group who mentored me during my PhD research. Dr. Adam Stieg has been helping me on many occasions with great advices on atomic force microscopy, microelectromechanical systems, instrumentation in Nano&Pico Core Lab in the California NanoSystem Institute as well as science and project managements. He has shared a great dealt of knowledge; encouraged me to thrive in science research. Dr. Jason Reed has trained me on live-cell interferometry and mechanical imaging interferometry technique. He also helped me and advice on how to adapt in working with biological systems. Dr. Cristina Martin gave me advice and opportunity to work with fabricated micro-cantilevers that we were developing for biological measurements. Dr. Shivani Sharma has also helped and giving advice on force spectroscopy and cell mechanics of a single cell.

For gas sensors and biosensors projects, I would like to acknowledge and thank Dr. Matthias Steiert and Dr. Michael Cable from Matrix Sensors Inc. for their support and advice

in collaboration. I have gained insight into the industry and learnt great details about sensors from them through working with them at California NanoSystem Insitute.

I would like to thanks other Gimzewki's group members that I was fortunate to work with: Dr. Russeen Wali, Audrius Avizienis, Henry Silin for their support on my research. Thank you also to supporting classmates and friends: Dr. Timothy Dong, Dr. Patrick Allen, Dr. Carlos Hernandez, Christopher Sukhaphadhana and Dr. Carlin Hseush, who were consulting me and supported my decisions as well as encouraged me throughout the PhD program.

Last, but not least, I am grateful and thankful for my loving and supporting family. I would not be where I am without them. My parents, Vinai and Pratum Eaimkhong, have always encouraged me with my study and walked with me during tough times. Thank you also to my brothers, Prachya Eaimkhong, for always being supportive of me and looking after everyone in the family.

VITA

2006 MSci Chemical Physics with Industrial Experience

University of Bristol, United Kingdom

2006-2012 Teaching and research fellow in Chemistry

Department of Chemistry and Biochemistry

University of California, Los Angeles

Selected Publications:

S. Eaimkhong, M.Steiert, T.F. Harper, M.D. Cable, J.K. Gimzewski, *Label-free biodetection using capacitive micro-machined ultrasonic transducers (CMUTs) and its application for cardiovascular disease diagnostics*, Journal of Nanotechnology and Nanomedicine, 2012, 3, p144-148

R.Wali, P.Wilkinson, S.Eaimkhong, J.Gimzewski, *Fourier transform mechanical spectroscopy of micro-fabricated electromechanical resonators: a novel, information-rich pulse method for sensor applications*, Sensors and Actuator B, 2010, 147 (2), p508-516

T.A.Wood, G.S.Roberts, S.Eaimkhong, P.Bartlett, *Characterization of microparticles with driven optical tweezers*, Faraday Discuss.,2007, 137 (17), p1-15

Selected Poster Presentation:

"the 3rd AnnualGlobal Symposium on Nanobiotechnology", California NanoSystem Institute, UCLA, 2009

"the Seaborg Symposium", California NanoSystem Institute, UCLA, 2009 and 2010

Chapter 1

Introduction

In this study, potential applications of nanotechnology in chemical detection, bio-sensing, medical diagnostic and cellular biology were investigated. This is possible through the use of resonators that generate scalable miniature motion. As nanotechnology becomes more advance, devices such as resonators are fabricated to be smaller, and hence miniature amplitude in oscillation is achieved. Motion of resonators and their behavior are explained later in this chapter.

Many instruments in nanotechnology rely on resonators to perform characterization and measurement. This is done by acquiring date related to certain characteristics of resonators' movement (e.g., resonant frequency, quality factor) to interpret and assist in measurements. Some instruments that use resonating devices in measurements are such as scanning probe microscope (SPM) and atomic force microscopy. Scanning probe microscope (SPM) has a cantilever probe that can vibrate and resonate with specific characteristics. When this probe is brought close to the sample of interest, it interacts with the sample and oscillates differently than before. For instance, the probe can resonates at lower frequency if attraction between the probe and the sample is high, or quality factor of the resonation might be low when a soft surface is measured. As changes in these characteristics occur, we can draw information that will tell us about the sample. This concept and process will be explained in more detail in chapter 2 and 5. We will focus on a few selected nanotechnological tools

which are atomic force microscopy (AFM), interferometer, and discuss on how these instruments can be adapted to use in biology.

The other part of the thesis is focusing on chemical and biological sensing by using resonators created from nanofabrication. In general, chemical sensing and biosensing systems are built to rely on mechanical movements of resonators. These sensors utilize similar concept explained earlier. By monitoring the change in resonant frequency or quality factor, abundance of certain chemicals can be quantitatively quantified. Since most of the resonators are made of traditional materials which are quartz and silicon, specific fabrication and functionalization techniques need to be performed on their surface before the resonators can be used for chemical and biological detection. In this study, certain chemicals are selected, and the detection process are explained further in chapter 2 and 5

1.1 Motion of resonators

Resonator is a device that vibrates and oscillates with highest amplitude at a specific frequency depending on the nature of the resonator (e.g., shape, material) as well as its environment (e.g., vacuums, air). Oscillation of resonators can be ideally described as a simple harmonic oscillation. However, friction or external force resists the motion and causes the oscillation to decelerate (see 1.1.2). Since many nanotechnological techniques rely on the use of resonators, application of nanotechnology on research usually requires us to understand fundamental concepts of resonators and their behavior.

1.1.1 Simple harmonic oscillation

Mechanical motion such as harmonic oscillation is a well-known phenomenal describing periodic motion in many mechanical systems. Repeatedly, we utilize this mechanical motion in simple devices such as pendulum in clocks, mechanical mechanism in watches. It can be expressed as shown in equation 1.1,

$$x(t) = A\cos(2\pi ft + \phi), \quad \ldots (1.1)$$

where x is a position at time t, f is the resonant frequency of an oscillator with mass m experiencing a single force, F. Equation 1.1 is a solution from solving Newton's second law for a simple harmonic motion (equation 1.2)

$$F = ma = m\frac{\mathrm{d}^2x}{\mathrm{d}t^2} = -kx \quad \ldots (1.2)$$

In this case, the motion is periodic, neither driven nor damped. It repeats itself in sinusoidal fashion with constant amplitude, A. The potential energy, U, stored in this simple harmonic oscillator at a position, x, is expressed in equation 1.3

$$U = \frac{1}{2}kx^2 \quad \ldots (1.3)$$

1.1.2 Damped harmonic oscillation

1.1.2.1 Damped harmonic oscillation

In reality, all resonators experience friction, which causes the motion of the system to slow down. In many vibrating systems such as tuning fork, Newton's second law with damping is adjusted with damping coefficient, c, shown in equation 1.4

$$F = -kx - c\frac{\mathrm{d}x}{\mathrm{d}t} = m\frac{\mathrm{d}^2x}{\mathrm{d}t^2} \quad \ldots (1.4)$$

This equation can be rewritten in equation 1.5

$$\frac{\mathrm{d}^2x}{\mathrm{d}t^2} + 2\zeta\omega_0\frac{\mathrm{d}x}{\mathrm{d}t} + \omega_0^2 x = 0 \quad , \qquad \ldots (1.5)$$

where ω_0 is called "undamped angular frequency of the oscillator", and ς is the damping ratio. Oscillators that undergo damping require a driving force to compensate energy loss during oscillations and to maintain the amplitude. The ratio between energy required to drive the oscillator and energy dissipated is called "quality factor (Q-factor)"..

1.1.2.2 Quality Factor

Because of damping in the motion, it is then necessary to drive the oscillation to maintain the amplitude for periodic cycles. One way to describe how under-damped resonators are is by quantify the ratio between the energy stored in the system and energy lost per a cycle. This ratio is known as quality factor, Q, and described in equation 1.6:

$$Q = 2\pi \times \frac{\text{Energy stored}}{\text{Energy lost per cycle}} \qquad \ldots(1.6)$$

According to equation 1.6, higher quality factor indicates a lower rate of energy loss relative to the stored energy in an oscillator; In other words, the oscillation ceases more slowly. On the other hand, Lower quality factor indicates a higher rate of energy loss, and the oscillation ceases more quickly.

Another way to characterize a resonator and measure Q-factor is to observe the bandwidth of frequency, Δf , generated by the resonator with respect to the resonant frequency, f_0. An example of a frequency spectrum of a resonator is shown in fig 1.1

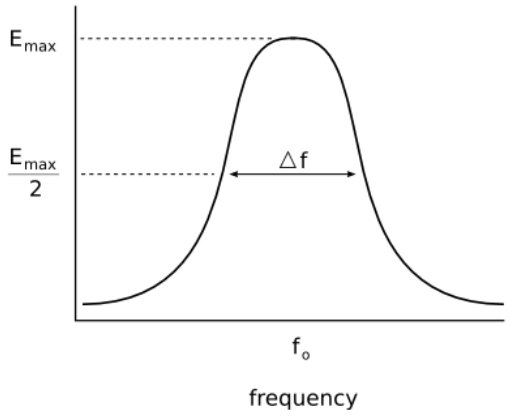

Fig1.1 The bandwidth Δf, of a damped oscillator is shown on a graph of energy versus frequency.

The Q factor of an oscillator can be defined as $f_0/\Delta f$ as shown in equation 1.7. The width of the peak indicates whether the oscillation have a high or low Q-factor. Since Q is proportional to $f_0/\Delta f$, broader peak (high Δf) will result in low Q-factor. On the other hand, narrow peak (small Δf) will result in high Q-factor. For sensitive measurements or applications that need high precision in frequency, resonators with high Q-factor is necessary. According to the spectrum in fig 1.1, Q-factor can be calculated using the following formulae:

$$Q = \frac{f_r}{\Delta f} = \frac{\omega_r}{\Delta \omega}, \qquad \ldots(1.7)$$

where f_r is the resonant frequency of the resonator, ω_r and $\Delta\omega$ are angular resonant frequency and angular frequency bandwidth.

For any instrument with a resonator integrated in, high Q-factor is desired for high quality and reliability of data. In chemical sensing and characterization application, low Q-factor

may result in insufficient quality and precision of the data. Hence, it is essential to assure high Q-factor during the measurements.

1.2 Application of resonators for chemical sensing

When a resonator oscillates, the resonant frequency and the Q-factor are commonly used to identify quality and characteristic of the resonator. As described in fig 1.1, resonant frequency is the frequency that resonator vibrates at the highest amplitude. Resonant frequency is a unique property to a resonator and depends on many factors such as shape, material, and mass of the resonator. When a resonator oscillates in different environments (e.g., vacuum, air), its resonant frequency will change according to the drag force and resistance caused by the media the resonator vibrates in. Similarly, Q-factor is also affected by the environment of the resonator. In heavier media, the oscillation becomes more restricted and damping happens more greatly; This will result in a lower Q-factor and yield a broader frequency spectrum (see fig 1.2).

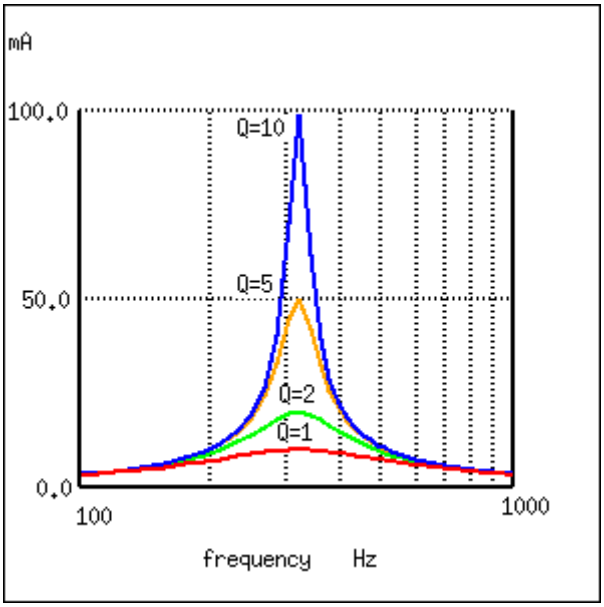

Fig 1.2 Four different frequency domain spectrums with different Q-factor. The most narrow peak represent an oscillation with highest Q-factor (Q=10) while the broadest peak represents an oscillation with the loswest Q-factor (Q=1)[1]

In this work, application of resonators for chemical detection was emphasized. We utilized the fact that resonant frequency of a resonator was changed when the mass of the resonator was altered by chemical adsorption. Generally, when mass of a resonator changes, the relationship between mass adsorbed and resonant frequency can be described below.

$$\frac{\Delta f}{f} \alpha - \frac{\Delta m}{m} \quad \ldots(1.8)$$

From this equation, Δf is the change in resonant frequency from the original resonant frequency f. Δm is the mass change due to adsorption of chemicals in relative to the mass m of the resonator. When the mass of the resonator increases, the movement of the resonator becomes more sluggish and slower. The oscillation will happen at lower frequency.

To detect certain chemicals, interaction at the interface of resonators has to be optimized for adsorption of the chemicals. In other words, the surface has to be functionalized by a selective layer to maximize the interaction and adsorption of the analyte.

1.3 Resonators design for chemical sensing

Most of the resonators are made of piezoelectric materials (e.g., quartz, lead zirconate titanate (PZT)), which convert electric energy into mechanical energy. The electric signal applied to these materials can induce the movement according to the signal. If AC current is applied,

oscillation of the resonator can be induced through difference in dipole moment. As micro and nano-fabrication advances, more complicated designs and features are possible. The resonators mainly used in this study are tuning fork and Capacitive Micromachine Ultrasonic Transducer (CMUT); they are introduced in this section.

1.3.1 Tuning fork

Tuning fork comprises of two prongs that resonates towards each other. It is a classic and simple resonator used in many devices (e.g., radio frequency generation, watches). Many scientists and engineer also found its applications in many instrumentation systems and in electronics. Examples of these applications are such as radar gun to detect car speed [2-4], hearing assessment tools [5], surface analysis tools [6, 7], sensors and actuators [7, 8]

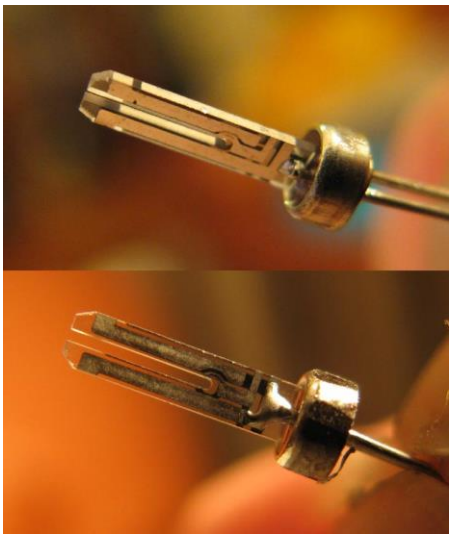

Fig 1.3 micro-resonator or micro tuning fork

In chemical detection, quartz crystal tuning forks are used and excited to resonate with AC current. A measurement of frequency bandwidth similarly to fig 1.2 is obtained from

frequency tuning. We also developed an algorithm using Fourier transform technique to increase the speed of the detection and to extract more parameters from the oscillation [9]. As expected, the spectrum obtained from our system shows a peak representing the resonant frequency of the tuning fork similarly to fig 1.2 at a much quicker speed than frequency sweeping method.

The use of tuning forks in our research was to use them for polymer and material screening for chemical and biochemical sensors. Tuning forks are inexpensive and simple to use with our platform. They are also available commercially with many specifications. Hence, for the first part of the development when we select polymers as selective layers for chemical reactions, it was convenient and cost-effective to use tuning forks as our model.

1.3.2 Capacitive Micromachine Ultrasonic Transducer (CMUT)

A capacitive micromachined ultrasonic transducer (CMUT) with more advanced fabrication technology and improved performance was introduced in 1993 by M. Haller and B. T. Khuri-Yakub [7]. Advanced IC fabrication processes enabled realization of the submicron gaps between the electrodes that make it possible to achieve high electric fields with low applied voltage. These processes also provide a precise control on device dimensions in the vertical and lateral directions. The wide bandwidth and the potential for integration with electronic circuits are other advantages associated with CMUTs. Since the first demonstration of CMUTs in early 1990s, extensive research on this device has been conducted both to improve fabrication process and to explore its potential application [7-12].

A CMUT resonator is operated by applying AC potential between the top and bottom electrodes to induce a periodic vibration of the membrane, which is caused by the electrostatic

attraction. An insulating layer is included to prevent the two electrodes from shorting in case of contact. A single transducer element uses many small capacitor cells that are connected in parallel. The shape of a device containing multiple single CMUTs can be tailored into much geometry. The structure of a basic CMUT cell is shown in fig. 1.4.

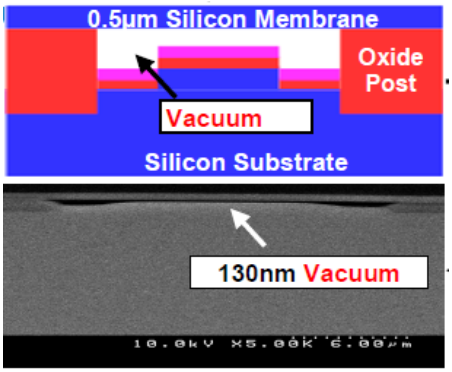

Fig 1.4 Basic CMUT structure (cell). This picture represent a side view of CMUTs and shows a thin gap between the two membrane electrodes.

In the past couple years, advanced CMUTs have been fabricated with the goal to achieve higher sensitivity for chemical detection and enhanced signal-to-noise ratio. In 2009, Khuri-Yakub *et al.* fabricated CMUTs composed of approximately 1000 resonator cells electrically connected in parallel shown in fig.3.12.

The optimal design for CMUTs device was shown to be hexagon with a dimension of 200-300 micrometer. Each hexagon contains around 1000 resonator cells, and the device can be driven with resonant frequency of 42.7MHz – greater compared to 17.5 MHz in the previous design. This 42.7 MHz CMUT model achieves a phase noise of -105 dBc/Hz and -148 dBc/Hz at offset frequency of 1 kHz and 1 MHz respectively in air [3]. This improved design also has higher sensitivity and many enhanced properties, which are summarized in table 3.1.

Since the silicon technology and fabrication techniques has been advanced in the past decades, non-piezoelectric transducers such as CMUTs are gaining interest and may replace systems with piezoelectric materials in a soon future in some area of applications. In this study, CMUTs were used and applied as chemical sensors for carbon dioxide and protein detection. Because of its high sensitivity, CMUTs are considered to be a promising device that will improve diseases diagnostics. This application will be very significant for critical diseases that cures are only available at early stage (e.g., cancers), or diseases that are highly contagious (e.g., tuberculosis).

1.4 Mechanical motion and effect of physical environment in biological system

In this study, mechanical and physical inducers were applied to cells. A background in mechanical and physical responses of cells and biological systems including basic understanding of cell movements, nanomehanotransduction and how physical properties may affect cells are discussed in this section. With the focus on the development of cardiac cells in particular, motion and mechanical aspects of cells and heart cells are also emphasized.

1.4.1 Mechanic of cells and effect of physical stimuli

Muscles are made up of subunits called Sarcomeres. Within Sarcomeres, actin and myosin filaments are responsible for many types of cell movements. Inside this subunit, thin filaments of actins (red thin filaments in fig 1.5) lie transversely across from both ends of Sarcomere. During muscle contraction and relaxation, two proteins called troponin and tropomyosin bind closely at cue to actin filaments in order to regulate muscle contraction. Troponin is associated with actin filament and bind to the actin molecules (one troponin for

every 6-8 actin molecules). Tropomyosin is a long thin protein and usually prevents myosin (green filaments in fig 1.5) heads from contacting actin, and help control contraction.

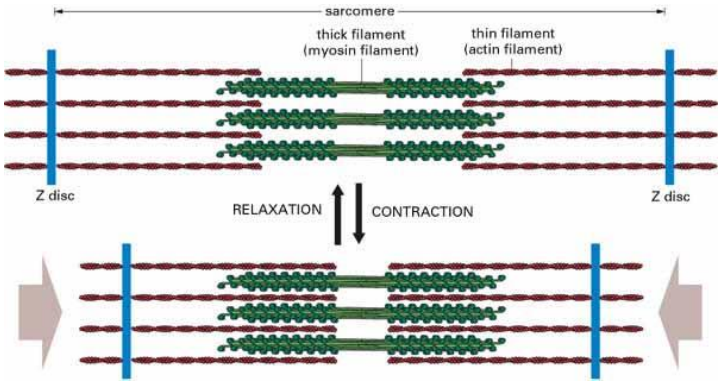

Fig 1.5 Overview of actin filament (red) and myosin (green) in sarcomere during muscle contraction cycles [10]

Myosin is a protein that plays a great role in muscle contraction and assists the conversion of chemical energy in term of adenosine triphosphate (ATP) to mechanical energy. It is sometimes known as motor protein that works together with actin filaments to initiate muscle contraction. At the end of myosin, there is an active site, "head of myosin", allowing myosin to bind to an actin molecule. Through series of this binding, actin filament is moved and controlled by myosin.

Before the muscle contraction, tropomysin and tropomyosin blocks the binding between myosin and actin filaments. When the muscle contraction process was stimulated by an inducer such as force or electricity, Ca^{2+} ions in sarcoplasmic reticulum were released into the muscle cells. Once Ca^{2+} binds to troponin, troponin disconnects from actin, and tropomyosin unblocks the myosin from binding to the actin filament. With energy from ATP, myosin heads start to move actin filament towards the center of sarcomere in each cycle until the stimuli are removed.

This process causes sarcomere to shorten after many cycles of the actin movement. When muscles relax, myosin heads disconnect from actin filaments, and sarcomeres return to their original length.

1.4.2. Contraction of cardiac muscle

Cardiac muscles are involuntary muscles found in the walls and foundation of the heart. This muscle comprises of cardiomyocytes. Contraction of cardiomyocytes is important for blood regulation through atria and ventricles and coordinated by nuclei of these cells. Contraction of cardiac muscles occurs regularly in cycles and result in blood pressure throughout the body.

Cardiac cycles can be monitored through many physical means and methods (e.g, atrial pressure, ventricular pressure, electrocardiogram, phonocardiogram) summarized in fig 1.6.

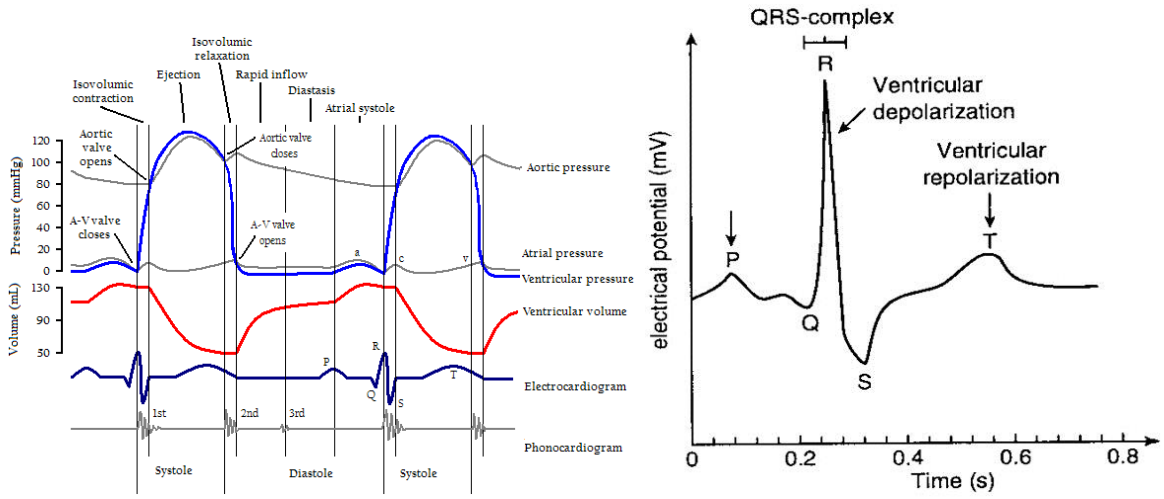

Fig 1.6 a typical heart signal of a 26 year old male adult [11]

These cycles are periodic, and frequency of the contraction motion can be characterized; This frequency is typically referred to as “heart beat”. A typical method to measure this frequency is through electrocardiogram which typically looks like a blue signal in fig.1.3. It is used wildly by physicians to monitor health condition of patients.

In this study, the origin of beating motion of cardiomyocytes is investigated and discussed in chapter 5. As stem cell research has gain more attention, it is unclear on how stationary cells such as embryonic stem cell can generate a motion to start contraction when it differentiate to become cardiomyocytes. It was suggested that the differentiation of stem cells towards mesoderm, i.e., muscle, cardiac cells, might be also influenced by non-biochemical signals such as force, electric field and stiffness of the substrate. These physical inducers may be applied to direct the differentiation of stem cells in addition to biochemical signals and are our focus in the investigation in chapter 5.

1.4.3. Force and mechanical motion in cellular level

As discussed briefly in section 1.2.1, actin-myosin interaction is responsible the cellular motion. Before those cycle happens, many biophysicists believe that cells can sense their physical environment and can respond appropriately through biochemical reaction within the cells [12]. These physical inducers are such as external force, stiffness of the substrate, electric field, and magnetic field. Recent works have illustrated the effects that these physical inducers may have on many cell types, especially stem cells. For example, stiffness or elasticity of the substrate was shown to affect differentiation of stem cells to become mesoderm [13]; Direction of forces and geometry of substrates for cell culture can influence cells to change in morphology [14].

When these physical inducers are applied on cells, it is suggested that cellular response will occur in 3 steps : (1) Force Sensing (2) Mechanotransduction (3) Mechanoresponses.

In the force sensing step, force induces changes in protein conformation and pressure within cells. As a result, the interactions are locally transduced into biochemical signals that activate various mechanosensitive signalling pathways, ultimately regulating cellular mechanoresponses [12, 15]. Force sensing can occur through three mechanisms (fig 1.7): (1) protein unfolding (2) membrane tension changes (3) Catch bond, receptor-ligand bond. All of these mechanisms will result to changes in biochemistry inside the cells. And hence, mechanotransduction occurs in response to regulate and maintain cells' survival.

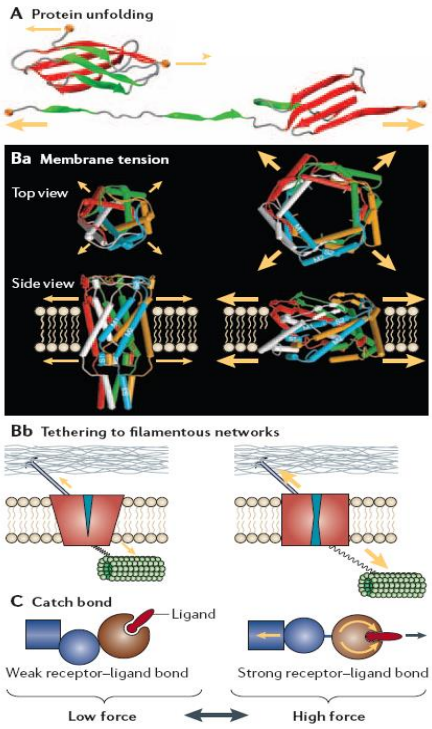

Fig 1.7 Mechanisms of force sensing by cells**. A** | Conversion of force into biochemical signals by partial protein unfolding[16]; This can result in the gain or loss of binding sites, increased separation between protein domains, or the gain or loss of enzyme function. **B** | The opening of some mechanosensitive ion channels can be regulated by membrane tension[17] (**Ba**), whereas the opening of others requires that their

intra- and/or extracellular domains are physically connected to force-bearing filaments (**Bb**). **C** | Stabilizing receptor–ligand bonds by switching them to a long-lived state by force (catch bonds)[18]. Yellow arrows indicate forces. Pictures are duplicated with permission from [12, 18]

In mechanotransduction, certain biochemical pathways are triggered and converted to mechanical responses. For example, Integrin cluster – cells adhesion protein- enlarges to maintain cellular adhesion when a sheer force is applied on cells [18]. Effect of force on mechanical cellular responses is investigated on embryonic stem cells and will be discussed in chapter 5.

1.5 Application of nanotechnology in biological research

Nanotechnology is an emerging field allowing studies of material and systems at nanometer scale. Many instruments in this field utilize a probe to scan across a specimen surface. These probes are usually nanoscale cantilevers that can interact with the surface to characterize nanoscale feathers accurately. As the field is emerging, the instruments are being developed to achieve higher resolution and to characterize small features (e.g., sub-nanometer) more precisely. Nanotechnology initially used in the study of solid state or hard material (e.g. silicon, semiconductor). However, after "single cell force spectroscopy (SCFS)" was developed in our laboratory[19], the potential of nanotechnological tools such as atomic force microscopes in biological research was recognized. The use of this technique was proved to reveal information additionally to information available from conventional methods in biological science; and the application of nanotechnological techniques in biology is gaining more attention from many scientists in biological research.

While nanotechnology has been around for several decades, only a small fraction of research has applied these tools in biological studies. Accordingly, there are potentially much information that have not been explored in fundamental biology because of limitation in instruments but may be discovered through the application of nanotechnological instruments. For example, a cell's Young modulus measurement- not available in a conventional method such as optical microscopy- showed us that cancer cells were 70% softer than normal cells using atomic force microscopy (AFM)[19-21]. After these works, more research has focus on force and mechanical aspect of cells more than before, and young modulus is being considered as an indicator to diagnose certain types of cancer [22]. This innovation became an inspiration and a motivation for many parts of this study in the Gimzewski laboratory. To pursue and develop more technology to advance biological research, we conducted research base on the application of nanotechnological tools in biological studies, which can be categorized into two main areas: (1) cell mechanical study at nano- and microscopic scale, (2) biochemical detection and gas sensing.

The first direction focuses on adaptation of nanotechnological microscopy to visualize biological material (e.g. stem cells, antibodies) in 3 dimensions. Selected techniques for this study include interferometry and atomic force microscopy. These instruments were adapted and modified to perform mechanical measurements on stem cells as they differentiated. A highly sensitive fluorescent microscope is also used to confirm our finding and provide a good comparison to the results from our new method. In addition to force application, nanofabricated platform was made and used for pulsation of stem cells. Electrical pulse was supplied and used to excite stem cells to drive the differentiation. During this process, we expected to visualize

mechanical motion or biological markers indicating changes in cell mechanics of the stem cells (e.g, cardiac gene expression). More details in this part will be discussed in chapter 5.

For the second direction, I was interested in developing and optimizing a nano-fabricated mechanicalelectronicmachine systems (MEMS), for biochemical detection purposes. This system is called capacitive micromachined ultrasonic transducers (CMUTs) and was demonstrated to detect specific antibodies and biomarkers for cardiovascular diseases at a very low concentration (e.g. ng/ml, pg/ml) for the first time. Ability to detect protein at very low concentration implies that detection of diseases with CMUTs may be possible at early stage; this is very important for many critical diseases such as cancer. CMUTs system was designed for high sensitive detection and only required small amount of sample ~1µl for detection. This high throughput sensing system can provide reading within a second and would improve the time, accuracy of the detection significantly. In this study, possibility of this technology for disease detection other than cardiovascular disease is also discussed. Results from the detection were compared to the conventional immunological technique (i.e., ELISA).

Lastly, we explored the opportunity of using CMUTs to detect carbon dioxide gas. Carbon dioxide is related to metabolism and organelle activities. However, high concentration of carbon dioxide is toxic to human bodies. With high sensitivity of CMUTs, low concentration of carbon dioxide was detected. Other organic volatiles were also considered and detected as well in chapter 3.

Reference

1. **Allaboutcircuits.com.** ***Q and bandwidth of a resonant circuit*** **2012; Available from: http://www.allaboutcircuits.com/vol_2/chpt_6/6.html.**
2. **Brzoticky, F.H.,** ***Calibration of police radar instruments,*** **in** ***Report of the 60th National Conference on Weights and Measures 1975*****. 1976, Metrologist Weights and Measures Section, Department of Agriculture State of Colorado: Boulder Colorado. p. 42-47.**
3. **Radarguns.com.** ***Radar guns FAQ.*** **2010; Available from: http://www.radarguns.com/radar-guns-faq.html.**
4. **Radars.com.au.** ***A detailed explanation of how police radars work.*** **2008; Available from: http://radars.com.au/police-radar.php.**
5. **B.Yueh, N.S., C.H.MacLean,P.G.Shkelle,** ***Screening and management of adult hearing loss in primary care: scientific review.*** **Journal of the America Medical Association, 2007. 298(15): p. 1976-1985.**
6. **V.T.Tung, S.A.C., T.X.Hoai,N.T.Tinh,V.V.Chikunov,** ***Tuning Fork Scanning Probe Microscopes – Applications for the Nano-Analysis of the Material Surface and Local Physico-Mechanical Properties,*** **in** ***Scanning Probe Microscopy-Physical Property Characterization at Nanoscale,*** **V.Nalladega, Editor. 2012, InTech.**
7. **B.J.Eves,** ***Design of a large measurement-volume metrological atomic force microscope (AFM).*** **Measurement Science and Technology, 2009. 20: p. 084003-8.**
8. **H.Edwards, L.T., W.Duncan,A.J.Melmed,** ***Fast, high-resolution atomic force microscopy using a quartz tuning fork as actuator and sensor.*** **Journal of Applied Physics, 1997. 82(3): p. 980-984.**
9. **R. P. Wali, P.R.W., S. Eaimkhong, J. Hernando-Garcia, J. L. Sánchez-Rojas, A. Ababneh, J. K. Gimzewski,** ***Fourier transform mechanical spectroscopy of micro-fabricated electromechanical resonators: A novel, information-rich pulse method for sensor applications.*** **Sensors and Actualtors B, 2010. 147: p. 508-516.**

10. **Pernick, N. *Stains Actin-general*. 2011; Available from: http://www.pathologyoutlines.com/topic/stainsactin.html.**

11. **Chang, D. *Cardiac cycle, A Wiggers diagram, showing the cardiac cycle events occuring in the left ventricle*. 2011; Available from: http://en.wikipedia.org/wiki/Cardiac_cycle.**

12. **Sheetz, V.V.a.M., *Local force and geometry sensing regulate cell functions.* Nature Reviews: Molecular Cell Biology, 2006. 7: p. 265-275.**

13. **Adam J. Engler, S.S., H. Lee Sweeney, and Dennis E. Discher, *Matrix Elasticity Directs Stem Cell Lineage Specification.* Cell, 2006. 126: p. 677-689.**

14. **F.Grinnell, C.H.H., E. Tamariz, D.J.Lee, G.Skuta, *Dendritic Fibroblasts in Three-dimensional Collagen Matrices.* Molecular Biology of the Cell, 2003. 14: p. 384-395.**

15. **R.I. Wilson, D.P.C., *The Force Be With You: A Mechanoreceptor Channel in Proprioception and Touch.* Neuron, 2010. 67.**

16. **M. Gao, D.C., V Vogel, K. Schulten, *Identifying Unfolding Intermediates of FN-III10 by Steered Molecular Dynamics.* Journal of Molecular Biology, 2002. 323(5): p. 939-950.**

17. **C.Kung, *A possible unifying principle for mechanosensation.* Nature, 2005. 436: p. 647-654.**

18. **W.E. Thomas, E.T., M. Forero, V. Vogel, .E.V. Sokurenko, *Bacterial Adhesion to TargetCellsEnhanced by ShearForce.* Cell, 2002. 109(7): p. 913-923.**

19. **S.E. Cross, Y.S.J., J. Rao, J.K. Gimzewski, *Nanomechanical analysis of cells from cancer patients.* Nature Nanotechnology, 2007. 2: p. 780.**

20. **S. Cross, Y.S.J., J.Tondre, R.Wong, J.Y. Rao, J.K. Gimzewski, *AFM-based analysis of human metastatic cancer cells.* Nanotechnology, 2008. 19: p. 384003.**

21. **J.Reed, B.M., B.PIttenger, S.Magonov, J.Troke, M.A.Teitell,J.K.Gimzewski, *Single molecule transcription profiling with AFM.* Nanotechnology, 2007. 18.**

22. **M.Lekka, P.L., *Applicability of AFM in cancer detection.* Nature Nanotechnology, 2009. 4(72).**

Chapter 2

Review of Techniques for Surface Functionalization and Characterization

As discussed in chapter 1, chemical detection, diagnostics and nanotechnology are the fields that rely on interaction and visualization of sample at interface. After the rise of silicon technology in 90s, the most popular interface has become air-solid silicon and liquid-solid silicon depending on the application. As a result, functionalization and surface modification of a hard substrate such as silicon became an important area and fundamental for much research. To apply nanotechonology in biological research, preparation of soft material and biological material for surface analysis (e.g. DNA gene profiling performed on silicon surface [1, 2]) has to be optimized for the finest measurement. In this chapter, techniques and materials used for surface functionalization and characterization in this study are discussed.

To deposit soft material (e.g., protein, polymer) appropriately on a surface, multiple steps protocols involving variety of instrumentations were developed. In this work, all these techniques were tested and applied to achieve an optimum layer of material with the desired property, e.g., high porosity, low surface tension. These properties are important in order for certain surface chemistries and interactions to occur. To confirm that the desire properties of the material layer on surface are achieved, characterization of the deposited film layer was performed. In this chapter, characterization techniques used in this work are also discussed and explained in details along with the functionalization techniques.

2.1 Material deposition and surface functionalization

Surface chemistry has become a great part in much research in chemistry, physics, electrical engineering, material science and biology. Since most of the interaction between molecules occur at interface (i.e. solid-liquid, solid-air), process of material deposition on substrates such as silicon wafer is very important to activate these interaction. Nowadays, many deposition techniques are available for many types of materials ranging from metals to soft matters, (e.g., polymers and proteins). In many occasions, achieving a desired layer at an interface requires multiple depositions of initial layers before the final layer. This means that deposition protocol have to be optimized for certain surface of interest.

Study at a nano-scale is a delicate and sensitive process, hence functionalization techniques used in this field have to be precise in positioning and give high quality of deposit layers. For application of nanotechnology in biological research manipulation and handling of soft materials on a flat surface for nanotechnological characterization such as AFM and optical profiler analysis have to be optimized. For this to happen, instruments and techniques with high precision in materials patterning were used in this work. These techniques are discussed in this chapter including advantages and examples of functionalized surface.

2.1.1 Material printer

Material printers allow the user to create a pattern and print it on any substrate, e.g., silicon, resonators, using ink formulated. In particular, the two machines used are Dimatix Material Printer (DMP) by Fuji (fig 2.1) and Sonoplot (fig 2.2).

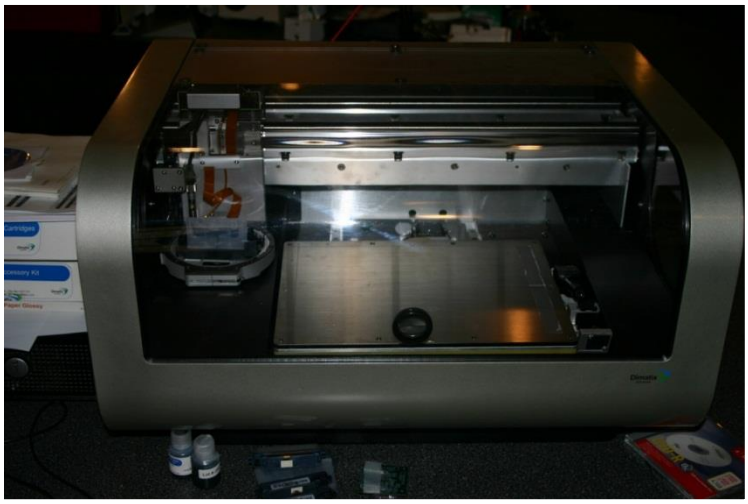

Fig 2.1 Dimatix Material Printer

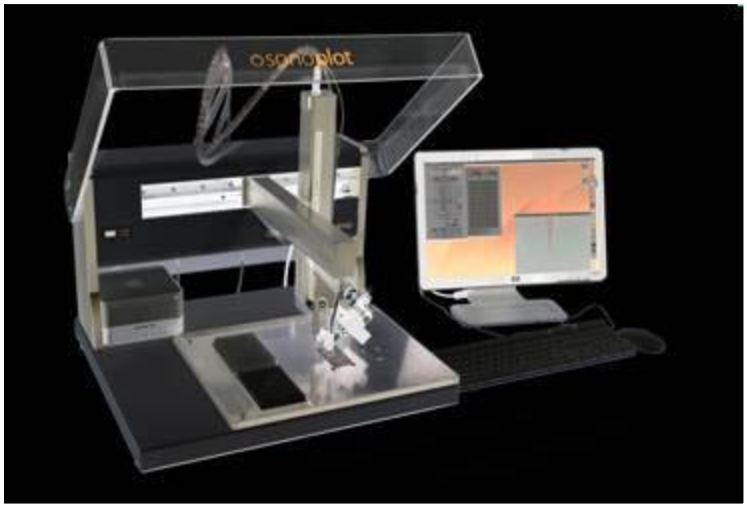

Fig 2.2 Sonoplot

The principal of these two machines are to apply vibration to a nozzle within a liquid holder or cartridge to dispense the liquid. In case of DMP, the nozzles inside a cartridge, made of small pieces of piezoelectric material, actuate according to the waveform created by users. In the waveform function menu, users can design a squeezing and releasing pattern to control the

movement of the nozzles; This will allow the users to control the characteristics of a liquid drop (e.g. volume, shape, stray) using different waveforms. Dimatix Material Printer (DMP) has high accuracy in deposition, i.e., +/- 10μm, compared to Sonoplot, and a dispensed droplet has volume of around 20nL. Although DMP offers many advanced features, it requires complicated formulation of ink solutions in order for them to be jetted off the nozzles. In particular, the machine requires these solutions to have viscosity of 10-12 cP and surface tension of 0.028-0.033 N/m. Since the polymer inks for our experiments were not commercially available, the inks were made and formulated. During this process, viscosity was tested by a viscometer, and surface tension was measured from a pendant drop of the solution using a contact angle machine to assure that the ink solutions had viscosity and surface tension as required.

To formulate ink for DMP printing, the solvents for ink formulation were chosen carefully. In this study, mixture of ethoxy glycol and dimethyl sulfoxide (DMSO) were used as a base solvent to produce ink of selected polymers. Both DMSO and ethoxy glycol were selected because they are non-volatile, and hence the ink properties would not change drastically due to vaporization. DMSO is known to be an universal solvent that can dissolve many polymers effectively. For our formulation, the formulation process started by dissolving the selected polymer powder in DMSO, ~ 1% w/w, before ethoxy glycol was added. DMSO has low viscosity and high surface tension that is outside the desired range. By adding ethoxy glycol, viscosity of the mixture increases while its surface tension decreases. Variation in composition between these two solvents then allows us to optimize a solution mixture to have viscosity and surface tension in the desired range. Surface tension and viscosity of a DMSO/ ethoxy glycol mixture at a different percent composition were shown in fig 2.3.

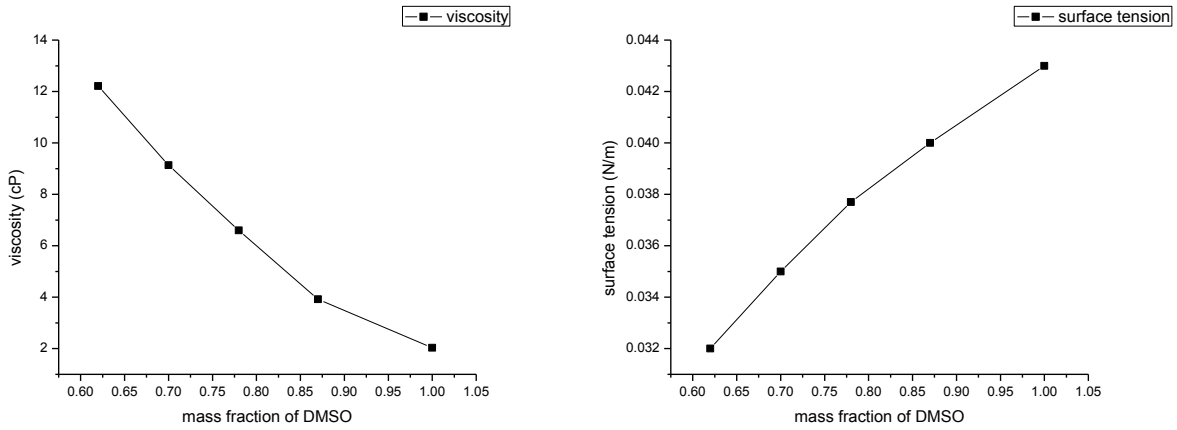

Fig 2.3 viscosity (left) and surface tension (right) of DMSO and ethoxy glycol mixture for ink formuation. According to the table, the most optimum mixture is 38% w/w ethoxy glycol in DMSO or 0.62 mass fraction of DMSO.

Once polymer inks were made, printing patterns were created on a computer to be transferred onto the substrate. The DMP has a camera to assist with the alignment for printing on a substrate for an accurate printing. Alignment for printing was then done carefully to make sure that the polymer solutions were transferred to accurate position and the printed pattern appeared as designed.

In this work, four polymer inks: polyvinyl alcohol (PVA), polyaniline (PA), polystyrene (PS) and polyphenylsulphide (PPS) were successfully formulated using DMSO and ethoxylate glycol mixture as the base solvent. Printing patterns including hexagon (~100-200 microns) for polymer printing on CMUTs and micro-rectangular for printing on micro-tuning fork are shown in fig 2.4 and 2.5 respectively.

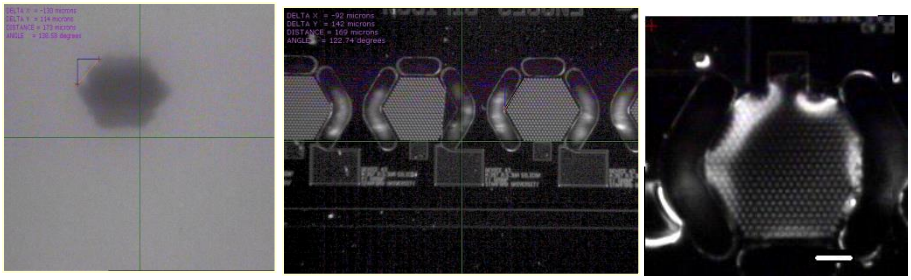

(a) (b) (c)

Fig 2.4 Printed patterns by DMP (a) a hexagon printed out on a photopaper by DMP (b) hexagon CMUT arrays (c) polyaniline deposition on CMUT device (scale bar is 75µm)

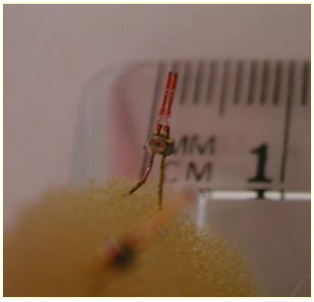

(a) Quartz resonators as model systems for mass sensors

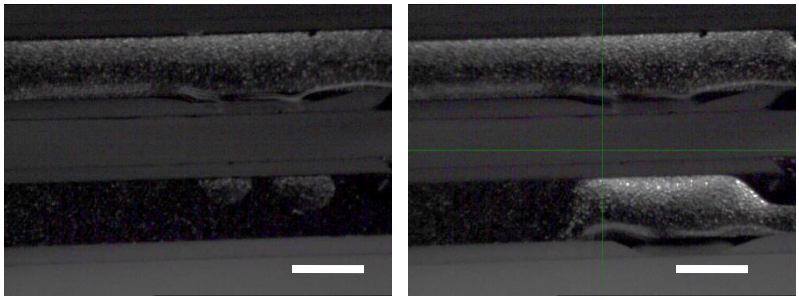

(b) (c)

Fig 2.5 Polymer deposition on quartz tuning fork using DMP (a) a quartz tuning fork before coating (b) deposition of tuning fork on the top arm (c) deposition of tuning fork on the top arm top arm and half right of the bottom arm (scale bar is around 200 µm)

Fig 2.4 illustrates that polymer inks were deposited on the surface of the CMUT devices accurately. The hexagon pattern with dimension of CMUT device was created and print on a photopaper. Then the same pattern was used to deposit polyaniline on top of a CMUT device and

demonstrated high precision in printing in fig 2.4c. Similarly, fig 2.5 shows an accurate deposition of polyaniline layer by DMP on a quartz oscillator. Once the printing was completed, the ink was left to dry at 120 °C for 2 hours in an oven.

Similarly to DMP, Sonoplot can deposit liquid considerably well for larger target using simple patterns, e.g., line, rectangular. For our investigation, many devices such as CMUT have complex shapes or small dimension, therefore Sonoplot was not accurate enough to be used in experiments requiring high precision in the deposition. However, Sonoplot is simple to operate and can jet any solution without requirement on ink formulation and properties. It is a good candidate for protein deposition because it can load protein solutions and dispense them quickly at a short period of time to minimize protein denature. For our biosensing experiments in chapter 4, CMUT chips were functionalized using Sonoplot.

2.1.2 Vapor deposition of silane

Vapor deposition is a method that chemicals are evaporated into vapor phase before they adsorb onto a solid substrate. This is sometimes known as chemical vapor deposition (CVD). In a typical CVD process, the substrate is exposed to one or more volatile, which react to form a layer on the substrate surface. Vaporization of these chemicals- typically silane for surface modification- can be performed by many methods depending on the nature of materials. For instance, heating of silanes to 120 °C is sufficient to generate enough vapor pressure of silane for deposition process. A setup for vapor deposition of silane on a silicon substrate is shown in fig 2.6.

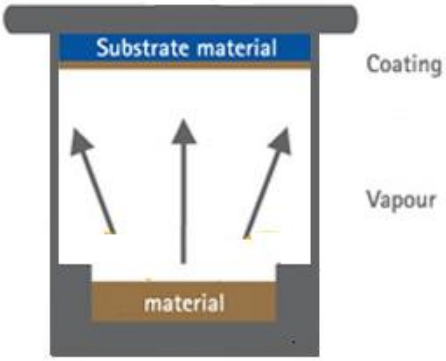

Fig 2.6 Vapor deposition setup. Vapor deposition chamber was placed on a heat source and caused vaporization of material such as silane. Substrates, usually silicon dice, were attached to the lid of the chamber. Once the vapor reaches the substrates, the deposition of the material takes place.

In this study, silanization of silicon surface is focused because it is a simple procedure to modify silicon surface using alkoxysilane (fig 2.7). With a large library of alkoxysilane that are commercially available, desired surface properties (e.g., hydrophobic, hydrophilic) of the substrate can be easily achieved. The silanization process on silicon, shown in fig 2.8, is very proactive because silane is a derivative of silicon. However, to obtain a monolayer self-assembly of silane on the silicon wafer, an optimum protocol for vapor deposition of certain silanes has to be developed for the specific substrate. This involves optimization of conditions, e.g., vapor pressure, temperature, deposition time.

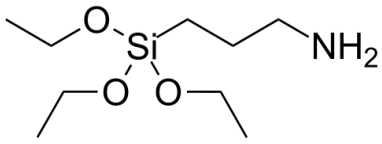

Fig 2.7 structure of (3-Aminopropyl)triethoxysilane (APTES), an example of alkyl silane molecules used in the study.

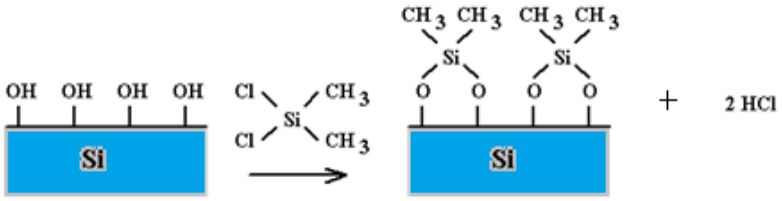

Fig. 2.8 an example of Silanization, a self-assembly process of aloxysilane on silicon surface, using dimethyldichlorosilane. In this process, small molecule such as HCl condense out and evaporate.

The chemistry of silanization usually contains the reaction between Si-OH group on silicon surface and Si-X of silane, where X refers to a halide and alkyl group. The condensation of small molecule, e.g., HCl, water, is expected during silanization, and hence these molecules have to be removed and cleansed from the surface. For higher coverage, silicon surface was treated with oxygen plasma (see section 2.1.4) to convert silicon dioxide layer to silicon hydroxide, which is a more reactive functional group for silanization. Fig 2.10 illustrates the hydropilicity of silicon substrate after oxygen plasma treatment.

Another method used to achieve high coverage of Si-OH is by treating silicon surface with piranha- mixture of sulfuric acid and hydrogen peroxide. The disadvantage of this process is the environmental impact and complex waste management because piranha is a hazardous, requiring special handling protocol. To avoid generation of hazardous chemical wastes, oxygen plasma was preferred and used mostly in this study.

2.1.3 Spin coating

Spin coating is a technique used in photolithography to control the thickness of the polymers and photoresist used to coat silicon wafers. These photoresists, e.g., SU8, have high

viscosity. By applying centrifugal force, polymer is spun on a wafer to create a thin homogenous layer of this polymer on the silicon wafer. Spinning rate can range from 1000 to 3000rpm to vary the thickness of the layer. By changing the spinning rate to higher, polymer layer is forced to spread out and hence the layer becomes thinner. More advanced spin coater allows the user to create a spinning profile to vary the spinning rate over time. This technique was used in SU8 cantilever fabrication and silane deposition on CMUTs.

2.1.4 Oxygen plasma

In plasma, gas atoms are excited to higher energy states and ionized. As the atoms and molecules 'relax' to their normal (lower energy states), they release photons, which result in the characteristic “glow” or light associated with plasma.

Plasma was adapted in a surface cleaning and modifying known as “plasma surface treatment”. During this process, high energy ions in plasma corrode the artifacts on surface such as silicon and eventually remove them from the surface. This process is similarly to sanding a surface using a sand paper. In other words, these ions in plasma act as the sand particles that corrode and remove the artifacts on surface at the molecular level. Depending on the type of gas ionized, the outcome of the treatment may be varied. For example, using oxygen plasma on silicon will add hydrophilic layer (i.e., Si–OH terminal) to silicon surface. Using plasma of different gas may yield to other results.

Plasma surface treatment can be used to modify the surface property of silicon substrate depending on the application on the surface. In our system, oxygen and helium gas were used to treat silicon surface and increase hydrophilicity of the silicon surface by adding Si-OH. This

layer is readily reactive with most silanes, and hence higher efficiency of silanization reaction (i.e., higher silane surface coverage).

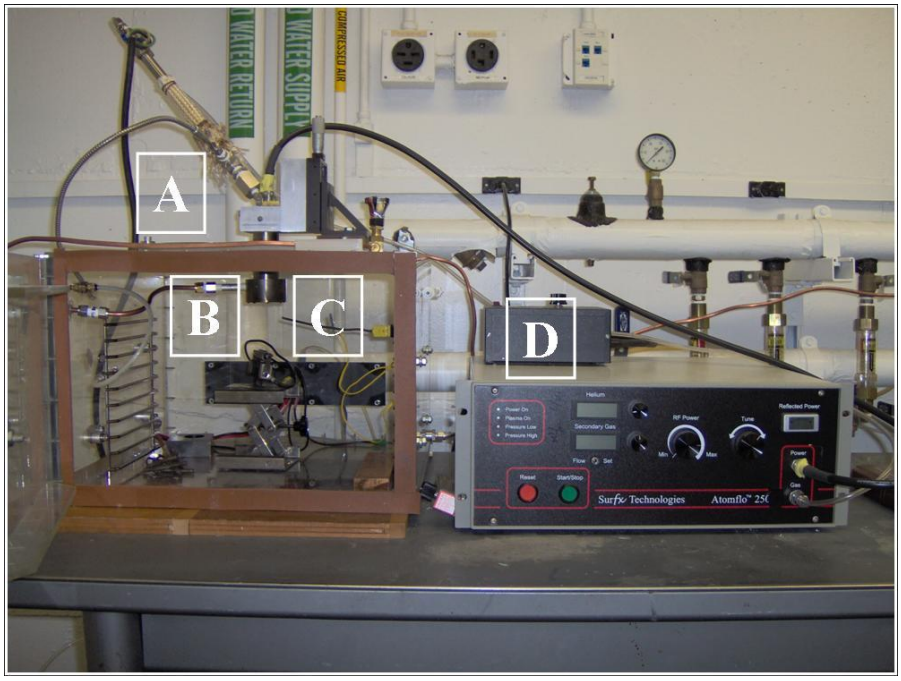

Fig 2.9 Plasma surface treatment system.

Fig 2.10 a demonstration of increase in hydrophilicity of silicon surface after oxygen plasma treatment (left) compared to the original silicon (right) through the contact angle of a water drop. In contact angel analysis, small contact angle or flat water drop illustrates high hydrophilicity of the surface.

Other than silanization, functionalization of biological materials would also benefit from hydrophilicity of substrate because proteins are zwitteric ions with net charges. By increasing

hydrophilicity of the susbstrate, we can achieve higher protein coverage yield on the surface through attraction from electrostatic charges.

2.1.5 Metal sputtering

Gold sputtering is a technique to coat a gold layer on a desired substrate. It is a physical vapor deposition (PVD) method to deposit a thin film of metal. This metal was place in a slot and known as a "target". During the process, sputtering gas such as argon bombards the gold target and ejecting the gold material from target onto a substrate.

2.1.6 Protein patterning

Many researchers have demonstrated strategies and methods to functionalize surface such as silicon with proteins for many biological applications. These applications include biosensing [3, 4], disease diagnostics [3, 5-7] , and cell patterning [8, 9]. Before a protein can adhere onto a silicon substrate efficiently, the surface has to be treated and modified to accommodate that specific protein. In this case, protein coupling agents were used to assist protein functionalization. Some of the reactions used in protein coupling are well-known interactions such as antibody-antigen, biotin-stepavidin. For example, to functionalize CRP protein, Anti-CRP was deposited on the surface as an initial layer, to functionalize TNFa, biotinylated Anti-TNFa is deposited on previously coated step-avidin layer. Some other coupling agents such as aminosilane can also assist protein functionalization as well by providing amine ($–NH_2$) terminus at the interface.

Since proteins usually carry charges, hydrophilic surface is sufficient to initiate the deposition process. By utilizing surface charges, the protein functionalization protocol can be simplified to fewer steps. In this study, we applied BSA and protein A as an initial layer onto

hydrophilic silicon, which was pre-treated with oxygen plasma and ethanol. Protein A is a protein known to adhere to the Fc domain of antibody and readily adsorbed on a hydrophilic silicon surface. As a result, the Fab domain of antibody is then exposed at the interface and available for binding to antigen. Similarly, BSA adsorbs very readily on hydrophilic silicon, and it was used as an initial layer for protein fabrication. For example, biotynilated BSA was deposited at the beginning of a sequential protocol before stepavidin conjugated molecules was deposited.

2.2 Surface characterization

2.2.1 Interferometric optical profiler

Interferometry of light is a technique that reflected beams of light are superimposed and gave fringes pattern, interferogram, similarly to the result in a double-slit experiment. Generally, when two beams of light with the same frequency combine, the resultant pattern is determined by the phase difference observed. The phase difference is usually caused by the path that these two waves travel. This may be because of the difference in media or length in each path that they travel. At the detector, waves that are in phase will undergo constructive interference while waves that are half a cycle out of phase will undergo destructive interference.

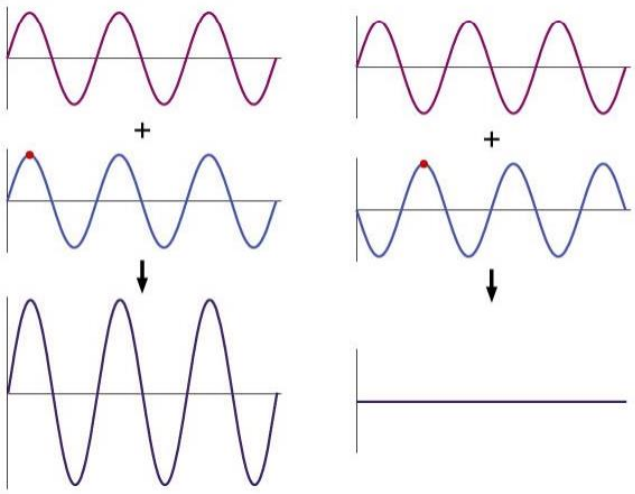

Fig 2.11 Constructive (left) and destructive (right) interference of any two waves.

In many decades, this concept has adapted and utilized to create an instrument called interferometer, which is used to measure distance or thickness of objects accurately in macroscopic and microscopic scale. A commonly used interferometric configuration is called Michelson interferometer, which was invented in 1887 by Albert Michelson (fig 2.12). In his configuration, a coherent light source provides incident light that is later split into two halves on a beam splitter. First half is transmitted to a stationary mirror and reflected back to the splitter while the other half is reflected and passes through the splitter to the adjustable mirror before reflected back to the splitter. Once both beams recombine at the splitter and reach the detector, an interference pattern can be observed at the detector. As previously described, this pattern depends on the optical path difference (OPD) or refractive properties of the media that these waves travel in.

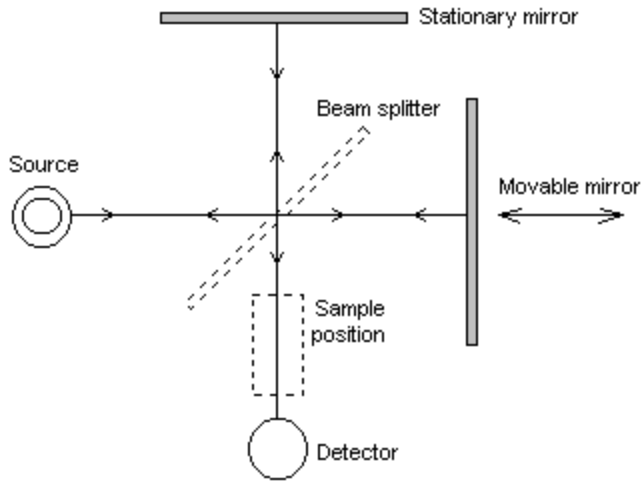

Fig 2.12 a schematic of an interferometer[10]

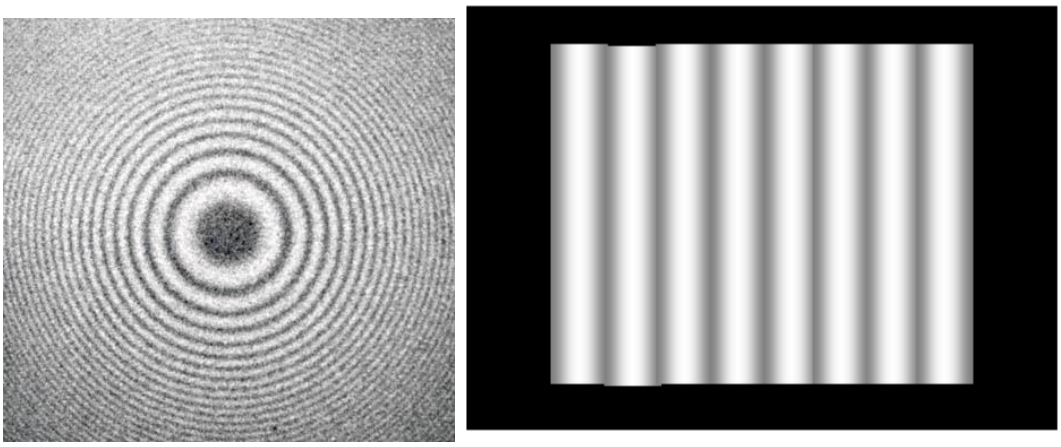

Fig.2.13 Interferogram or interferrence pattern from an interferometer using a point light (left) and a parallel light (right)

The operation of length measurement by interferometry can be divided into two common techniques: vertical scanning interferometry (VSI) and phase shifting interferometry (PSI). VSI is the more popular technique of interferometry while PSI has higher resolution in measurement

over a shorter range. An observation of the fringes pattern from the interference in VSI mode can provide length estimation. This relationship is expressed in equation (2.1).

$$L = (N + f)\,\lambda/2, \qquad \ldots(2.1)$$

where L is the length being measured, λ is the wavelength, N is an integer and f is a fraction ($0 < f < 1$) that can be derived from a calibration.

Commonly the optics are arranged such that the light beam measures exactly double the required length, in which case the measurement units, 'fringes', are half-wavelengths. In other words, length can be calculated in term of multiple of $\lambda / 2$. By using a light source for which λ is known, measurement of N and f leads directly to a value for L.

For example, one fringe on an interferogram from an interferometer that use visible light with wavelength of 400-700nm is around 200-350nm in dimension. For higher sensitivity, it is possible to calibrate of *f* to a resolution of 1/100 to 1/1000 of a fringe to increase sensitivity of the measurement. This will make measurement more accurate, similarly to using a ruler that has minor tick mark as small as 1nm with white light source. For higher sensitivity, utilizing light sources with smaller wavelengths will improve measurement resolution and quality of the measurement. For instance, using x-ray yield a resolution of picometer range [11]

Early applications of interferometry for distance measurement were mostly in astronomy to measure distances of stars and objects in the sky. In the past several decades, much research has illustrated the use of interferometer in metrology because of its high resolution (e.g., nanometer and picometer resolution) that was desired in nanotechnology. For measurement of small features such as surface roughness, thin-film thickness, an interferometer was incorporated to an optical microscope and algorithm for accurate visualization and analysis of fringes pattern.

This system is known as interferometric optical profiler (fig 2.14). Similarly to an interferometer, the system has a beam splitter that divides coherence light into two halves to travel along two paths. The first half is transmitted directly to the stage where samples are placed. It is crucial for samples to be reflective so that light can be reflected back and superimpose with the other beam at the splitter. The other half is reflected to the reference mirror before recombining with the transmitted beam to create an interferogram. CCD camera is used to record a series of interferogram emerged from the system, and a computer algorithm can analyze these intensity patterns to create representative topological surface map of the test surface.

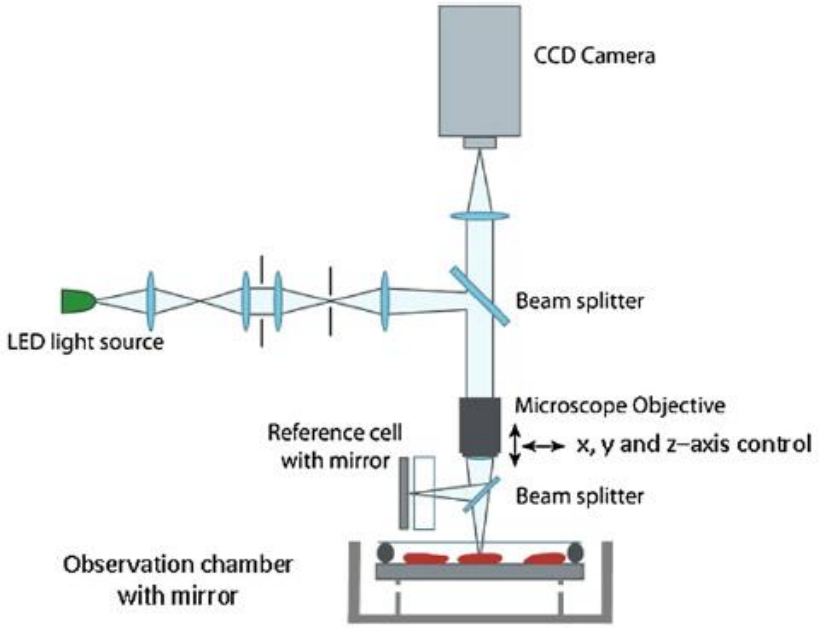

Fig 2.14 a schematic of an interferometric optical profiler

In an interferometric optical profiler, optical lens are placed to convert light from a point light source into parallel beams. As a result, the fringes pattern will form alternating bight and dark along one direction as shown in fig. 2.15, which is different from radial fringes observed in fig. 2.13

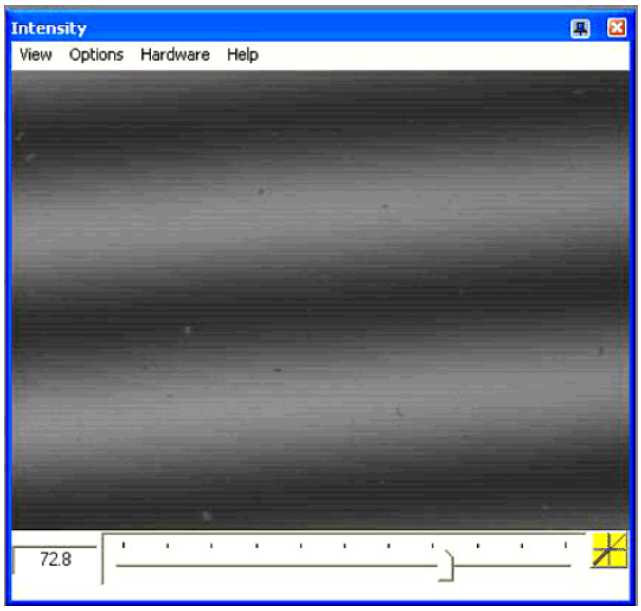

Fig 2.15 a fringes pattern observed from a WYKO NT9300 interferometric optical profiler.

During a VSI measurement with a profiler, multiple interferometric fringes patterns are recorded as the machine scans over a desired range in the vertical direction. As the sample is being scanned, the reference mirror and the microscope objective are being adjusted accordingly to the parameter [12]

In this study, we are using a WYKO NT 9300 interferometric optical profiler (fig 2.14) from Bruker that has a computer control and allows the measuring range of up to 10mm vertically in VSI mode [12]

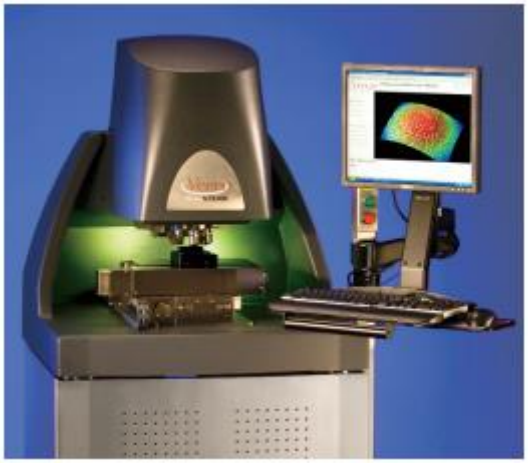

Fig 2.16 WYKO NT 9300 interferometric optical profiler

An advanced computer algorithm is used to analyze the fringes pattern observed from the Michelson interferometer within the profiler and provide height profile of the surface (fig 2.18). With this machine, 3D- surface contour map and contour profile are constructed from the algorithm. This allows the users to visualize their samples in 3-dimensions (fig.2.17)

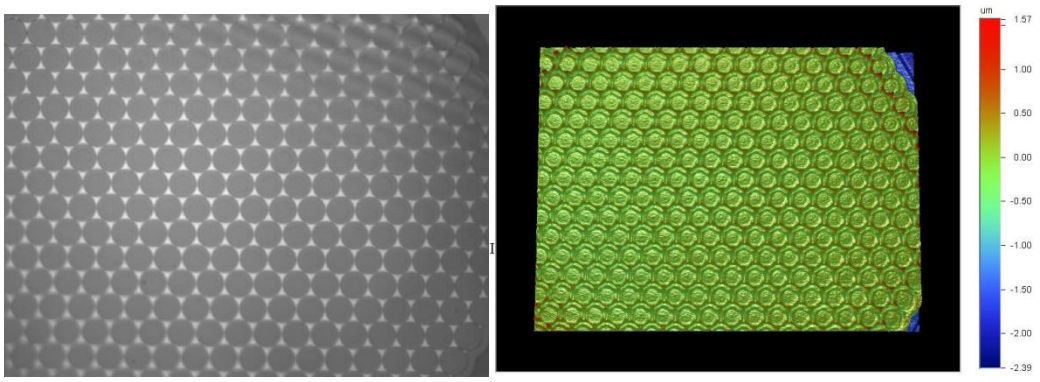

Fig 2.17 Example of images from WYKONT9300.2D (left) and 3D (right) surface map from optical profiler

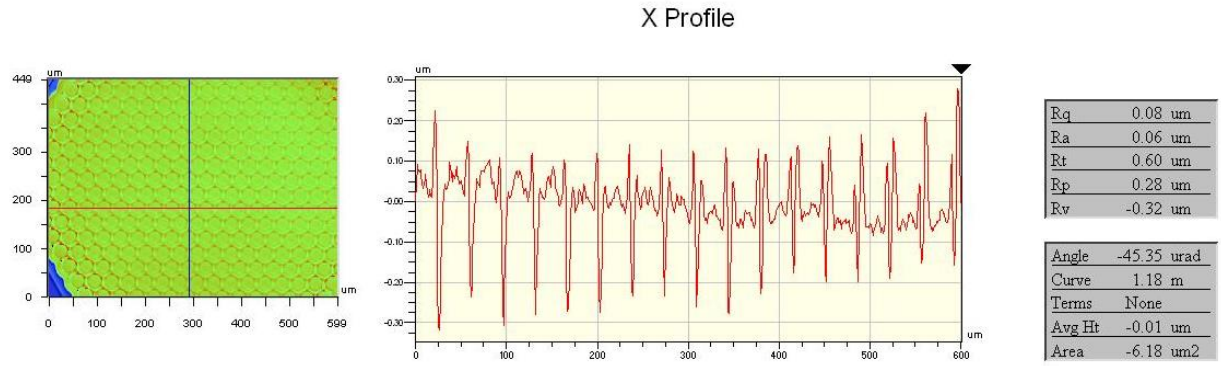

Fig.2.18 3D contour map and height profile of a MEMs (CMUTs)

In an advanced optical profiling system, Phase Shifting Interferometry (PSI) is enabled in addition to VSI for applications that require higher precision. Instead of analyzing a series of interference patterns of low coherence light such as white light with known optical path difference among them, PSI utilizes monochromatic light source to obtain a phase data during the measurement. During a measurement, a piezoelectric transducer (PZT) moves the reference mirror by a small, known distance to cause a phase shift (ϕ) between the test and reference beams. The optical path difference created by motion of the reference mirror can be calculated using this relationship:

$$\phi = (2\pi/\lambda)\ (\mathrm{OPD}) \qquad \ldots(2.2)$$

For example, to introduce phase-shifting step of $\pi/2$, the reference mirror will be moved by $\lambda/4$.

The intensity of the interference pattern at many different relative phase shifts are recorded and then converted into the phase data or phase map. For instance, if A(x, y), B(x, y), C(x, y) and D(x, y) are the resulting interference light intensities corresponding to phase-shifting steps of 0, $\pi/2$, π and $3\pi/2$, the phase map data $\Phi(x,y)$ of a sample will be given by a relationship:

$$\Phi(x,y) = \frac{B(x,y)-D(x,y)}{A(x,y)-C(x,y)} \quad \ldots(2.3)$$

The local height contour, h(x,y), on the test surface is given by

$$h(x,y) = \frac{\lambda}{4\pi}\,\Phi(\mathrm{x},\mathrm{y}) \quad \ldots(2.4)$$

Generally, PSI provides higher resolution in measurement over VSI, because it does not heavily relies on locating center of fringes. The location determination of the fringe center introduces an inherent limit to precision of VSI. Although smaller features can be measured accurately with PSI, this technique has limitation and works well only on smooth test surface that has vertical variation within λ/4. If the surface roughness or vertical variation of the surface is high, VSI is more appropriate for that particular test surface.

With WYKO NT9300, both modes are available depending on the size of the feature on the specimen. The key features of VSI and PSI modes on the WYKO NT9300 are summarized in table 2.1.

Table 2.1: Comparison between VSI and PSI modes

	VSI	PSI
Light Source	White light	Monochromatic light (filtered from white light)
Measurement	Vertical scans – the objective moves through focus	Phase shift at a single focus point – the objective does not move

Analytical Method	Process fringe modulation data from the intensity signal to calculate surface height	Processes phase data from the intensity signal to calculate surface heights
Range	2mm	160nm

In summary, the optical profiler is a powerful instrument that provides a topographic surface map of a reflective test surface. Its accuracy, fast measuring speed and high-throughput capability are attractive attributes that would benefit the study of biological samples. Biological samples such as proteins and cells need to be kept in liquid media to prevent denaturation, and this prompts a challenge to image the sample through liquid media. Additionally, biological samples are non-reflective and may not provide enough reflection to construct interferogram. According to these problems, we developed a technique called Live-Cell Interferometry that allows optical profiling of any biological samples. This technique is based on modification of WYKO interferometric optical profiling system for protein characterization, biopolymers characterization and cells imaging. It will be discussed in full details in Chapter 5.

2.2.2 Atomic force microscopy (AFM)

Atomic Force Microscopy was created by Gerd Binning, Steve Quate and Christoph Gerber at IBM Zurich Labolatory in 1986 after the development of scanning tunneling microscope that earned Gerd Binning and Heinrich Rohrer the Nobel Prize for Physics. One of the most important components of the AFM is its probe, which consist of a cantilever with a sharp tip at its free end. The probe plays a great role and is in contact with the test surface during

a scan. Typically, cantilevers of AFM probes are made of silicon or silicon nitride and are reflective to deflect laser beam. When the tip is brought close to a surface, forces between the tip and the sample lead to a deflection off the cantilever. The deflection of the cantilever is, hence, interpreted to construct a profile image of that particular specimen surface. A topographic surface map can also be constructed from the deflection data collected from the machine. Other than topographic information, AFM also quantifies the force between the tip and the test surface and leads to many elasticity measurements such as young modulus on a miniature sample.

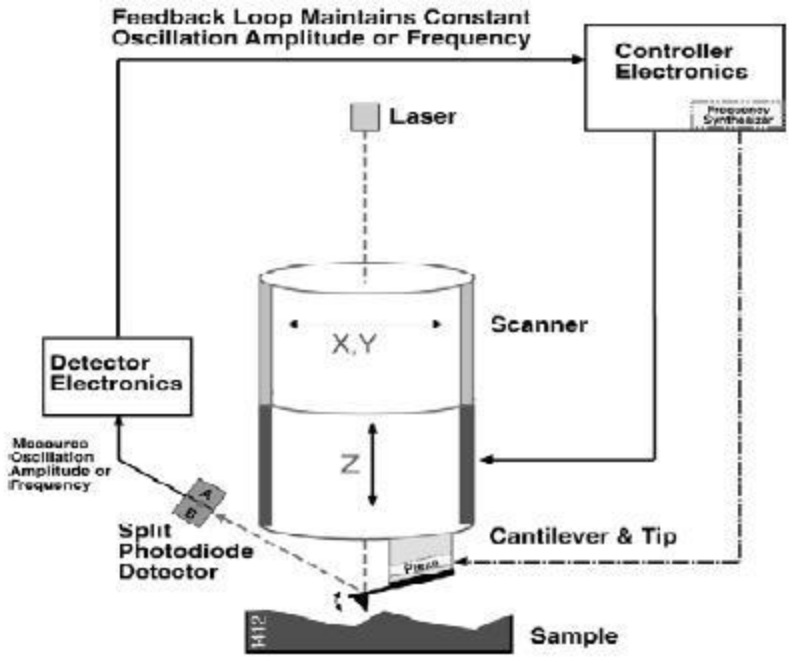

Fig 2.19 schematic of AFM operation [13]

AFM is a very high-resolution scanning probe microscopy comprised of four main units: stage and stage control; optical head; tip and tip holder; software. When a surface analysis is performed with an AFM, a sample is placed on a stage equipped with motors that control the

direction of the scan along the test surface in x- and y-direction. Usually a stage has slots that fit silicon wafers, glass slides or vacuum suctions to keep the samples firmly in place. In AFM optical head, a laser source is aligned to provide an incident beam that is deflected off an AFM tip. Within this unit, a photodiode is used to collect the intensity of the beam which will be turned into a deflection data. The position of the laser beam has to be adjusted to give maximum intensity on photodiode after deflected of the cantilever. Furthermore, the beam should also directly hit the center of the photodiode as shown in fig 2.20.

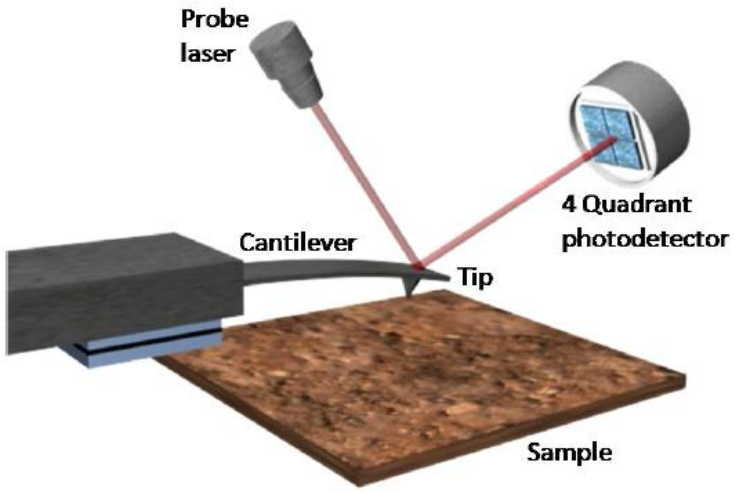

Fig 2.20 Overview of the deflection of a laser beam to photodetector in AFM measurement. This deflection data leads to phase and height analysis [14]

As mentioned earlier, AFM probes are the most important piece of the technique because they interact directly with the specimen surface. The AFM probes are usually placed on a probe holder with the tip pointing away from the holder. The holder is then connected to the optical head. At this point, the tip is facing towards the stage and ready for measurement. All the holders have a glass window, allowing the user to visualize the top of the sample to help with the

alignment. Probe holders are varied in designs depending on the manufacturers. For imaging in water, a special probe holder is required to prevent water in the system.

After the laser beam is deflected off the probe and reaches the photodiode, the intensity on a quadrant photodetector is recorded and analyzed by the AFM software. After analysis, a topographic surface map of the test surface is constructed from the deflection data. Example of AFM images and topographic surface map of CMUTs are shown in fig 2.21.

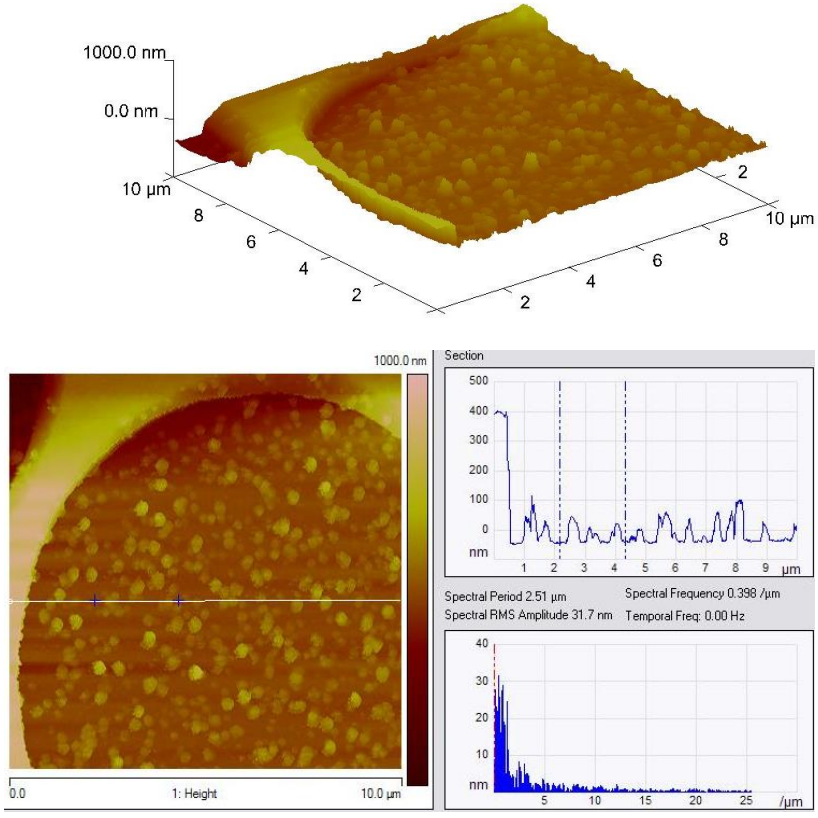

Fig 2.21 AFM images of a MEMS device with height profile

Potentials of AFM as a characterization tool have been improved over the past decades with many different modes. The primary modes of AFM operation are: contact, non-contact and dynamic mode. These modes are suitable to operate for different probe-surface separation range

(fig 2.22). In contact mode, the tip is almost at the contact with the surface, and the overall force is repulsive. The force between the tip and the surface is kept constant during scanning by maintaining a constant deflection, and hence the force is sensed directly by the deflection induced on the cantilever. In dynamic mode [15], the tip is kept at a small distance from the surface, and a small oscillation is applied to vibrate the tip near its resonant frequency. As a result, this dynamic detection method can be used to detect a small force between the tip and the sample via changes in the amplitude, phase or frequency in response to interaction to the sample. Furthermore, in normal tapping mode operation, the probe taps on the surface only at the maxima or minima point of each modulation cycle of the sinusoidal driving signal, and hence frictional forces between the probe and the sample is minimize. This technique gives a substantial improvement in imaging quality and stability of the measurement over the standard contact mode[16]. Since the contact is minimized in this mode, AFM tips and soft samples do not suffer from degradation that is sometimes observed after taking numerous scans in the contact mode.

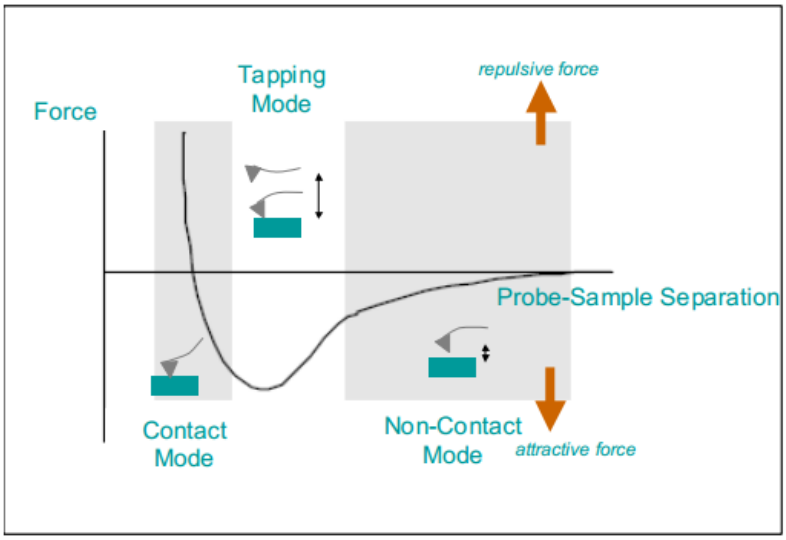

Fig 2.22 Regime of AFM modes according to probe-surface separation [17]

Non-contact mode is similar to dynamic mode in term of tip vibration. However, the separation between probe-sample is greater and the overall force is attractive Van der Waal force during the operation. Table 2.2 summarize advantage and disadvantages of these three modes

Table 2.2 Comparison of contact, dynamic and non-contact modes of AFM.

AFM mode	Advantages	Disadvantages
Contact	Fast Scanning, Suitable for rough samples, support friction and elasticity analysis	Invasive to samples: force can damage/deform soft samples
Dynamic (Tapping)	High resolution image of sample that are easily damaged or loosely attached to a surface, suitable for biological samples	Slower scan speed, more challenging to image in liquids due to vibrational damping
Non-contact	Very low force exerted on the sample, extended probe lifetime	Lower resolution, contaminant layer on surface can interfere with oscillation, need ultra-high vacuum (UHV) to have best imaging

In this study, AFM was used to characterize MEMs, polymer and biopolymer layers on silicon to understand the topology, surface roughness and surface chemistry of processes such as silanization, deposition of proteins and antibody on CMUTs for biosensing. We used two

commercial AFM machines: Bruker Catalyst and Asylum, both of which are capable to image in liquid.

2.2.3 Contact angle and surface tension

Contact angle is an angle measured on a dispensed liquid droplet as it is sitting on a solid surface (fig 2.23). At the edge of this droplet, liquid-vapour interface meets with a solid surface.

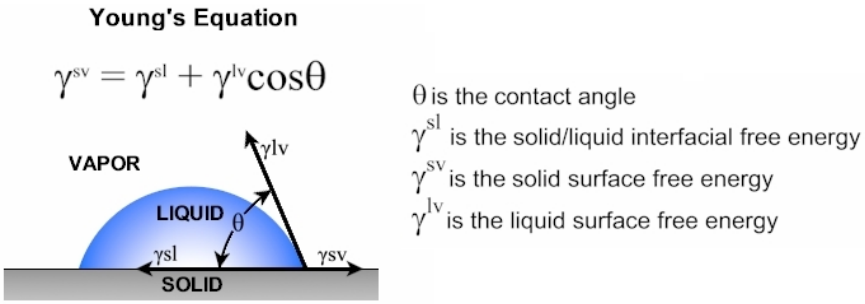

Fig 2.23 Interfacial forces and surface tension acting on a droplet on a solid surface

On a droplet, the three surface free energy: solid/liquid interfacial free energy, solid/vapor surface energy and liquid/vapor surface energy are in equilibrium as shown in equation (2.5).

$$0 = \gamma_{SG} - \gamma_{SL} - \gamma_{LG}\cos\theta_C \qquad \ldots(2.5)$$

Contact angle between a surface and a droplet is a unique property between a specific liquid and solid pair. It suggests the wettability of the liquid on a solid substrate, which depends on the surface chemistry between them. For example, a water droplet on a hydrophobic substrate such as Teflon will appear round to minimize the contact with the unfavorable surface. This can be explained in term of adhesive and cohesive forces within the liquid droplet. The adhesive

force or solid/liquid surface energy between the solid surface and liquid is causing a liquid drop to spread, while the cohesive force between liquid molecules is causing the droplet to ball up. In this case, because the interaction or adhesive force between Teflon and water is weak, the cohesive force dominates and causes the liquid to form a nearly spherical droplet.

On the other hand, if the interaction between the solid surface and liquid is strong, adhesive force will dominate, and the droplet will spread out over the solid surface (e.g., water droplet on a hydrophilic surface).

Contact angle measurement was performed by analyzing a snap shot of a water droplet dispensed on a solid surface (fig 2.24). Once the picture was shown on the screen, the machine allowed manual fitting on the droplet picture to estimate the contact angle.

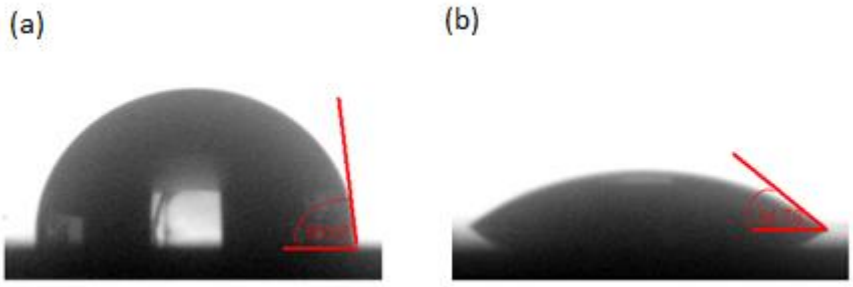

Fig 2.24 An example of droplet snapshots taken in a contact angle measurement. Different coating change wettibility of the silicon surface measured by contact angle of water droplet on (a) non-treated silicon surface substrate and silicon surface after treated with (b) trifluoropropyl dimethyl chlorosilane. In comparition

Every time when a surface modification is performed, contact angle is a great technique to estimate whether the surface becomes more hydrophilic or hydrophobic by using a water droplet. For example, hydrophilic and hydrophobic surface are illustrated in fig 2.24. The surface that cause larger contact angle(labeled in red) is more hydrophobic than the one with smaller angle.

Reference

1. **D. Nawarathna, R.C., E. Nelson, H. Kumar Wickramasinghe, *Targeted mRNA Profiling of Transfected Breast Cancer Gene in a Living Cell.* Analytical Biochemistry, 2011. 408(2): p. 342-344.**
2. **C. Hsueh, H.C., J. K. Gimzewski, J. Reed, T. M Abdel-Fattah, *Localized nanoscopic surface measurements of nickel-modified mica for single-molecule DNA sequence sampling.* ACS Applied Materials and Interfaces, 2010. 2(11): p. 3249-3256.**
3. **S.Eaimkhong, M.S., T. F. Harper, M.D.Cable, J. Gimzewski, *Label-Free Biodetection Using Capacitive Micromachined Ultrasonic Transducers (CMUTs) and Its Application for Cardiovascular Disease Diagnostics.* Journal of Nanomedicine and Nanotechnology, 2012. 3(5): p. 1000144.**
4. **R. Raiteri, M.G., B.Hans-Jurgen Butt, P. Skladal, *Micromechanical cantilever-based biosensors.* Sensors and Actuator B, 2001. 4010: p. 1-12.**
5. **S.Cross, Y.S.J., J. Rao, J.K. Gimzewski, *Nanomechanical analysis of cells from cancer patients.* Nature Nanotechnology, 2007. 2: p. 780.**
6. **S. Cross, Y.S.J., J.Tondre, R.Wong, J.Y. Rao, J.K. Gimzewski, *AFM-based analysis of human metastatic cancer cells.* Nanotechnology, 2008. 19: p. 384003.**
7. **S.Sharma, C.S., L.Bentolila, J.Rao, O.Dorigo, J.K.Gimzewski, *Correlative nanomechanical profiling with super resolution F-actin imaging reveals novel insights into mechanisms of cisplatin resistance in ovarian cancer cells.* Nanomedicine, 2012. 8(5): p. 757-66.**
8. **R.Craven, *Cell patterning by preferential adhesion.* Nature Reviews Neuroscience, 2005. 6: p. 585.**

9. **B. Kaehra, J.L.T., R. M. Kalinich, Y. H. Awad, B. S. Swartzentruber, D. R. Dunphy, C. Jeffrey Brinker, *Cellular complexity captured in durable silica biocomposites.* PNAS, 2012.**

10. **C.Bustamante, *Of torques, forces, and protein machines.* Protein Science, 2004. 13: p. 3061-3065.**

11. **A.Frank, *Nanometric surface metrology at the National Physical Laborator.* Metrologia, 1992. 28: p. 471-482.**

12. **Veeco.Inc *Wyko NT Series Optical Profilers*.**

13. **WikiFoundation. 2013; Available from: http://en.wikipedia.org/wiki/File:AFM_noncontactmode.jpg.**

14. **C.M.Olmos, *Micro/Nano fabrication of polymer-based device*, in *Centre Nacional de Microelectronica* 2008, Universitat Autonoma de Barcelona: Barcelona. p. 288.**

15. **R.Perez, R.G., *Dynamic atomic force microscopy methods.* Surface Sciences Reports, 2002. 47: p. 197-301.**

16. **P.K.Hansma, J.P.C., M.Radmacher, D.A. Walters, P.E. Hillner, M.Bezanilla,. M.Fritz, D.Vie, H.G. Hansma, *Tapping Mode atomica force microscopy in liquids.* Appl.Phys.Lett, 1994. 64(13): p. 1738-1740.**

17. **R.A. Wilson, H.A.B. *Introduction to Scanning Probe Microscopy (SPM)*.**

Chapter 3

Application of Resonators and Microelectromechanical Systems (MEMS) for chemical detection

In this chapter, we discuss the applications of micro-resonators and micro-transducers on chemical sensing of selected gas and volatile organic compounds. Generally, chemical sensors are categorized into four general groups: (1) Chromatography and spectrometry; (2) electrochemical sensors; (3) mass sensors; and (4) optical sensors [1]. However, in our study, we focus only on detecting mass changes from adsorption of chemicals or analytes on sensors, and hence mass sensing techniques are discussed throughout this chapter.

During chemical adsorption, adsorbed mass affects certain characteristics of resonators (e.g., resonant frequency, quality factor), and hence quantifying the change of these properties would provide estimation of chemical mass adsorbed on the resonators. To achieve high sensitivity, many systems with high resonant frequency were developed. At the same time, quality factor of these device have to be high for sensitive detections.

Nowaday, nanotechnology and nanofabrication provide many methods to fabricate sophisticated and miniature resonators. The platform and data acquisition technique have been also developed for faster and more accurate reading to accommodate these resonators and their utilities. The fabrication of a selective layer on resonators will allow resonators to interact better with the analytes for more accurate reading. All of these topics are discussed in this chapter with specific examples on volatile organic compounds and carbon dioxide detection.

3.1 Introduction to chemical detection: mass sensing

Chemical sensing continues to gain interest as we are more concern with our health and environment. There are many benefits to sense and detect chemicals in atmosphere because this information will allow us to rapidly respond to many incidents. For example, toxic gas detection would alert workers about potential threats caused by leakage in a factory, or explosive chemicals detection would prevent potential terrorist attacks at airports. Other than industrial and security applications, environmental monitoring and medical screening can benefit from chemical sensing.

Chemical sensors have been around for a long time. One classic example is, for instance, breath alcohol detector equipped by police patrols. Most of these alcohol sensors rely on electrochemistry for colour change indication after alcohol interact with the reagents [2]. This type of sensors has been made automated using LED and colour detector to analyse the results. For ultra-low concentration of chemicals, the conventional analysis heavily relies on optical instrument and spectroscopy such as IR spectrometer, NMR, which are expensive and large in dimension. Once nanotechnology and nanofabrication were established, miniature devices suitable for measuring small quantity of chemicals have been invented with anticipation to replace the use of expensive and sluggish instruments. To date, the most sensitive mass sensor fabricated has the resonant frequency of 2GHz and yoctogram resolution [3]. This is the first device that has reached a resolution to weight a single atom.

Chemical mass sensing continues to gain much attention with its literature continues to grow at an increasing speed [4]. This is partly because nanofabrication techniques allow scientists and researchers to fabricate miniature and complicated devices (e.g., sub-nanometer

cantilever) at a higher cost-efficiency. This type of miniature sensors is generally known as microeleactricalmechanical systems (MEMS), which are resonators vibrating at relatively high resonant frequency than conventional ones. These are devices (e.g., quartz crystal microbalance, microcantilever) made with piezoelectric materials, which generate mechanical motion from electrical energy. New nanofabrication techniques made the development of resonators without piezoelectric material possible. These resonators rely on certain physical effect such as capacity, surface acoustic wave to cause vibration.

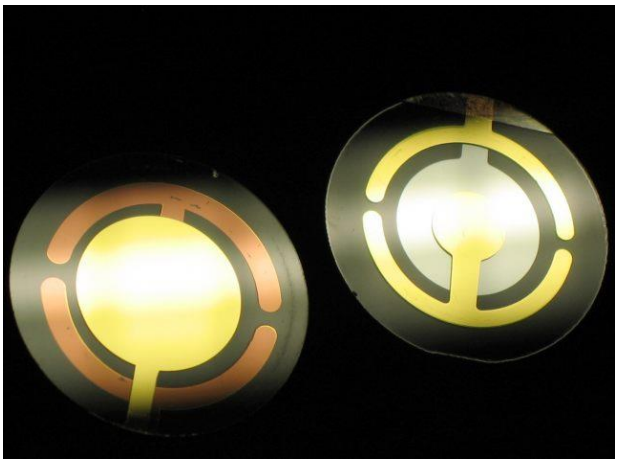

Fig 3.1 An example of quartz crystal microbalance (permission is granted under the terms of GNU Free Documentation License).

One of the first commercial mass sensors derived from quartz micro-resonator (micro tuning forks), microcantilever and quartz crystal microbalance (QCM). These mass sensors have been around for many years as analytical instruments for alcohol, aromatics, ketones, esters, alkanes, perfume [5-7], toxic gas (e.g., NO, cyanide derivatives, dimethyl methylphosphonate (DMMP)) [8-10] . During the detection process, a resonant frequency of a resonator without analyte is initially recorded before a measurement as a reference frequency. Subsequently,

analytes or chemicals are introduced to the system, and this exposure usually causes resonator to vibrate at lower resonant frequency following a relationship described below:

$$\frac{\Delta f}{f} = - \mathrm{k} \frac{\Delta m}{m} \quad , \tag{3.1}$$

Where Δf is change in resonant frequency of the resonator f, Δm is change in mass according to the analyte on the resonator with mass *m,* and k is a constant depending on the type, dimension of resonators. This relationship is illustrated graphically in fig 3.2.

From this equation, we can rearrange to estimate resolution of a resonator in term of mass sense per 1Hz of frequency shift:

$$\Delta m = -k \left(m \frac{1Hz}{f}\right), \tag{3.2}$$

which suggests that a resonator with higher resonant frequency should have higher mass sensing resolution. In other words, reading of 1Hz from a resonator with higher resonant frequency refers to smaller amount of mass that can be detected by the resonator.

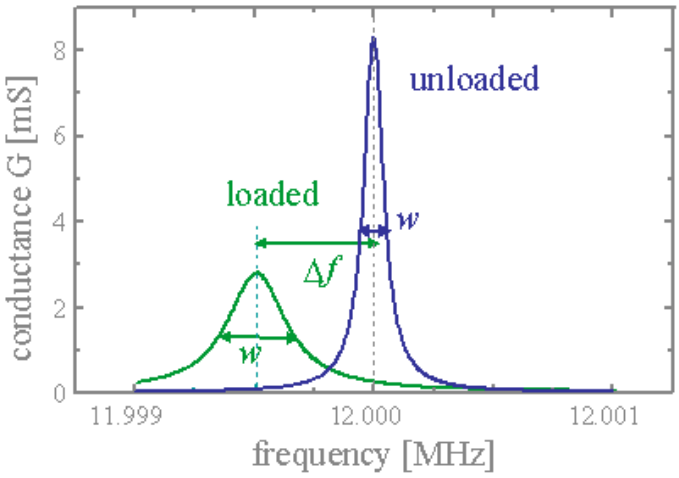

Fig 3.2 Impedance analysis is based on electrical conductance curve of a quartz crystal microbalance. The central parameters of measurement (highest maximum point) are the resonance frequency and the bandwidth, *w*. As described in equation 3.1, the resonant frequency shift to lower when mass is loaded on the device (blue to green). Mass loading may also affect quality factor of the device as well.

For accurate mass sensing, resonant frequency determination on these resonators has to be accurate and robust. The circuitry design usually starts to excite the resonators with signal from low to high frequency within the pre-set frequency bandwidth. Once the system realizes the resonant frequency for each resonator from the feedback signal, it will record that frequency and report the value at the end of a sweep. For example, tuning resonant frequency for AFM cantilever is tuned by similar method. The frequency sweep is very useful, but it can take up a long time to sweep over a large domain of frequency for an unknown frequency. Hence, frequency sweep may not be suitable for complicated system that requires results spontaneously. Many researchers have developed many circuit design and method to overcome this problem. In our laboratory, we applied “Fast Fourier Transform (FFT)” to filter out the irrelevant frequency [11]. This, hence, should reduce the amount of time for frequency read out compared to frequency sweeping. This process is shown and summarized in fig 3.3.

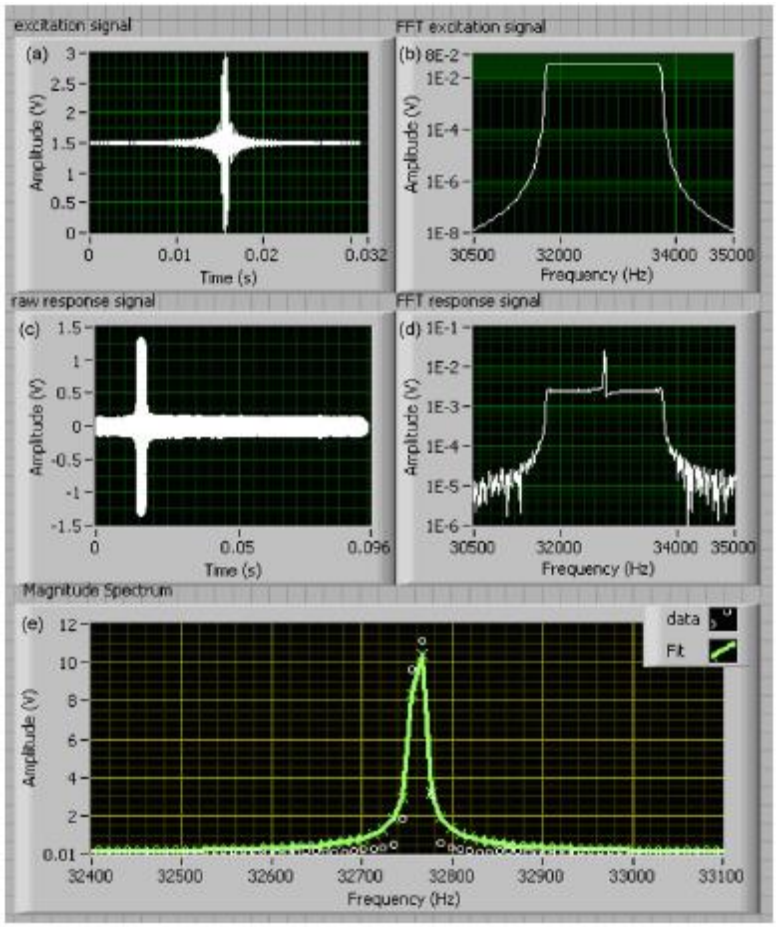

Fig 3.3 Pulses and responses before and after signal processing. (a) a wave package of excitation signals with frequency ranging within the excitation domain specified by user (b) FFT of the excitation signal (c) raw magnitude response from a single resonator (d) FTT of the magnitude response (e) Lorentzian fitting (opened circle) of the FFT magnitude response (green) [11]

For sensing to be effective, the adsorption of chemicals or analytes at the surface of resonators must be maximized. Since most of the resonators are made of quartz or silicon, they may not interact well with many analyte and chemicals in the gas phase. A typical process to increase adsorption isotherm is to deposit or coat a thin layer of polymer or materials that interact selectively with the analyte. Once the analyte molecules interact and adsorb on this selective layer, they accumulate on the resonators and are "weighted" by the sensors for mass reading. During a measurement, adsorption of analytes can be categorized into two types: chemisorption

and physisorpsion. Chemisorption usually refers to adsorption occurring through chemical reaction to create new bonds between adsorbate and surface. For instance, carbon dioxide detection using N,N'-bis(2hydrixyethyl)ethylenediamine, tetraethylenepentamine and poly(ethyleneimine) relies on chemical interaction between CO_2 and amino groups on these polymer [12].

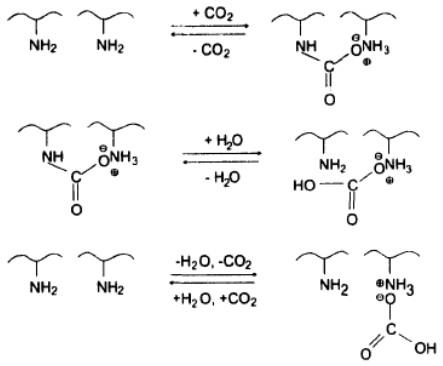

Fig 3.4 possible interaction mechanism between carbon dioxide molecules, water and the amino groups for carbon dioxide sensing[12]

Physisorption describes adsorption occurring through physical interaction depending on shape, size and intermolecular forces of molecules. Materials for physisorption in mass sensing are usually porous materials such as zeolite [13-16], metal organic framework (MOF) [17-20] because they have the ability to entrap the adsorbates. Although physisorption is weaker than chemisorption, but it has an advantage when desorption of the adsorbates is required.

In gas and VOC detection, it is important to distinguish the signal in response to the analyte from the noise background. Gas handling system is one option to help identify the signal. It is used to inject known concentration of analytes at a specific time interval. When analyte is introduced into the test chamber, resonant frequency continues to decrease until saturation in adsorption is reached. This limit could be due to maximum coverage on the sensor's surface.

After the analyte is removed in desorption cycles, the resonant frequency of mass sensors will continue to rise back to the original value. This analysis of resonant frequency in time-domain is a standard for gas sensing. To distinguish the signal from analyte, a background reading is established by flowing carrier gas onto the sensor. This step will also help remove any adsorbed gas from previous experiment and can be done by purging light gas such as nitrogen or clean air to remove any remaining adsorbates in the selective layer. This step is also known as "desorption" step. After desorption is completed, the analyte is introduced into the chamber by a carrier gas and this step is known as "adsorption" step; Adsorption of analytes causes the resonant frequency to drop as the selective layer becomes heavier. After the adsorption is completed, the system will end the cycle with desorption step again to clean and remove all the adsorbates. Some analytes such as helium gas exceptionally cause sensors an increase in the resonant frequency during adsorption cycle instead. This is because helium gas is lighter than most gas, and hence adsorption of helium will result to reduce the weight of the selective layer on the sensor.

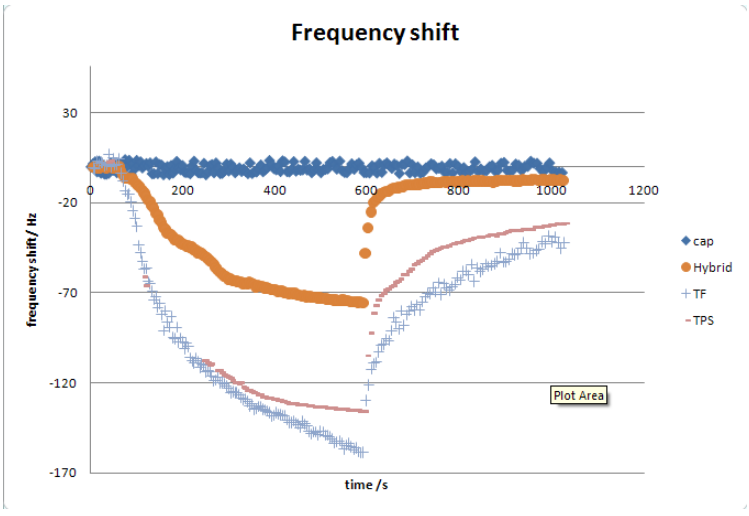

Fig 3.5 an example of normalized signal from frequency reading in time domain. A capsulated tuning fork was not exposed to an analyte and hence there was not any shift in the resonant frequency. When acetic acid was introduced, frequency drop was clearly observed until acetic acid was removed.

Desorption occurred, and frequency gradually reached the original value as acetic acid was being removed during desorption. The pattern of frequency drop on each device is different because they were coated with different polymers: tetrafluorosilane (TF), Trimethoxypropylsilane (TPS), TF/TPS 1:1 mix (hybrid), and hence they interacted with the same analyte differently.

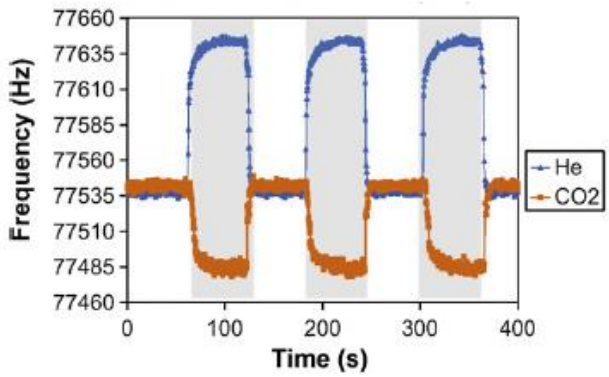

Fig 3.6 responses of a microcantilever to CO_2 and He gas during adsorption (shaded grey) and desorption (white background) cycles. Adsorption of CO_2 caused resonant frequency drops while He caused resonant frequency to rise.[11]

By analysing periodic signal within adsorption and desorption cycles, the characteristics such as rate of frequency shift and magnitude of frequency shift can be viewed and determined correctly. After resonant frequency shift was determined, these data were used to determine the mass of the analyte or to estimate the gas concentration.

3.2 Gas handling systems

As a part of gas detection system, gas handling system is important to control the concentration of the analyte into the test chamber. A precise and accurate flow control will help to create a recognizable pattern over time (see fig 3.6). This pattern of adsorption curve contains information such as rate, periodicity and magnitude of the frequency shift, which are key elements for measurement. For a VOC test, organic solvent vapors were introduced to the test chamber using lab air and a glass headspace sampler (fig 3.8) connected to two Aalborg mass flow controllers (MFC). In the system, one MFC controls the flow of the air passing through the

headspace sampler while the other MFC will adjust the total flow rate of gas entering the test chamber to the pre-set value. In this study, all the resonator responses and signals were monitored under room temperature with 1000 ml/min total flow rate.

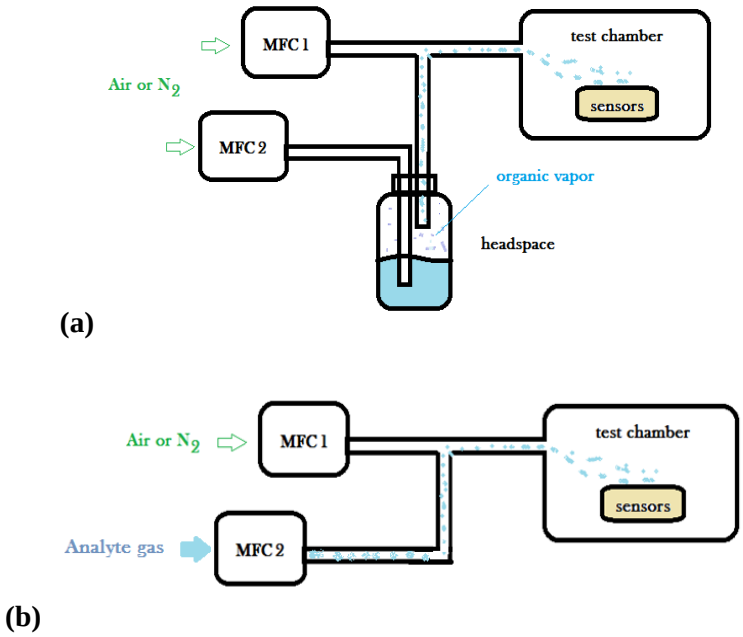

Fig 3.7 schematic of gas handling system for (a) volatile organic compound (b) gas detection

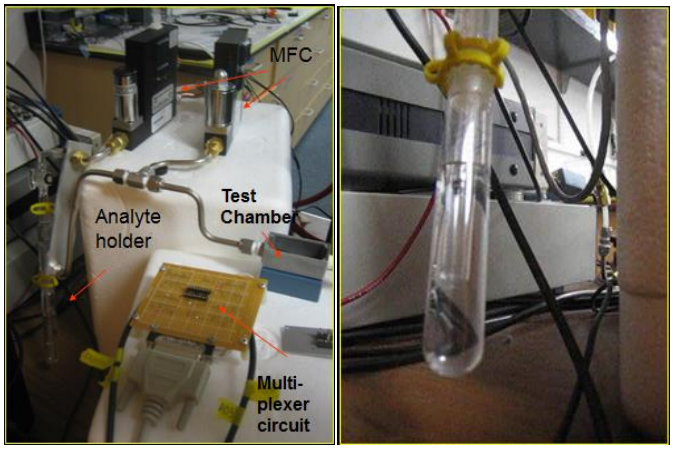

Fig 3.8 Components of the gas handling system**.** Left: Components of the gas handling system. Right: analyte holder or headspace for volatile organic compound detection.

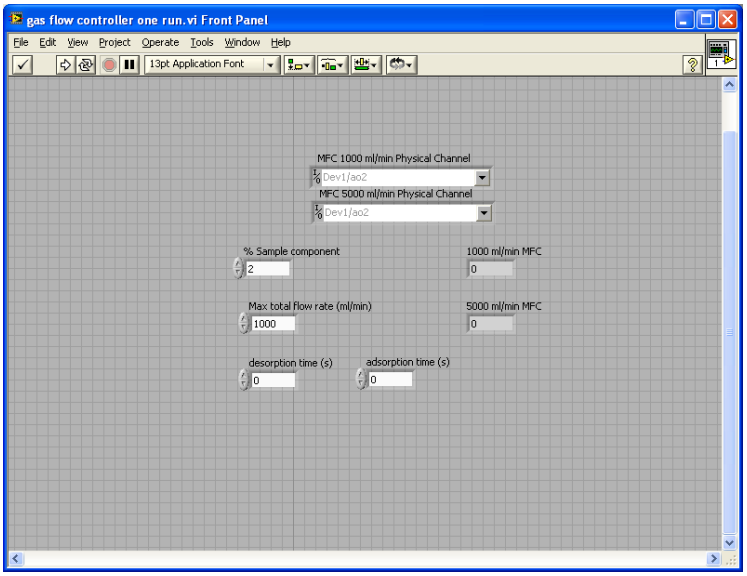

Fig 3.9 LabView user interface controller for the gas handling system

The gas handling system is computerized and controlled by a LabView VI program (fig 3.9). On the user interface, the user can select the % component of the gas mixture. After the selection, the algorithm will compute the flow rate that each MFC will operate at. For example, for 5% of an analyte in 1000ml/min flow rate, the first MFC will flow air at 50ml/min into the headspace to carry the saturated vapour of an analyte (usually organic solvent) above the liquid within the headspace into the test chamber. The second MFC will flow air at 950ml/min to mix with the flow from the first MFC just before the analyte reaches the test chamber to adjust the total flow rate to the pre-set value. For high accuracy, operating range of each MFC should be close to the actual flow rate used. In our system, the MFC connected to the headspace has the operating range from 0-100 ml/min, and the other MFC has the operating range from 0-1000 ml/min.

To perform gas sensing, the headspace or the analyte holder is removed. The MFC that is originally connected to the head space is switched to connect directly to the test chamber. Since this MFC is used to control the amount of the analyte gas, the gas supply is switched from a carrier gas to the gas of interest (e.g., carbon dioxide, helium) to be passed directly into the test chamber as illustrated in fig 3.7b.

3.3 Devices and Platform for chemical detection

In our laboratory, we used 3 different resonators for our sensing test. They have different advantages in term of resolution, control and price. Background information of each device is given in this section.

3.3.1 micro-tuning fork

Quartz tuning forks, with nominal resonance frequencies of 32,768 Hz ±20ppm were purchased from Frequency Management International (FMI). The metal capsules were removed so that both arms of the tuning fork were exposed to the surrounding atmosphere. An example of a quartz tuning fork used in our experiments is shown in fig 1.3. Usually, they have thin metal electrodes deposited as a pattern on the surface and connected to two wire leads. In our experiment we connected them into a 16-pin chip by soldering these two exposed wires (fig 3.16).

3.3.2 Aluminium Nitride (AlN) based microcantilever

Many micro-cantilevers were made with conventional piezoelectric materials: quartz crystal, lead zirconate titanate (PZT) and Zinc Oxide (ZnO). In addition, aluminum nitride is a promising material for MEMS fabrication and has been applied to create AlN-driven silicon-based microcantilevers [21-24]. We obtained cantilevers from Hernando *et.al*. These cantilevers have silicon base thickness of 20 μm with resistivity below 0.1 Ω.cm and 1μm thick polycrystalline AlN thin film on top of the silicon (see fig 3.10).

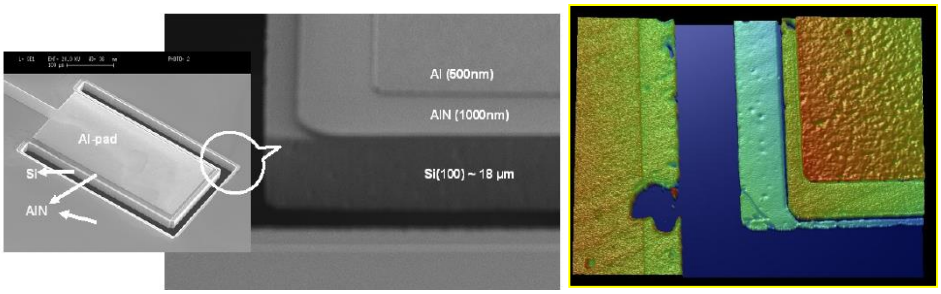

Fig 3.10 AlN based microcantilever used in mass sensing experiment [25]

This piezoelectric film was synthesized reactively from an aluminium target in a pure nitrogen atmosphere in an Ardenne sputter-deposition system. The top electrode consisted of a 500nm Al layer. The cantilever (top electrode) had a nominal length and width of 640 and 200 µm,respectively [25]. The nominal resonant frequency of these cantilevers is around 75-80 kHz.

3.3.3 Capacitive Micromachine Ultrasonic Transducers (CMUTs)

The reason why electrostatic or capacitive transducers have not been popular is the high electric fields that need to be maintained to achieve acceptable efficiencies. Recent advances in micro-fabrication technology have made it possible to build capacitive ultrasound transducers which compete well with piezoelectric transducers. There have been demonstrations of capacitive transducers in air dating back to the 1950s.

A capacitive micromachined ultrasonic transducer (CMUT), created by complementary metal–oxide–semiconductor (CMOS) fabrication technology, was introduced in 1993 by M. Haller and B. T. Khuri-Yakub [26]. Advanced integrated circuit (IC) fabrication processes enable realization of the submicron gaps between the electrodes that make it possible to achieve high electric fields with low applied voltage. These processes also provide a precise control on device dimensions in the vertical and lateral directions. The wide bandwidth and the potential for integration with electronic circuits are other advantages associated with CMUTs. Since the first

demonstration of CMUTs in the early 1990s, extensive research has been conducted on fabrication and modeling for this new transducer technology [26-30].

A CMUT resonator (fig 3.11) is operated by applying a time varying AC potential between the top and bottom electrodes to induce a resonant vibration of the membrane caused by the electrostatic charge attraction. An insulating layer is included to prevent the two electrodes from shorting in case of contact. A single transducer device (fig 3.12 right) comprises of many small capacitor cells (fig 3.11) connected in parallel and can be tailored into many geometries.

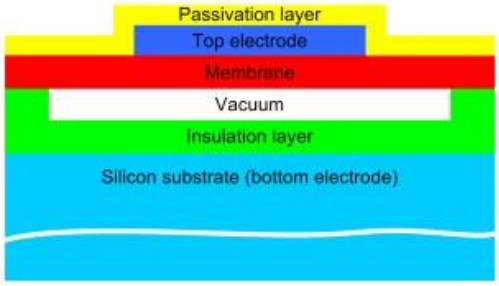

Fig 3.11. Basic CMUT structure (cell).

In the past couple years, advanced CMUTs have been fabricated with the goal to achieve higher sensitivity and enhance signal-to-noise ratio. In 2009, Khuri-Yakub *et al.* fabricated CMUTs device comprised of approximately 1000 resonator cells that are electrically connected in parallel (see in fig 3.12)

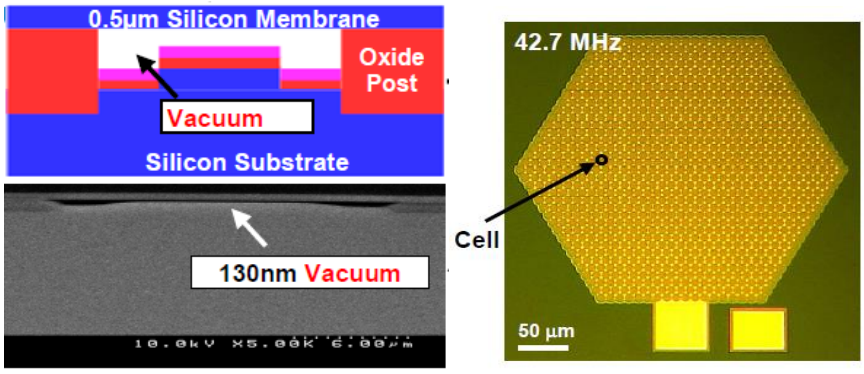

Fig 3.12 Nanofabricated CMUT cell (left) and CMUTs array (right) [31].

The optimal geometrical design for the elementary device was shown to be hexagonal having a dimension of 200-300 micrometer on each side. Each hexagon contains 1000 resonator cells, and the device can be driven with resonant frequency of 42.7MHz – compared with 17.5 MHz in earlier designs. This CMUT model achieved a phase noise of -105 dBc/Hz and -148 dBc/Hz at offset frequency of 1 kHz and 1 MHz, respectively in air [31]. This improved design also introduces improvement in sensitivity and many properties of CMUT which are summarized in table 3.1

Table 3.1 Summary of CMUTs performance

	17.5-MHz Oscillator	**42.7-MHz Oscillator**
CMUT Bias (V)	41	66
R_x (Ω)	50.2	73.7
Q	127	160
Power (mW)	6	16
Output Power (dBm)	4.6	-15.7
Allan Deviation	2.8×10^{-8}	4.7×10^{-9}
Mass Sensitivity (g/Hz)	27×10^{-18}	4.8×10^{-18}
Mass Resolution (ag)	13.3	0.96
Mass Resolution per Unit Area (ag/μm^2)	0.067	0.011

Since the silicon technology and fabrication techniques has been advanced in the past two decades, MEMs-based procedures such as CMUTs are gaining more significance and start to replace the use of piezoelectric materials.

CMUTs as chemical sensors

The idea of using transducers to measure the mass change was introduced in the past decades. A commercial example of these transducers is quartz crystal microbalance (QCM). The use of CMUTs as sensing devices offers advantages over many types of other sensing devices. One advantage is because they inherently provide a multi-resonator configuration, which results

in low motional impedance and a low false alarm rate. However for the highest potential in the detection, the CMUTs have to be functionalized to suite with the application and the analyte. The idea of using organic polymer film deposited on MEMS for sensing was done on a silicon based cantilever by Gerber and Gimzewski [32-34]. With much higher resonant frequency, CMUTs should allow higher resolution in mass detection in comparison to many transducers. The behavior of CMUTs and can be described approximately by the following expression

$$\frac{\Delta f}{f_0} = -\frac{1}{2}\frac{\Delta m}{m} \tag{3.3}$$

Equation 3.3 explains the relationship between the change of resonant frequency of a resonator as its mass changes. For CMUTs the estimated resolution, using this equation, is shown to be 4.8×10^{-18} g/Hz. This high resolution for detection allows the use of this device in many study involving materials with small masses (e.g., nanogram, picogram).

In 2007, CMUTs were reported as chemical sensors by Gimzewski, and Khuri-Yakub [35]. The experiments showed that by functionalizing the CMUTs surface with appropriate organic polymer as the selective layer, the device were made selective to a particular analyte. For example, different functionalized-CMUTs with polymer such as polyacrylamide, polyethyleneglycol, polyvinylalcohol were shown to respond to acetone vapor differently in fig 3.13.

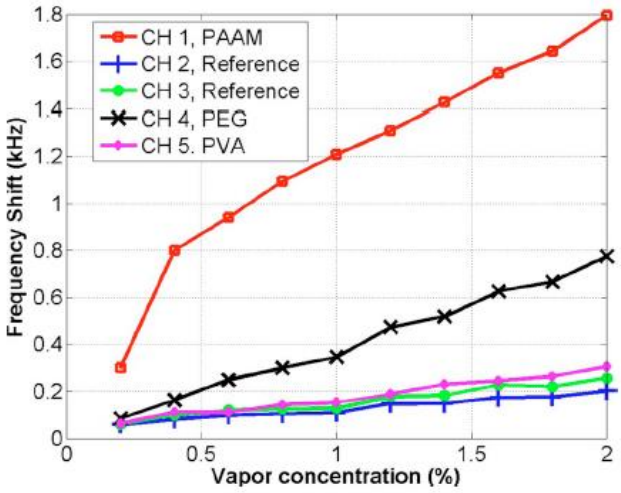

Fig 3.13 Frequency shift of several CMUTs channels coated with different polymers in the presence of acetone vapor. (PAAM = polyacrylamide , PEG = Polyethyleneglycol, PVA = polyvinylalcohol).

Functionalized CMUTs were also tested in the presence of many analytes other than acetone for sensitivity and selectivity and the results are summarized in table 3.2.

Table 3.2 Sensitivity of functionalized channels to several analytes. All values are in the unit of ppb/Hz.

	Water	Isopropanol	Acetone	Methanol
PAAM	41.6	101	3508	2150
PEG	410	1060	6420	2020
PVA	399	988	18800	5450

With an appropriate polymer with high selectivity to the desired analyte, small differences in concentration of the analyte can be clearly distinguished as shown in fig 3.14.

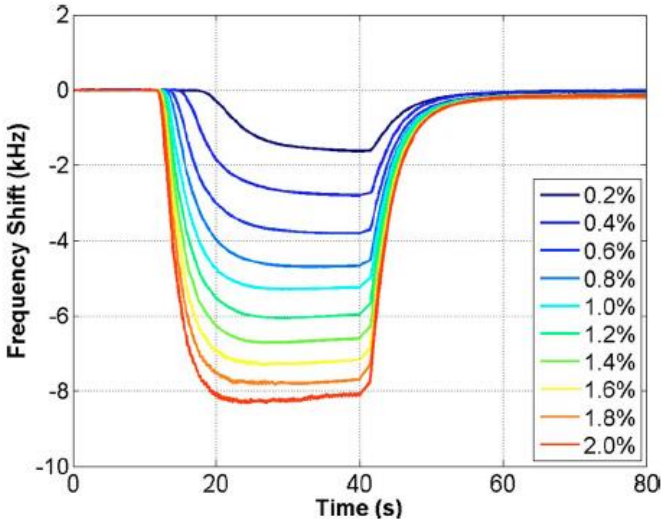

Fig 3.14 Frequency shift of PAAM coated channel due to the vapor of isopropanol. Analytical vapor starts flowing at the point of 10 s and stops at 40 s.

Based on preliminary results, CMUT sensors illustrated the potential to replace piezoelectric sensors in air phase because of its high resolution and high cost-effectiveness in production. In our laboratory, we focused on developing CMUTs for chemical and biological sensing by testing it with selected gas and VOCs of interest. The unique design and the compact size of the resonator cell (~20 µm in diameter) were a good attribute for developing a miniature device. We were able to create an array of 16 CMUTs per one chip ~2 mm x 5 mm (fig 3.15) on one chip. There is also a possibility to connect multiple chips to create larger array of devices for E-nose application but it will require the development of the circuitry and the software.

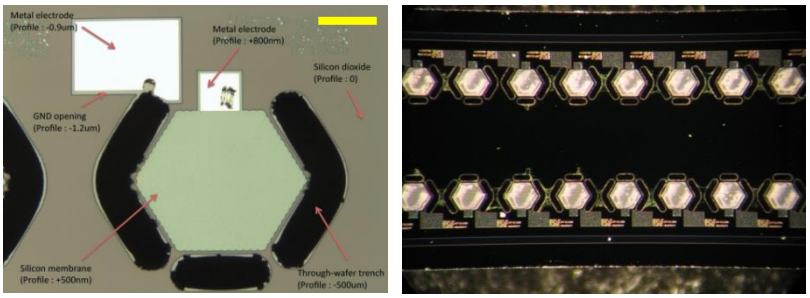

(a) (b)

Fig 3.15 (a) Overview of a CMUTs device (b) array of 16 CMUT devices on a single chip

3.4 Data Acquisition

For tuning fork and AlN micro-cantilever, a data acquisition system was built in our laboratory using a National Instrument data acquisition unit connected to the Labview program control (Fig 3.3). The Labview program generates a pulse to excite the resonator and performs a fitting algorithm on the response signal using initial input parameters for frequency and frequency bandwidth. After the fitting algorithm is performed, the program will determine the resonant frequency by choosing the central peak value on a fitted Lorentztian curve (see fig 3.3 e). The resonant frequency is monitored and recorded in a time domain until user terminates the program. Automation of measurements is desired and possible by synchronizing this program to the gas handling system program.

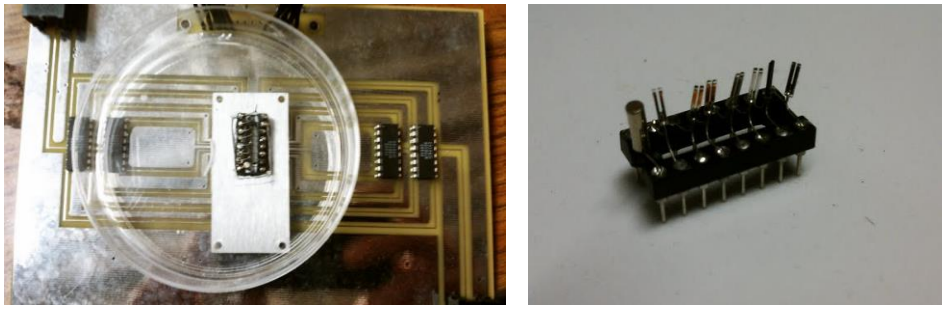

Fig 3.16 PCB circuit (left) for chemical detections with slots for a project chip with tuning fork soldered in (right) to be plugged in

To connect a resonator to the circuit, micro-cantilevers and tuning forks were connected by soldering to a chip socket (fig 3.16) that was plugged into a multiplexing circuit. This multiplexing circuit allows the data acquisition program to monitor the resonant frequency of 8 resonators simultaneously in less than 1 second for each frequency read out.

Since CMUTs resonate at much higher resonant frequency than the tuning forks (32 kHz) and the AlN microcatilever (75-80 kHz), the Labview NI data acquisition system is not applicable for CMUTs. Instead, a special data acquisition system was developed by Matrix Sensors Inc. for resonant frequency read out of CMUTs which ranges from 30-60 MHz. The system has a phase lock loop (PLL) circuit that sweeps over that frequency range. This unit has a circuit that controls the surface temperature of CMUTs. Additionally, it also includes circuits to measure temperature and humidity, which are important to verify the data from CMUTs detection. The CMUTs temperature control is a very important feature because temperature affects the performance of CMUTs greatly. Few Celsius changes in temperature can cause resonant frequency to change significantly and create high noise level. With this circuit, the surface temperature of CMUTs is controlled and can be monitored in order to help validify the data in each measurement. Furthermore, a humidity sensor is also placed inside the test chamber for parallel reading for measurements that might be affected by humidity (e.g., CO_2 detection).

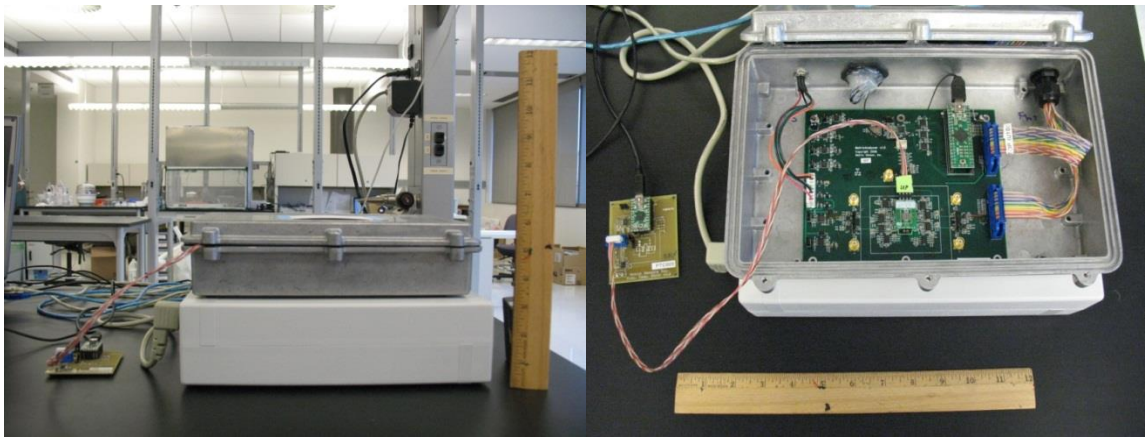

Fig 3.17 Data Acquisition Unit for CMUTs operation. The picture on the right shows a single CMUT chip plugged onto the circuit board inside the aluminium test chamber.

Since CMUTs chip is wire-bonded on a socket chip that can be plugged into the Matrix data acquisition unit, this allows plug-and-play measurement which is useful and practical for

measurements. For detections that require multiple functionalization steps such as biosensors (see chapter 4) on a single chip, this scheme provides convenience to the users to manipulate chemicals on the chip. The users can also run many different tests on the same platform by switching to different coated chips. The chip has large enough surface for functionalization on the surface. In an attempt to minimize noise and retain high Q-factor of the response, the exposed wires after wirebonding are protected and sealed (fig. 3.18) with an epoxy (e.g., SU8). This provides stability of the chips and allows the chips to be processed with a wider range of surface modification techniques such as oxygen plasma, ethanol cleaning.

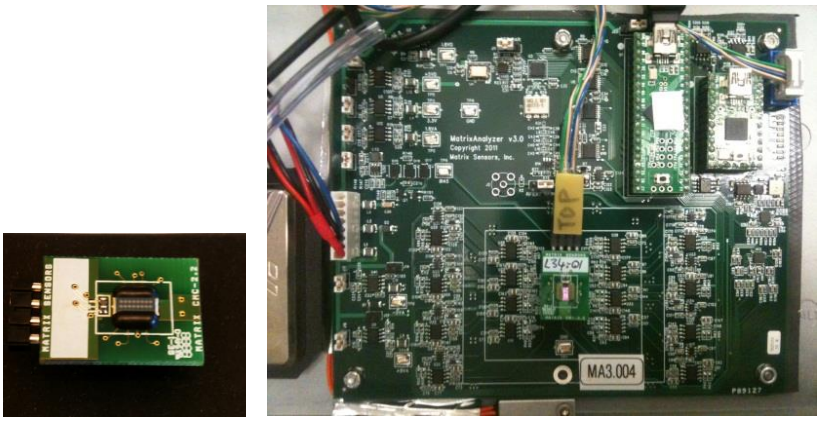

Fig 3.18 CMUT chip (left) plugged in data acquisition circuit (right)

3.5 volatile organic compounds (VOC) detection

While there has been a lot of success in sensor development for greenhouse gases (CO_2, CH_4, N_2O, NO, and CO), technology for detection of VOCs remains a weak point. Hence, the needs and requirements for environment monitoring, medical applications, homeland security

and agriculture have increased demand for portable volatile organic compounds (VOCs) sensors [36-38]. In the last decade, sensing devices have been developed to be miniature for stand-alone operation. There are two main approaches for VOC sensors development. First, the sensors are coated with a polymer or specific materials that have both high sensitivity and selectivity to the substances or analytes. The challenge for this approach is finding a suitable material that can provide a clear response to the specific analyte with small noise level (responses from other background chemicals). Since this approach can be challenging to find a sufficient material, combination of multi-channel signals from sensors with different polymer coated would provide a signature or specific data set for each particular analyte. For example, a CMUT chip contains 16 CMUT sensors that can be used to detect an analyte simultaneously. By coating these sensors with different polymers or materials, the signal from each sensor will be different. Hence the combination of these specific signals is specific to the analyte. We refer to this technique as "electronic nose".

In our laboratory, we performed VOC-sensing using a combination of many materials that might be good selective materials for detecting alcohol, chloroform ($CHCl_3$), dimethyl sulfoxide (DMSO), hexane and acetonitrile (ACN). We applied these solvent into the test chamber using the headspace, and the responses of sensors with different coated materials were tested by the customized data acquisition system [11]. The resonators for this experiment were commercial tuning forks (section 3.3.1), which were inexpensive, cost-effective and easy to handle. This system is hence an adequate system for VOC sensing on its own for many application. However, we are also interested in developing a sensitive VOCs sensoring system using CMUTs. Since the production of CMUTs required long lead-time and substantial development cost, the use of tuning forks with this system to screen materials for sensing

applications on CMUTs platform helped save unnecessary cost and time, and were more sensible than applying the materials directly onto CMUT sensors.

The first VOC sample tested was ethanol using tuning forks coated with a polyaniline layer. This is because polyaniline was the first successful ink made for the DMP material printer. During the measurement, MFCs were switched on and off to provide the ethanol vapour for the adsorption/desorption cycle as explained earlier. We applied different concentrations of ethanol to the device to test the sensitivity of polyaniline to ethanol in presence of water. Signals for different concentrations are distinct in fig 3.19. This implies certain level of sensitivity of polyaniline to ethanol. Since the signals were clearly distinguishable between different concentration, we assumed that this polymer or material was good for this analyte (alcohol). For other analyte, we can perform similar screening or test on a specific material before using it with the CMUT platform.

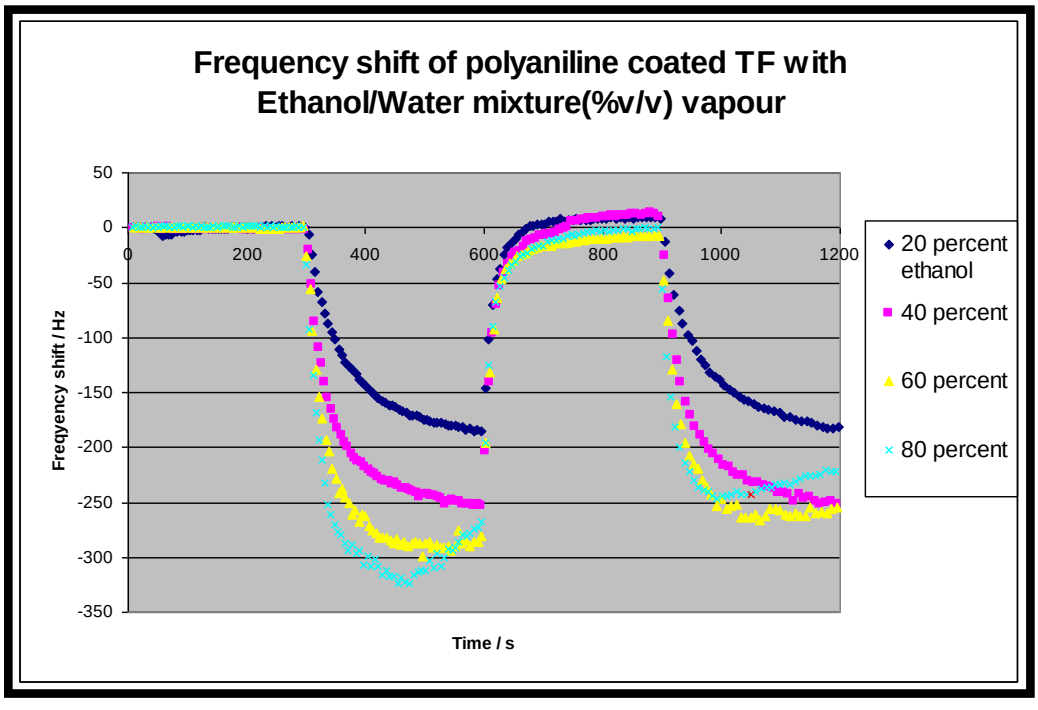

Fig 3.19 ethanol detection using polyaniline-coated tuning forks using Dimatix printer.

Sensitivity test of many polymers such as polyethylenimine (PEI), polyaniline (PAn) and polyvinyl alcohol (PVA) as a selective layer for many VOCs were performed and shown in fig 3.20. The responses of the tuning forks coated with these polymers to CHCl3, isopropyl alcohol (IPA), simethyl sulfoxide (DMSO), hexane, acetonitrile and toluene were shown in fig 3.20.

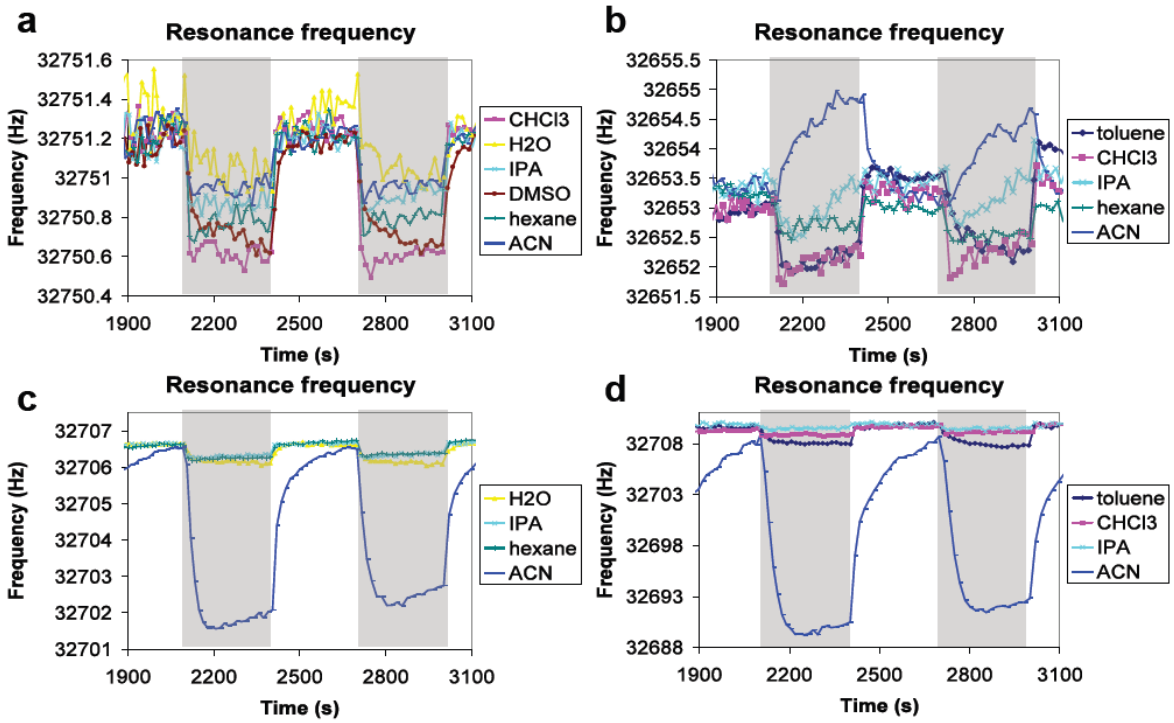

Fig 3.20 chemical responses from tuning fork coated with (b) polyethylenimine (PEI) , (c) polyaniline (PAn) and (d) polyvinyl alcohol (PVA) compared to bare tuning fork in (a) [11]

In fig 3.20a the VOCs were passed into a chamber with uncoated tuning forks. The data from the same tuning fork for different VOCs was overlaid. As we can see, bare tuning forks provide different response to the different VOCs. However, the signals were not clearly resolved, and this would be a problem to assure the existence of a particular VOC without a selective layer on tuning forks. However, when the same VOCs were introduced to the coated tuning forks with different polymer layer coated as described in fig 3.20 b-c, the responses became distinguishable.

In this experiment, acetonitrile was shown to interact with polyethulenimine, polyaniline and polyvinyl alcohol very well and, hence, caused a significant resonant frequency change more than any other VOCs. This would be an expectation of the result after screening material to be used in the detection of acetonitrile. To choose selective material, we focused on exclusivity and size of the signal. This means that for acetonitrile detection, polyvinyl alcohol is a good polymer for the application because it caused a larger signal than polyethylenimine and polyaniline.

Similar material screening processes can be performed for any analyte. For many gas sensing application, synthesis of materials for VOC or gas sensing are gaining popularity as a research area. This system would provide a mean to narrow down and verify the range of materials selected for synthesis. It is recommended that the material should be tested for sensitivity before production at a large scale is performed.

3.6 Carbon dioxide detection

Carbon dioxide is a gas that exists in the life cycle of most living organisms, including human beings. Detection of carbon dioxide is hence related to us and is growing in demand for many fields such as environment monitoring, food and agricultural quality control. In an environmental context, carbon dioxide is a greenhouse gas that leads to global warming. Monitoring the emission of carbon dioxide is critical. Importantly, for indoor atmosphere, carbon dioxide is toxic at a level higher than 1% in air, and hence needs to be regulated accordingly.

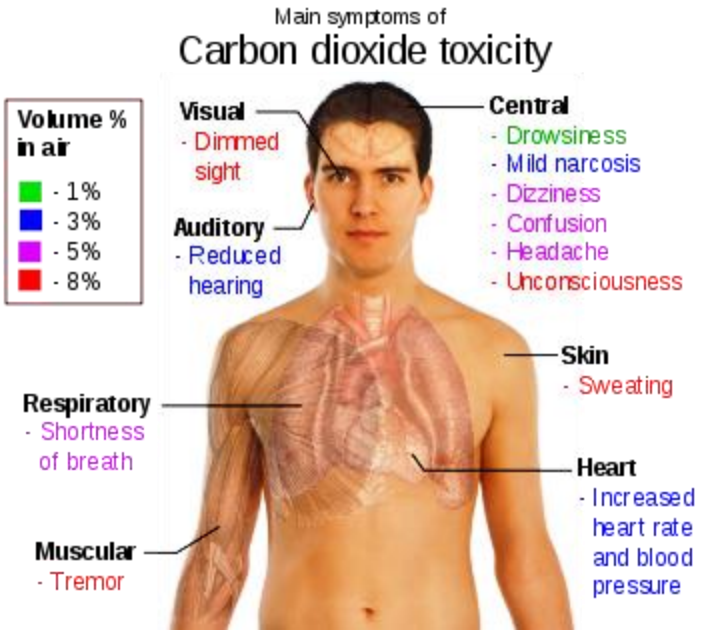

Fig 3.21 Toxicity of carbon dioxide to our body

Other demands for carbon dioxide are found in the food and agricultural industry. Carbon dioxide level is an indicator for incipient spoilage in bulk food storage. Early response and carbon dioxide regulation canl ensure high quality and maintain freshness of these products; hence sensors are being used for the process control, monitoring quality and assessing safety in this industry. Currently, carbon dioxide sensors are expensive (>$100 per unit) despite increasing demand. This could be because of a complicated mechanism of detection compared to many other gases [39]. The market potential for a reliable and inexpensive carbon dioxide sensor is significant due to its wide range of applications.

Efforts to use MEMs and resonators as carbon dioxide mass sensors have been done in the past. This requires a selective material that can capture and interact well with the gas. Amino-functionalized polymers were known among those materials that undergo chemical interaction with CO_2 gas (fig 3.4) and used as a selective layer for CO_2 detection[12, 40, 41]. In these works, the amine group of the polymer is an active group that can interact with carbon dioxide in the

presence of moisture. Other polymers without an amine group and silanes (e.g.,Teflon [42], poly(dimethylsiloxane)bis(12-hydroxystearate), fluoroalkylacrylate [43]) also has potential as a selective material. Advanced porous materials such as carbon nanotubes, polypyrole, porous silica and zeolites are also possible for CO_2 detection because CO_2 can be entrapped inside the pores within these compounds [44-49]

In 2009, Yaghi's group introduced a new group of molecules called metal organic framework (MOF), which is comprised of metal and organic ligands. By selecting the ligands and metal, the pore size of the material can be tailored[50]. This class of materials is claimed to be one of the most porous materials; and with the correct pore size, it can be tuned for specific functionality such as capturing carbon dioxide gas. In Yaghi's work, MOF-74 was shown to have high selectivity to carbon dioxide and can be used as a CO_2 capturing materials[51]

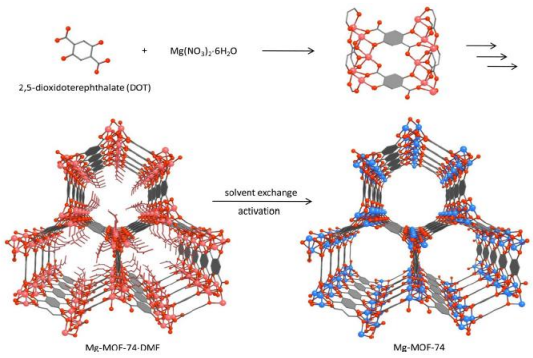

Fig 3.22 structure and synthesis of MOF-74 [51]

From our collaboration, we acquired MOF-74 and attempted to use it as our selective layer on CMUTs sensors. Early results in our development were obtained from using selected polymers as our selective layers. They have shown great selectivity and potential to assist CO_2 detection. However, the results from MOF-74 material illustrate the superiority of using an advanced material for carbon dioxide sensing.

3.6.1 Carbon dioxide detection using tuning fork and selective polymers

3-aminopropyltrimethoxysilane (AMO) was successfully used as a selective polymer for carbon dioxide detection in the past [12, 41]. We applied this polymer onto our tuning fork system to assure the validity of our system and results derived from this system for material screening by starting with this known selective material. Concentration of CO_2 was varied before entering the test chamber in a periodic fashion of alternate desorption/adsorption. A simple resonator such as the tuning fork illustrated its capability to distinguish the concentration of CO_2 shown in fig 3.23.

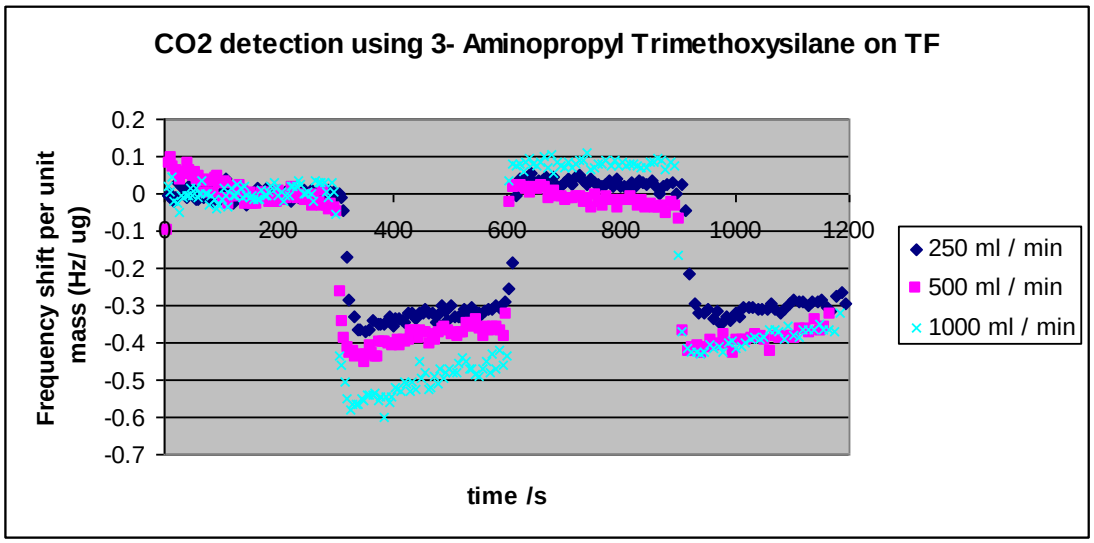

Fig 3.23 CO_2 detection on AMO coated tuning fork. The signals from different concentration are distinguished clearly by this platform.

In fig 3.23, a clear distinction of the signal curve for 250 ml/min, 500 ml/min and 1000ml/min are clearly shown. However, these signals illustrate a drifting effect that may be caused by a temperature drop during the carbon dioxide flow. If the viewing window is short

enough, this effect can be neglected by performing certain data analyses. In response to this effect, it is noted that several improvements such as data correction analysis or temperature control must be implemented to achieve more consistent data and eliminate drifting in the signal.

After a test with a known selective polymer was performed, we selected other possible polymers for CO_2 detection such as tetrafluorosilane (TF) and trimethoxypropylsilane (TPS) to coat five tuning forks. We include five different tuning forks: non-coated, amino-silane coated, TF-coated, TPS coated and 1:1 TPS/AMO coated (hybrid), for the screening test.

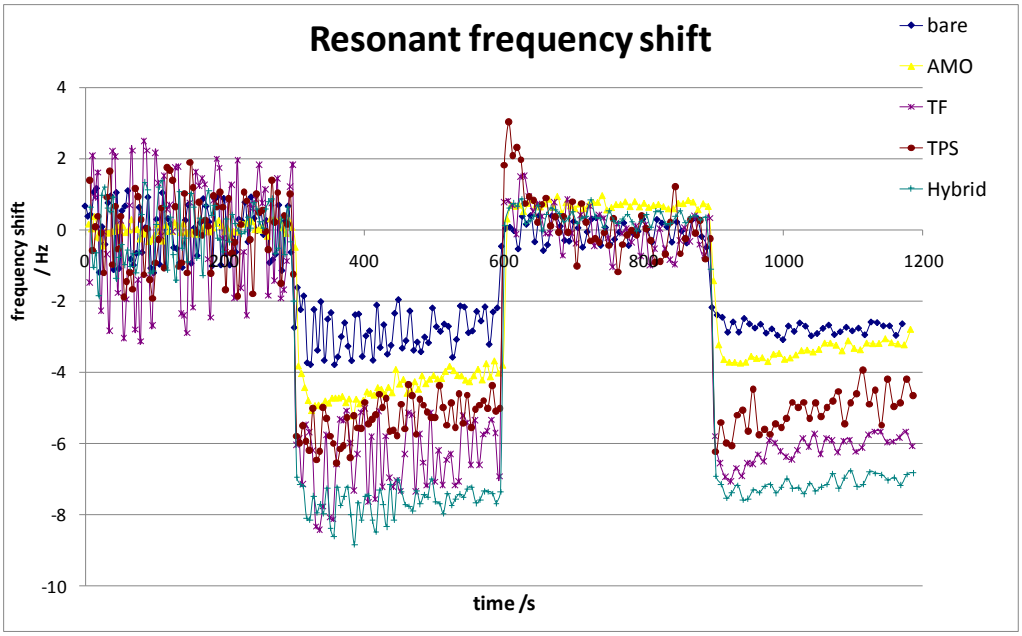

Fig. 3.24 response of tuning forks with different selective polymer coating to CO2 flow

In this test, the signals from pure CO_2 were detected by each tuning fork differently. A bare tuning fork illustrated a shift according to CO_2 and was used as a reference. Fig 3.24 shows that the mix of TPS/AMO illustrated the highest potential as a selective layer for CO_2 because of the highest drop in resonant frequency in the presence of carbon dioxide. However, in this figure, the amount of material coated was not taken into account. Therefore, we must compare the signal

per the amount of material deposited on tuning fork to be conclusive. To do that, we previously recorded the resonant frequency of each tuning fork both before and after the polymer coating. The difference between these two resonant frequencies allowed us to calculate the mass of polymer coated on each tuning fork. Hence, for a more reliable comparison, the drop in the resonant frequency from each tuning fork was then normalized with the mass of the polymer layer on the tuning fork (fig 3.25)

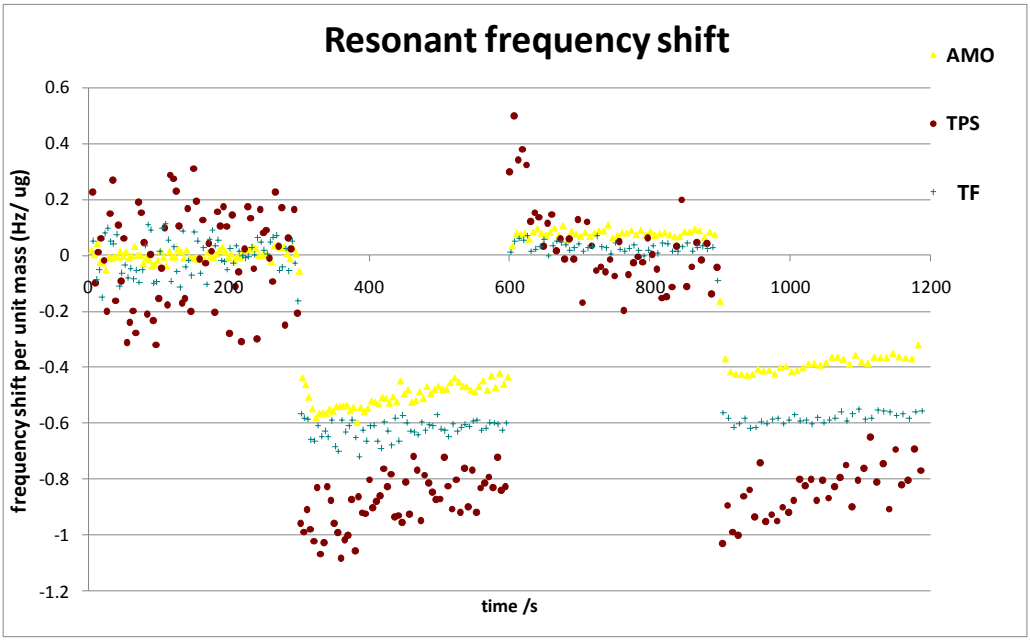

Fig 3.25 Shift in Resonant Frequency per unit mass (µg) upon CO_2 flow

The characteristic of TF in fig 3.25 is an example of a signal derived from layer that is too sensitive to use for CO_2 because it would introduce too much noise as a result, especially for low a CO_2 concentration application. After normalization, the signal/mass of each tuning fork is shown in fig 3.25. TPS is shown to induce to highest decrease in resonant frequency, but at the same time the signal from his tuning fork fluctuates much more than the one from AMO layer. In this case, it is not perfectly conclusive that TPS is a better selective layer for CO_2 than AMO because AMO can be much more reliable at a lower concentration of CO_2.Also, the mixture of AMO/TPS (hybrid) induces the frequency drop roughly half-

way between the signal by AMO and TPS which was expected. After this screening, we conclude that AMO and TPS would be a good candidate to use as a selective layer for CO2 detection which would be done on CMUTs. For the next step, the ink of AMO and TPS were made for DMP material printer so that they can be printed and deposited on CMUTs. Completing the screening is useful to save time and cost in developing an ineffective selective layer for CMUTs.

3.6.2 Carbon dioxide detection using CMUTs.

After the material screening, the AMO ink was made successfully for the DMP material printer, while the TPS ink required a larger adjustment on surface tension and viscosity to improve its jettability. Since detection of CO_2 on CMUTs was aimed towards the low concentration range, we believed that AMO may outperform TPS nevertheless according to less fluctuation of signal observed. The detection was then pursued with AMO layer deposited on CMUTs using DMP material printer.

In the experiment, we applied different concentration of CO_2 to be between 1-5%. The responses from CMUTs are shown in fig 3.26-3.27. In this case, the resonant frequency increased in the presence of CO_2. After several repetitions, the results were consistent with resonant frequency shifted up when CO_2 was introduced.

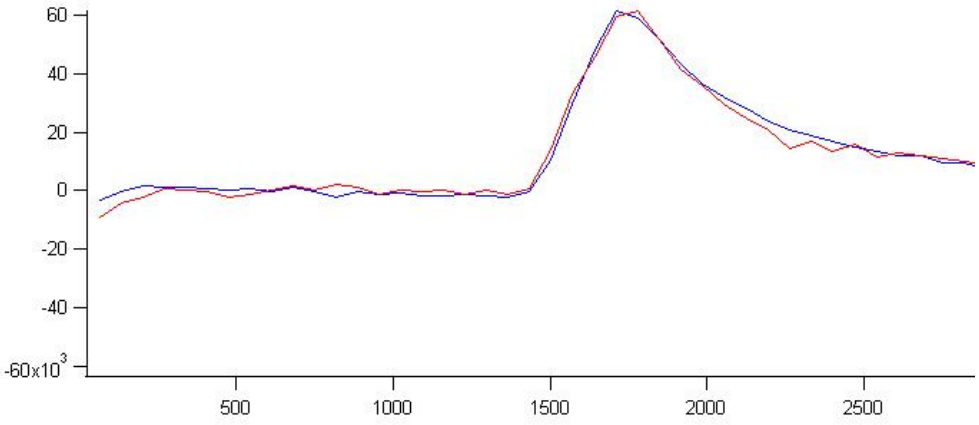

Fig 3.26 an example of response to 1.5% CO_2 from a AMO coated CMUTs.

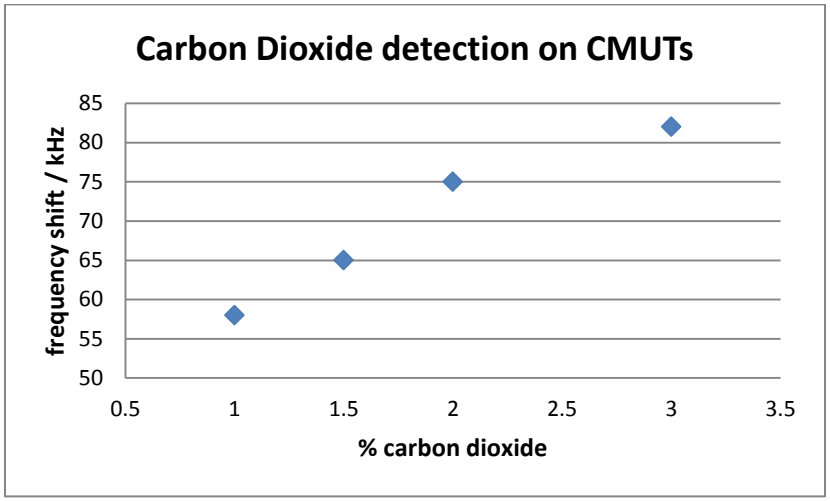

Fig 3.27 calibration curve of carbon dioxide detection on AMO coated CMUTs

This can be explained by the fact that the AMO coating became more flexible when it interacted with CO_2 through the reaction explained in fig 3.4. This flexibility allowed the CMUT membrane to vibrate at a higher frequency than before its exposure to CO_2. However, the same effect on the tuning fork was not observed. This could be because the size of the tuning forks is much larger than the thickness of the polymer so that this effect is negligible unlike in a micro-resonator such as CMUT. In this experiment, the lowest concentration that we used was 1%. We

seemed to reach the limitation of the MFC and could not provide a lower concentration of CO_2 without increasing the total flow rate from 1000ml/min. The new MFC with the lower flow rate limitation (e.g., 100ml/min) will be used in a future experiment to provide the range of CO_2 concentration below 1%.

In addition to AMO, we acquired MOF-74 through our collaboration with Dr.Yaghi. As highlighted earlier, MOF-74 was used as a CO_2 capturing material because it has the comparable pore size to the gas molecule. A critical step for MOF-74 deposition is to be able to disperse the material throughout which might be difficult for MOF-74 because it is insoluble in most solvents. We believe that the best approach for the deposition is to grow these crystals of metal organic framework directly on the sensors. However, it is a time consuming process and harsh during MOF synthesizing may damage the structure of CMUTs. In this study, we obtained preliminary results by dispersing MOF-74 using acetone as a solvent on CMUTs sensors. The concentration of MOF-74 in acetone is roughly 1mg/ml, and only 10 µl was used to cover the CMUTs chip. After acetone dried, the chip was left with a layer of MOF-74. It was then placed in the test chamber and exposed to the flow of CO_2.

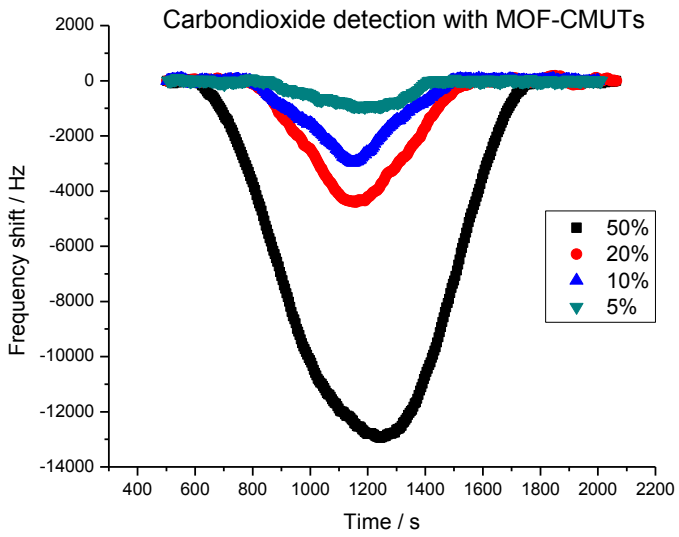

Fig 3.28 response of MOF-74 coated CMUTs to CO2 at different concentration

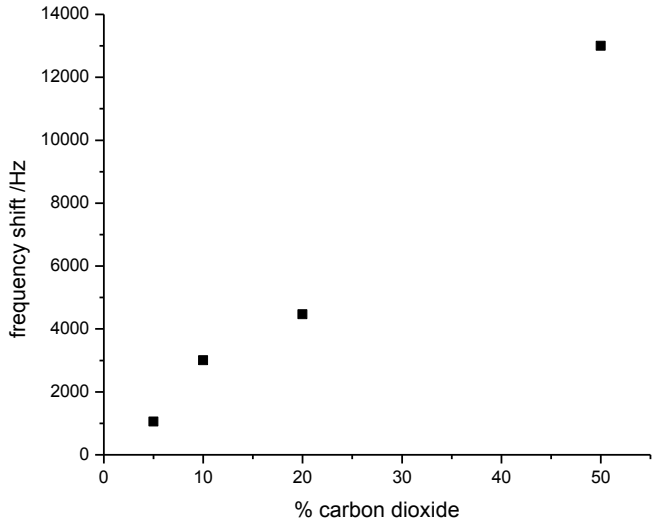

Fig 3.29 calibration curve of CMUTs for carbon dioxide detection- plot of frequency shift signal (frequency dip determined in fig 3.28) against % carbon dioxide

The CO_2 responses from MOF-74 layer on CMUTs are shown in fig 3.28. In this case, we applied the CO_2 concentration ranging from 2%-50% and collected the signal over a gas flow

cycle with 5 minutes of CO_2 desorption and adsorption alternate. The frequency drop on CMUT illustrates a good linearity in fig 3.29 and shows that MOF-74 on CMUT can be used as an alternative analytical tool for CO_2 concentration. In the future, we would like to explore in the lower range of CO_2 concentration. To be more accurate, we need to implement a more sensitive MFC that can control CO_2 gas at a lower flow rate. This is to assure that we will have an accurate control on the concentration. Also in the future, a standard CO_2 sensor will be implemented to provide a reference in parallel to the detected signal.

Since CMUTs were illustrated to detect CO_2 with AMO and MOF-74 as a coated selective layer on the device, we were interested in weather our device can be used in a real environment for a long period of time. This is an important verification if we aim for our sensors to be used in a real application for CO_2 monitoring. Hence, we designed a 4-weeks experiment to follow the CO_2 level in parallel to an optical based CO_2 sensor or NDIR, which is an industrial standard. Fig 3.30 shows the result from the first day of the experiment (top) and the last day after 4 weeks (bottom) as CO_2 level was randomly changed in a constant air pressure, constant atmosphere temperature, constant humidity and constant chip temperature condition.

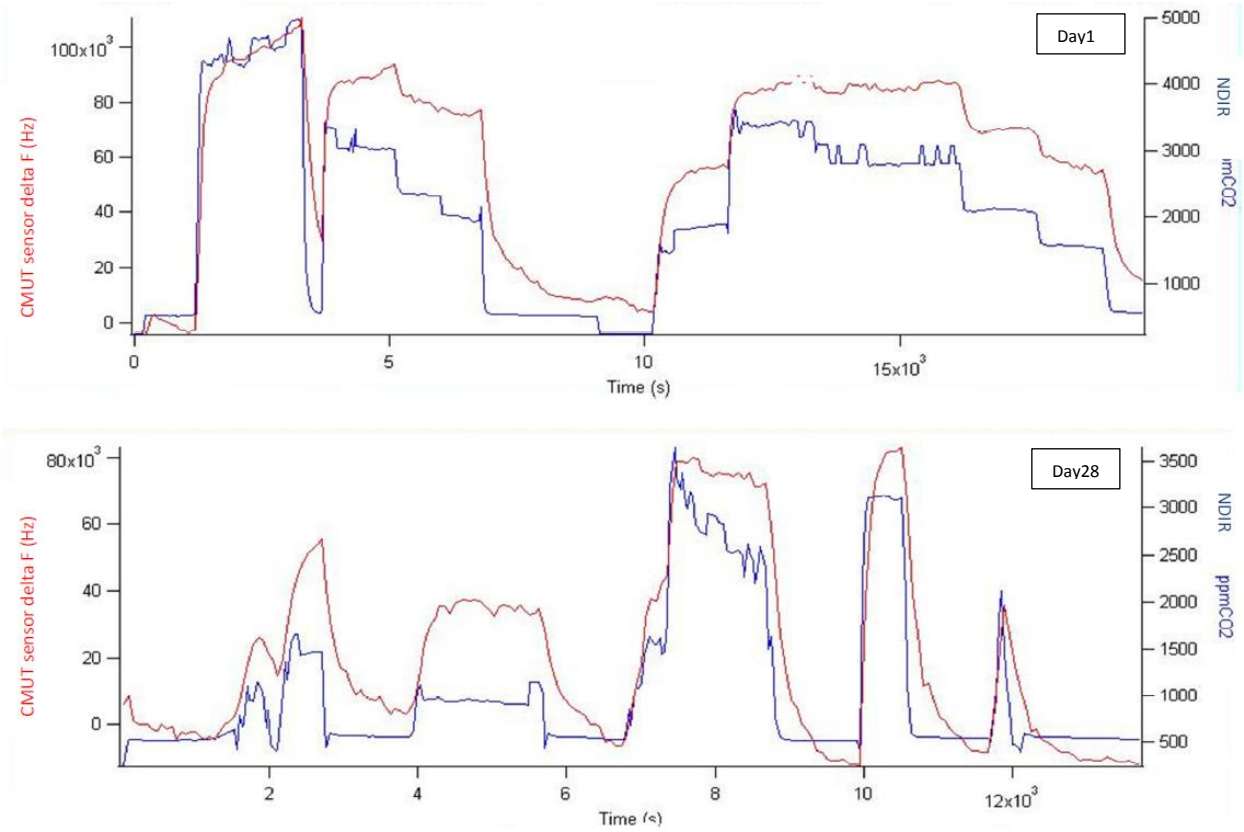

Fig 3.30 The signal of the CMUT sensor (red) tracks the NDIR reference sensor signal (blue) very well. CMUT sensor signal recovers to baseline (laboratory air) in reasonable time. We still observe a very strong signal after over 4 weeks of extensive use of this sensor device.

We observed that level of CO_2 reading from our sensor is comparable to the reference reading from a NDIR sensor. The signal from CMUT sensor matches well and shows similar trend and characteristics to the standard signal. For a good comparison, CMUT sensor should be calibrated for reading in ppm, similarly unit to NDIR.

It would be interesting to perform similar experiment with MOF-74 on CMUT. After some calibrations CMUTs might be tunable to match up perfectly with the reading from NDIR sensor. This might require effort to modify MOF-74 and AMO layer so that CMUTs sensors will be highly accurate and reliable. For further development, robustness and responsiveness of the sensor should be verified. In fig 3.30, CMUTs illustrated a slow response to CO_2 concentration

changes at a few time points. We can see that the trace of the CMUT signal implies that the sensors responded slower to the frequency drops compared to the NDIR sensor. This means CMUTs sensor might be satisfactory to use in certain applications that small error is acceptable. However, this issue will be addressed in the future development.

References

1. C.K.Ho, M.T.I., M.Kelly, R.C.Hughes, *Review of Chemical Sensors for In-Situ Monitoring of Volatile Contaminants*. 2001, Sandia National Laboratories: Abouquerque. p. 2.
2. Institute, A.B. *Alcohol Detection Technologies: Present and Future*
3. J. Chaste, A.E., J. Moser, G. Ceballos, R. Rurali, A. Bachtold, *A nanomechanical mass sensor with yoctogram resolution.* Nature Nanotechnology Letter, 2012. **7**: p. 301-304.
4. Jiii Janata, M.J., and D. Michael DeVaney, *Chemical Sensors.* Analytical Chemistry, 1994. **66**: p. 207-228.
5. K. Nakamura, T.N., T. Moriizumi, *Prediction of quartz crystal microbalance gas sensor responses using a computational chemistry method.* Sensors and Actualtors B, 1999. **61**: p. 6-11.
6. X.Jin, Y.H., A.Mason, X.Zeng, *Multichannel Monolithic Quartz Crystal Microbalance Gas Sensor Array.* Analytical Chemistry, 2009. **81**: p. 595-603.
7. P. Si, J.M., A.Komolov, J. Denborg, P.J. Moller, *Polymer coated quartz crystal microbalance sensors for detection of volatile organic compounds in gas mixtures.* Analytica Chimica Acta, 2007. **597**(2): p. 223-230.
8. J. Zhang, J.Q.H., F. R. Zhu , H. Gong, S. J. O'Shea, *Quartz Crystal Microbalance Coated with Sol-gel-derived Thin Films as Gas Sensor for NO Detection.* Sensors 2003. **3**(10): p. 404-414.
9. M.Yang, J.H., X Hu, C. Yan, Z. Cheng, *CuO nanostructures as quartz crystal microbalance sensing layers for detection of trace hydrogen cyanide gas.* Environmental Science and Technology, 2011. **45**: p. 6088-6094.

10. Z. Ying, Y.J., X. Du, G. Xie, J. Yu, H. Wang, *PVDF coated quartz crystal microbalance sensor for DMMP vapor detection.* Sensors and Actuators B, 2007. **125**(1): p. 167-172.

11. R. P. Wali, P.R.W., S. Eaimkhong, J. Hernando-Garcia, J. L. Sánchez-Rojas, A. Ababneh, J. K. Gimzewski, *Fourier transform mechanical spectroscopy of micro-fabricated electromechanical resonators: A novel, information-rich pulse method for sensor applications.* Sensors and Actualtors B, 2010. **147**: p. 508-516.

12. R.Zhou, D.S., W.Gopel, *Mass sensitive detection of carbon dioxide by amino group-functionalized polymers.* Sensors and Actuators B, 1996. **33**: p. 188-193.

13. X. Yu, J.W., Y. Long, *Zeolite-based Materials for Gas Sensors.* Sensors, 2006. **6**(12): p. 1751-1764.

14. I.Marr, S.R., G.Hagen, R.Moos, *Planar Zeolite Film-Based Potentiometric Gas Sensors Manufactured by a Combined Thick-Film and Electroplating Technique.* 2011.

15. I.Marr, A.N., D. Schonauer-Kamin, R.Moos. *Sensing of NO, NO_2, and NH_3 with Zeolite-Based Impedimetric Gas Sensors*. in *The 14th International Meeting on Chemical Sensors*. 2012.

16. X.X. Sun, Q.Y., J. Wang, Y. Huang. *Novel gas sensor based on nano-zeolite films for the nerve agent simulant dimethylmethylphosphonate detection*. in *7th International Conference on Solid-State and Integrated Circuits Technology, 2004. Proceedings.* 2004.

17. R.Pohle, A.T., P.Davydovskaya, M. Fleischer, *Metal Organic Frameworks as Promising High Surface Area Material for Work Function Gas Sensors* Procedia Engineering, 2011. **25**: p. 108-111.

18. A.Kondo, T.D., H.Noguchi, T.Ohba, K.Kaneko, H.Kanoh, *Adsorption of water on three-dimensional pillared-layer metal organic frameworks.* Journal of Colloid and Interface Science, 2007. **314**: p. 422-426.

19. P.Davydovskaya, R.P., A.Tawil, M.Fleischer, *Work function based gas sensing with Cu-BTC metal-organic framework for selective aldehyde detection.* Sensors and Actuators B, 2012.

20. N.Liu, Y.Y., J.J.Cha, M.T.Mcdowell, Y.Han, Y.Cui, *Functionalization of Silicon Nanowire Surfaces with Metal–Organic Frameworks* Nanotechnology Research, 2012. **5**(2): p. 109-116.

21. V.Cimalla, F.N., K.Tonisch, Ch.Foerster, K.Brueckner, I.Cimalla, T.Friedrich, J.Pezoldt,R.Stephan, M.Hein, O.Ambacher *Nanoelectromechanical devices for sensing applications.* Sensors and Actuators B, 2007. **126**: p. 24-37.

22. A.Andrei, K.K., M.Jozwik, P.Delobelle, L.Hirsinger, C.Gorecki, L.Nieradko, C.Meunier *AlN as an actuation material for MEMS applications. The case of AlN driven multilayered cantilevers.* Sensors and Actuators A, 2008. **141**: p. 565-576.

23. K, K., M.Józwik, C.Gorecki, A.Andrei, L.Nieradko, P.Delobelle, L.Hirsinger *Static and dynamic characterization of AlN-driven microcantilevers using optical interference microscopy.* Optical Laser Engineering, 2009. **47**: p. 211-216.

24. S.González-Castilla, J.O., M.Clement, E.Iborra, J.Sangrador, J.Malo, J.I.Izpura *Electrical detection of the mechanical resonances in AlN-actuated microbridges for mass sensing applications.* Applied Physics Letter, 2008. **92**: p. 183506.

25. J. L. Sánchez-Rojas, A.A., H. Seidel, Ü. Sökmen, E. Peiner, U. Schmid, *Characterization and simulation of high quality AlN-actuated resonant suspended beams.* Microsystem Technologies, 2010. **16**(5): p. 855-861.

26. Khuri-Yakub, M.I.H.a.B.T. *A surface micromachined electrostatic ultrasonic air transducer*. in. *IEEE Ultrason. Symp*. 1994.

27. D.W. Schindel, D.A.H., *The design and characterization of Micromachined air-coupled capacitance transducers*, in *IEEE Transactions on Ultrasonics, Ferroelectrics and Frequency Control*. 1995. p. 42-50.

28. M.I.Haller, B.T.K.-Y., *A Surface Micromachined Electrostatic Ultrasonic Air Transducer,* in *IEEE Transactions on Ultrasonics, Ferroelectrics and Frequency Control*. 1996. p. 1-6.

29. P.C.Eccardt, K.N., T.Scheiter, C.Hierhold *Surface micromachined ultrasound transducers in CMOS technology*. in *the 1997 IEEE International Ultrasonics Symposium*. 1996.

30. B.T.Khuri-Yakub, C.H.C., F.L.Degertekin, S.Ergun, S.Hansen, X.C.Jin, Ö,Oralkan, *Silicon Micromachined Ultrasonic Transducers,"* Japanese Journal of Applied Physics, 2000. **39**: p. 2883-2887.

31. H.J.Lee, K.K.P., P. Christman, O. Oralkan, M. Kupnik and B.T.Khuri-Yakib. *A low-noise oscillator based on a multi-membrane CMUT for high sensitivity resonant chemical sensors*. in *22th IEEE MEMS Conference*. 2009. Sorrento, Italy.

32. H.P. Lang, R.B., F. Battison, J.P. Ramseyer, E.Meyer, C.Andreoli, J. Brugger, P. Vettiger, M. Despont, T. Mezzacasa, L. Scandella, H.J. Guntherodt, Ch. Gerber, J.K.

Gimzewski, *A chemical sensor based on a micromechanical cantilever array for the identification of gases and vapors.* Applied Physics A, 1998. **66**: p. S61-S64.

33. F.M. Battison, J.P.R., H.P. Lang, M.K. Baller, Ch. Gerber, J.K. Gimzewski, E. Meyer, H.J. Guntherodt, *A chemical sensor based on a microfabricated cantilever array with simultaneous resonance-frequency and bending readout.* Sensors and Actuators B, 2001. **77**(1): p. 122-131.

34. H.P. Lang, J.P.R., W. Grange, T.Braun, D. Schmid, P. Hunziker, C. Jung, M. Hegner, C. Gerber, *An Artificial Nose Based on Microcantilever Array Sensors.* Journal of Physics: Conference Series, 2007. **61**: p. 663.

35. K. K. Park, H.J.L., G. G. Yaralioglu, A. S. Ergun, Ö. Oralkan, M. Kupnik, C. F. Quate, B. T. Khuri-Yakub, T. Braun, J.-P. Ramseyer, H. P. Lang, M. Hegner, and Ch. Gerber and J.K. Gimzewski, *Capacitive micromachined ultrasonic transducers for chemical detection in nitrogen.* Applied Physics Letter, 2007. **91**: p. 094102.

36. E. S. Snow, F.K.P., E. J. Houser, S. C. Badescu, T. L. Reinecke, *Chemical Detection with a Single-Walled Carbon Nanotube Capacitor.* Science, 2005. **307**: p. 1942-1945.

37. S. Ampuero, J.O.B., *The electronic nose applied to dairy products: a review.* Sensors and Actuators B, 2003. **94**: p. 1-12.

38. Srivastava, A.K., *Detection of volatile organic compounds (VOCs) using SnO2 gas-sensor array and artificial neural network.* Sensors and Actuators B, 2003. **96**: p. 24-37.

39. N.Yamazoe, N.M., *Development of Gas Sensors for Environmental Protection*, in *IEEE TRANSACTIONS ON COMPONENTS, PACKAGING, AND MANUFACTURING TECHNOLOGY*. 1995. p. 252-256.

40. F. Hutter, K.H.H., H. Schmidt. *Ormosiles A new class of materials for sensitive layers in the development of gas sensors*. in *2nd International meeting on chemical sensors*. 1989. Bordeaux, France.

41. H.Edres, R.H., M.Schwaiger,G.Gmelch,M.Roth, *A capacitive CO_2 sensor system with suppression of the humidity interference.* Sensors and Actuators B, 1999. **57**: p. 83-87.

42. W.Wang, K.L., T.Kim, I.Park,S.Yang, *A novel wireless, passive CO2 sensor incorporating a surface acoustic wave reflective delay line.* Smart Materials and Structures, 2007. **16**(4): p. 13821389.

43. N.Levit, D.P., G.Tepper, *High surface area polymer coatings for SAW-based chemical sensor application.* Sensors and Actuators B, 2002. **82**: p. 241-249.

44. I.G.Giannakopoulos, D.K., C.A.Grimes, V.Nikolakis, *Synthesis and Characterization of a Composite Zeoplite-Metglas Carbon Dioxide Sensor.* Advanced Functional Materials, 2005. **15**(7): p. 1165-1170.

45. X.Xu, J.W., Y.Long, *Zeolite-based materals for gas sensors.* Sensors, 2006. **6**(12): p. 1751-1764.

46. S.Reiss, G.H., R.Moos, *Zeolite-based Impedimetric Gas Sensor Device in Low-cost Technology for Hydrocarbon Gas Detection.* Sensors, 2008. **8**(12): p. 7904-7916.

47. A.Modi, N.K., E.Lass,B.Wei,P.M.Ajayan, *Miniaturized gas ionization sensors using carbon nanotubes.* Nature 2003. **424**: p. 171-174.

48. S.A. Waghuley, S.M.Y., S.S. Yawale, S.P. Yawale *Application of chemically synthesized conducting polymer-polypyrrole as a carbon dioxide gas sensor.* Sensors and Actuators B, 2008. **128**(2): p. 366-373.

49. H.J.Lee, K.K.P., M.Kupnik,N.A.Melosh,B.T.Khuri-Yakub, *Mesoporous Thin-Film on Highly-Sensitive Resonant Chemical Sensor for Relative Humidity and CO2 Detection.* Analytical Chemistry, 2012. **84**(7): p. 3063-3066.

50. H Deng, C.J.D., H. Furukawa, O.Yaghi, Science, 2010. **327**(5967): p. 846-850.

51. D.Britt, H.F., B.Wang, T.G.Grover,O.M.Yaghi, *Highly efficient separation of carbon dioxide by a metal-organic framework replete with open metal sites.* PNAS, 2009. **106**(49): p. 20637-20640.

Chapter 4

Label-free biodetection using Capacitive Micro-machined Ultrasonic Transducers (CMUTs) and its application for cardiovascular disease diagnostics

In this chapter, Capacitive Micro-machined Ultrasonic Transducers (CMUTs) were used to detect protein using two different schemes involving antibody detection and biomarker or antigen detection. For antibody detection, anti-human IgG Fab specific was used as an antibody that specifically adsorbs on human IgG functionalized CMUT devices and anti-Goat IgG was chosen as a non-specific negative control. We achieved a significant higher signal for the specific antibodies (~10-500 ng/ml) on CMUT devices in comparison to the non-specific negative control at low concentration. For antigen detection, we were interested in a cardiovascular disease biomarker and chose the tumor necrosis factor alpha (TNFα) as the analyte. We found a linear calibration curve for TNFα at very low concentrations and demonstrated that this label-free biodetection has a general applicability for assays including cardiovascular disease.

4.1.Introduction to biosensing

Capacitive Micro-machined Ultrasonic Transducer (CMUT) is a technology that was introduced as an alternative to piezoelectric resonators in the last decade. Currently the most recent models were designed to have high resonant frequency i.e. 40-52 MHz and the detection surface of an individual CMUT is approximately 20 μm in diameter[1-3]. Initially, CMUTs were developed

for medical imaging and therapeutic purposes [4-6]. CMUTs gained much attention for medical ultrasonic imaging and a lot of work has demonstrated significant improvements in CMUTs performance during the past decade. Less attention has focused on another aspect of this technology, which is its use as a mass sensor. Since the CMUT is a high frequency resonator, its oscillation and motion will be affected by mass change due to adsorption and desorption on its surface. For a cantilever resonator, its frequency is given by:

$$\frac{\Delta f}{f} = -\frac{1}{2}\frac{\Delta m}{m} \quad \text{...(4.1)}$$

Where Δf is the change in resonant frequency f and Δm is the change in mass of the resonator with mass m. For CMUTs with surface area A, the relationship between frequency and mass is,

$$\frac{\Delta m}{A} = 2\rho\,\frac{\Delta f}{f} \quad \text{…(4.2)}$$

The decrease in resonant frequency from its original value provides a measurement of the mass change in real time. This concept has been widely used in chemical sensing on many different types of oscillators such as SAW[7], QCM[8] and micro-fabricated cantilever devices [9, 10]. CMUTs with high resonant frequency can theoretically detect the mass of analytes in femtogram range or lower and with appropriate functionalization they can target specific analytes [1]. In the past, CMUTs were applied to detect low concentration chemical vapor such as dimethylmethylphosphonate (DMMP), decane, alcohol and acetone etc. [1, 3, 11], however their capabilities as biosensors have not been widely explored.

Coating CMUTs with biocompatible materials such as parylene-c and polydimethylsiloxane (PDMS) [12] is achievable and useful in biological detection applications. However, it is only until recently that CMUTs were reported as a biosensor using a label-free scheme to observe the

frequency change for antibodies against bovine leukemia virus protein gp51 (anti-gp51) [13] on previously gp51-coated CMUTs. In this communication, whole blood samples from cattle were used as a source of anti-gp51 and the measurement were done on CMUTs with a lower resonant frequency of 12MHz. For current demands in diagnostics and biomedical detection, quantitative detection of particular human disease markers at very low concentration (e.g pg/ml or ng/ml) is desired and they can benefit greatly from label-free detection technology [14]. In conventional labeling-dependent detection analyses (e.g. ELISA), some challenges such multiple label issues were observed [15]. Therefore, development of sensitive, reliable, high-throughput, label-free detection techniques are now attracting significant attention. These label-free detection techniques monitor biomolecular interactions and simplify the bioassays by eliminating the need for secondary reactants such as fluorescent, chemiluminescent or radioactive tags.

In this study, we used a CMUTs detection system developed by Matrix Sensors using CMUT devices with silicon surface that have resonant frequency of ~50 MHz to achieve high sensitivity in protein detection. To demonstrate a potential of CMUT in biosensing, we employed this technology in detecting biomolecules in two different schemes. Firstly antibody detection because when antigens infect the human body, several types of cells work together to recognize them and respond in producing excess amounts of antibodies to maintain normal regulation. However, detecting antigen still remains important to confirm precision and accuracy in diagnostics. Consequently, we also performed an antigen detection assay as a part of the experiments.

For antigen detection, we were interested in cardiovascular diseases (CVD) because these diseases can cause result in acute symptoms leading to fatality and are the leading cause of

mortality in the United States [16]. A rapid and accurate diagnosis of CVD is therefore critically important[17]. One common method to diagnose CVD is by detecting biomarkers known to have association with CVD such as C-reactive protein (CRP), tumor necrosis factor (TNFα) and Interleukin 6 (IL6) [17-21] by performing an immunological assay. A similar type of test can be performed on a single CMUT chip in a short period of time without requiring multistep protocols such as fluorescently labeled secondary antibodies required for microarray or ELISA. Since much research has suggested a stronger association between TNFα and CVD than most other biomarkers [19, 21], we decided to focus on detection of TNFα.

To perform an immunological assay, antibodies to capture antigens of interest have to be immobilized on the CMUTs surface so that the Fab domains are exposed [14]. We compared two methods for immobilization of antibodies. Both strategies aimed at binding the Fc domain of the antibody such that it is oriented towards the surface causing the Fab domains to be exposed to the specific antigen. For the first detection scheme, we used protein A that readily adsorbs onto silicon surfaces to immobilize human IgG onto the sensor in the desired orientation [22-24]. The second detection scheme utilized the non-specific affinity of bovine serum albumin (BSA) on silicon surface [25-27]. Biotinylated BSA functionalized sensors were therefore fabricated. This was followed by attachment of stepavidin, which provided additional biotin binding sites for subsequent capture of biotinylated antibodies.

We performed a calibration test using biotinylated Qantum Dots (Q-dots) that were captured using the same immobilization scheme as described above. After Q-dots were applied, the surface roughness parameter R_a was measured from an interferometer to provide a subsequent independent measurement confirming correlation between layer thickness and the mass of the protein layers on the CMUTs.

4.2. Material and methods

4.2.1 CMUTs sensor, data acquisition and frequency measurements

The CMUTs data acquisition platform with built-in temperature control (developed by Matrix Sensors Inc.), operates at a high frequency of ~ 20-60MHz which is in the range of the resonant frequency of current devices (~50-54 MHz). This platform can measure the resonant frequency and performs a frequency sweep in less than 1s. In this setup, a single 16 channel-CMUT chip was wire-bonded onto a PCB connector, which allows plug-and-play read-out with the acquisition unit. This allows for multiple assays or chemistries to be performed simultaneously on different sensors of the same chip or multiple chips by easily swapping out CMUT chips on the reader platform. Furthermore, the compact size of the chip, only ~10µl of liquid sample required for functionalization of the entire chip surface, or less than 1µl to functionalize individual sensors on a chip. Another advantage of the platform is that it uses USB connection and power supply for the system providing in-field portability and convenience for measurements at any location.

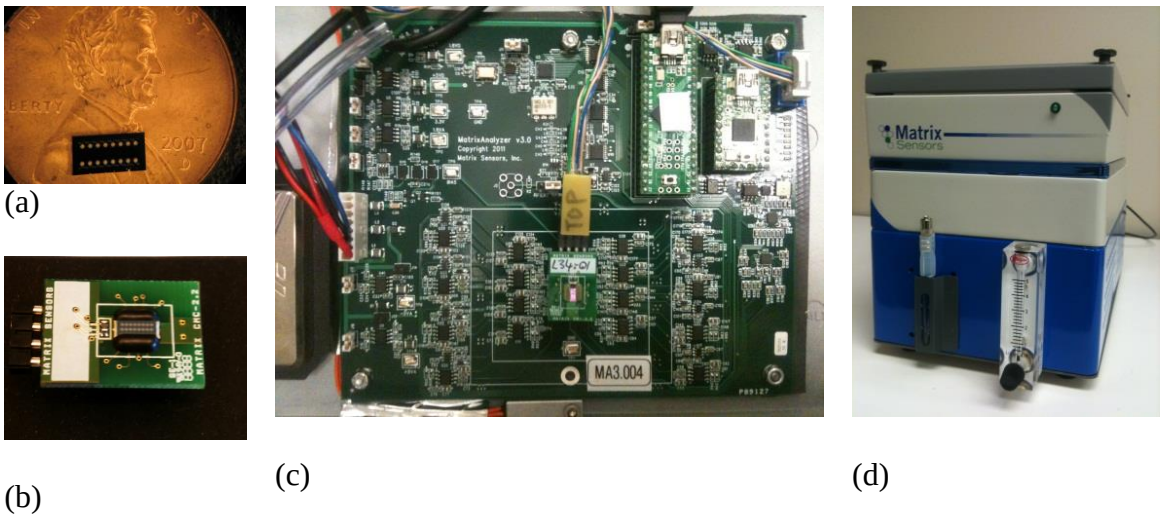

Fig 4.1 Overview of CMUTs and data acquisition. (a) wafer-fabricated CMUTs chip before wire-bonding (b) wire-bonded CMUTs chip (c) data acquisition circuit board (d) Matrix Sensor reader.

The electronics measure the resonant frequency of the CMUT device which decreases in response to the mass adsorbed onto the top of CMUT surface. This drop is converted to the mass adsorbed on the surfac as illustrated in fig 4.2.

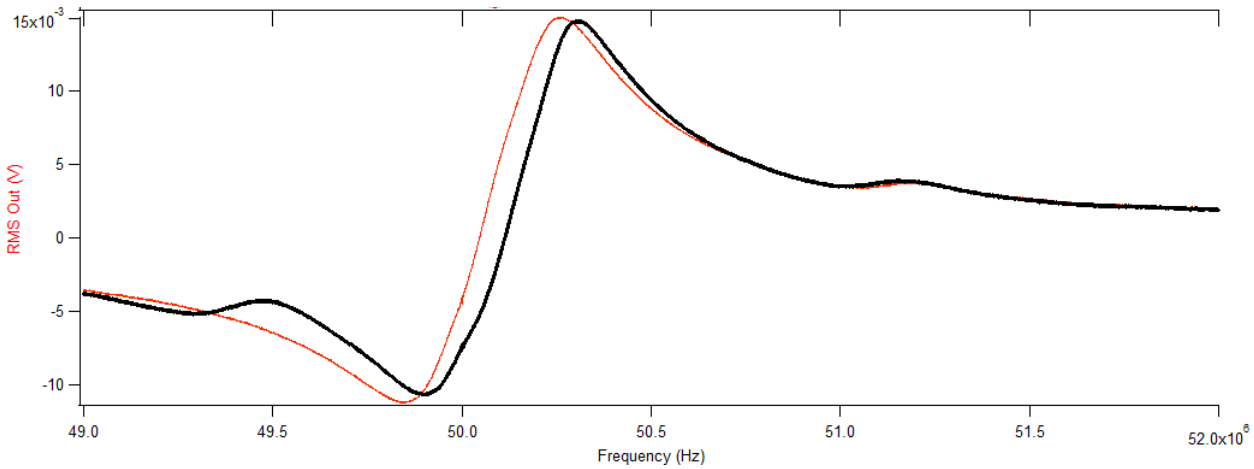

Fig 4.2. Frequency sweeps of an antibody-functionalized CMUT sensor- before capture of antigen (black curve) and after binding of antigen (red curve). The resonant frequency decreased by 80 kHz upon capture of antigen onto the antibody-functionalized sensor surface corresponding to a mass 300 pg of antigen/sensor.

4.2.2 Calibration of mass-detection using Quantum Dots

Before analytical detection at low concentration, CMUTs were calibrated for precision in mass detection using biotinylated Quantum Dots (655nm) (Invitrogen). For the assay, BSA-LC-biotin conjugate (ImmunoPure Biotinylated BSA, Thermo Scientific) in phosphate buffer saline (PBS) pH 7.4 was incubated over the chip surface at 200 µg/ml for 30 minutes at room temperature. The surface was then gently rinsed with PBS containing 0.05% Tween-20 (PBS-T) followed by a

rinse with DI water and air drying prior to measurement. Streptavidin (Thermo Scientific) in PBS pH 7.4 was then incubated over the BSA-LC-biotin coated chip surface for 30 min at room temperature. Rinsing, drying and measurement were repeated as described above. After that Q-Dots-biotin were incubated over the chip in concentrations ranging from 0.1 – 1000 nM. After the washing and drying steps were completed, the frequency difference between this step and the previous one provided the mass of Q-Dots attached onto CMUTs surface. To have a better understanding of the correlation of mass to frequency shift, the surface amplitude parameter (R_a) of the CMUTs surface were also recorded.

4.2.3Antibody detection: human IgG and anti-human IgG

4.2.3.1 Overview of detection scheme

In this experiment, we showed that immunological assays could be performed on the CMUTs without fluorescent tags. We chose a robust model of human IgG (Sigma Aldrich I4506) and anti-human IgG Fab-specific (Sigma Aldrich I9010) as the specific pair for immunological recognition while the anti-goat IgG (Sigma Aldrich A4187) served as the non-specific antigen.

To avoid denaturation of the proteins from drying out during the functionalization steps, measurements of mass adsorbed were obtained only after the end of the assays. We divided CMUTs chip into 3 sets providing 3 different measurements. The first set recorded the change in frequency of the device after being coated with protein A (Sigma Aldrich 82493), human IgG and bovine serum albumin (Δf_0). This was used as an arbitrary zero baseline before addition of the two antibodies. The second set measured the change in frequency of the device after being coated with protein A, human IgG, bovine serum albumin and anti-human IgG ($\Delta f_{specific}$), which served as a positive control. The final value recorded was the change in frequency of a device after being

coated with protein A, human IgG, bovine serum albumin and anti-goat IgG ($\Delta f_{non\text{-}specific}$), which served as a negative control.

After all three frequency changes were obtained, the difference between $\Delta f_{specific}$ and Δf_0 gave the frequency change corresponding to the mass of anti-human IgG Fab-specific of the specific antibodies bound. Similarly the difference between $\Delta f_{specific}$ and Δf_0 gave the frequency change corresponding to the mass of anti-goat IgG or the non-specific antibodies bound

The assays were performed with antibody concentration ranging from 10ng/ml – 500ng/ml under the same condition to minimize variation in protein performance.

4.2.3.2 Functionalization

Before protein functionalization, the surface of a CMUT device was cleaned using oxygen plasma for 2 minutes and then rinsed with ethanol. The chip surface was incubated in ethanol for 10 minutes to increase surface hydrophilicity before its frequency was recorded. The functionalization began with the addition of protein A (Sigma Aldrich 82493) at 500µg/ml in PBS (pH=7.4) and incubation for 2 hours. The surface was then washed and dried as previously described before 500µg/ml of Human IgG (Sigma Aldrich I4506) was applied and incubated for 2 hours. Washing and drying were repeated and, as before, 0.1% bovine serum albumin (BSA) was added and incubated for 30minutes (blocking step). After washing and drying, some of the chips were tested for frequency. The others were separated into two sets for positive and negative controls. For positive control or specific binding, Anti-Human IgG Fab-specific, at concentrations of 10ng/ml – 500ng/ml in 0.02% BSA in PBS, was added and incubated for 3 hours. Washing and drying was again repeated before frequency measurements. Similarly for negative control or non-specific binding, Anti-Human IgG Fab-specific at concentrations of 10ng/ml – 500ng/ml in 0.02%

BSA in PBS was added and incubated for 3 hours. Washing and drying was repeated before the frequency measurements.

4.2.3Quantitative TNFα detection on a single CMUTs chip

We performed the assay to detect TNFα on CMUTs system by immobilization of anti TNFα on the surface using biotin/stepavidin binding. The assay started by applying BSA-LC-biotin conjugate (ImmunoPure Biotinylated BSA, Thermo Scientific) in PBS pH 7.4 , which was incubated over the chip surface at 200 µg/ml for 30 minutes at room temperature. The surface was then gently rinsed with Phosphate Buffer Saline with 0.05% Tween-20 (PBS-T) followed by a rinse with DI water and air drying before measurement. Streptavidin (Thermo Scientific) in PBS pH 7.4 was then incubated over the BSA-LC-biotin coated chip surface for 30 min at room temperature. Rinsing, drying and measurement were repeated as described previously. After that 0.5 µg/ml of anti- TNFα-biotin conjugate (Anti Human TNF-alpha Biotinylated Affinity Purified PAB from R&D systems) were incubated on the chip. After the washing and drying steps were completed, TNFα antigens at different concentrations, over the rage from 0 – 400 ng/ml were applied onto the previously coated chips. The adsorbed mass of TNFα from each concentration was determined from the frequency difference between this and the previous step. A calibration curve of TNFα detection over the concentration was then created (fig 4.5).

4.3. Results and discussions

4.3.1Sensitivity and reliability of CMUTs for biodetection

Calibration of the CMUTs for biodetection was conducted by applying a layer of Q-dot onto the device utilizing commonly used biochemical reaction. Over concentration range of 0.01-1,000 nM, a calibration curve of the frequency drop from an average of 8 sensors over this range of concentration was obtained (fig 4.3)

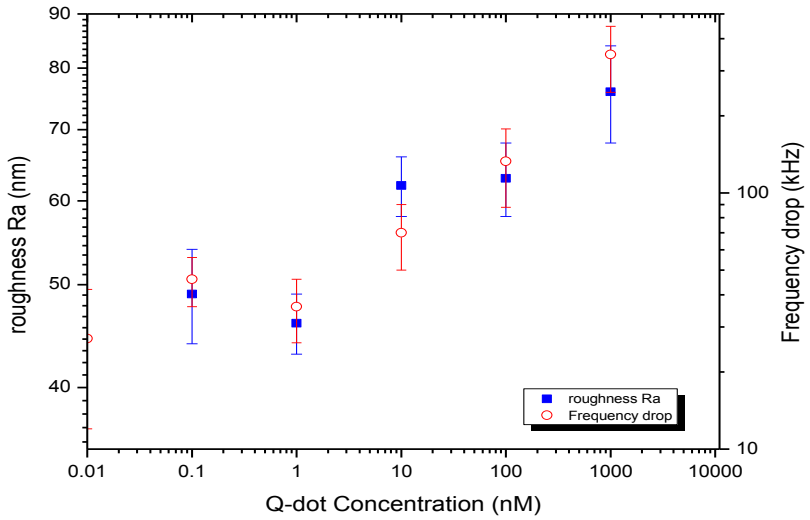

Fig 4.3. Calibration curve from frequency change corresponded to addition of Q-dot solution on CMUTs surface (open circle) and calibration curve from R_a surface roughness of the coated CMUTs chips (solid square).

In order to verify the reliability of the frequency drop as a good representation of the protein mass adsorbed on top of the device, the coated devices were observed under interferometer (Bruker NT9300) to measure the vertical surface roughness parameter (R_a). This value represents the thickness of the deposited layer on a surface from the average surface value and is a good indicator

for amount of material deposited on the surface. The R_a values of the coated devices were plotted against the Q-dot concentration and the calibration curve shows a linear relationship similarly to the graph obtained from frequency drop. Frequency drop is well correlated with R_a thickness with correlation efficient = 0.90. This means that the mass calculated from frequency drop can be used in biological mass sensing to detect the presence of a particular protein using appropriate coating techniques on CMUTs.

4.3.2 Antibody detection on CMUT sensor

As mentioned earlier, detection of antibodies are important and is an indirect detection method for disease-causing agents in our body. We chose to immobilize human IgG at its Fc position using protein A and hence the Fab domains of this antibody are exposed and available for antigen binding. When the anti-human IgG Fab specific was added, the Fab units of anti-human IgG should readily bind to the Fab units of previously coated human IgG. This interaction is strong enough in order for the specific antibody to remains on the device even after many washes. Unlike ELISA, our technique does not rely on secondary fluorescently labeled antibodies, where the signal from the fluorescent tags can be overestimated [15]. The signal obtained from this CMUT device is the direct representation of mass of the bound antibody bound and does not suffer from amplification from secondary antibody tags.

To assure that the mass derived from frequency difference in the specific antibody assay is primarily from a specific antibody and to ensure the observed signal is from the protein of interest, it is crucial to be able to clearly resolve between the mass of specific and non-specific antibody at the same concentrations. Both masses were compared in Fig 4 after both specific and non-specific

antibody assays were performed. For accuracy and reliability of the data, all assays were performed at the same time and under the same conditions in moist chambers to avoid variation in the protein performance and dehydration of the protein during surface incubation. The results below clearly show significant difference in mass between specific and non-specific antibodies bound to the surface for 4 antibody concentrations. Ideally, we expect the mass of non-specific to be negligible, however it is common that some cross binding of non-specific proteins or antibodies to the human IgG occurs on fig 4.4.

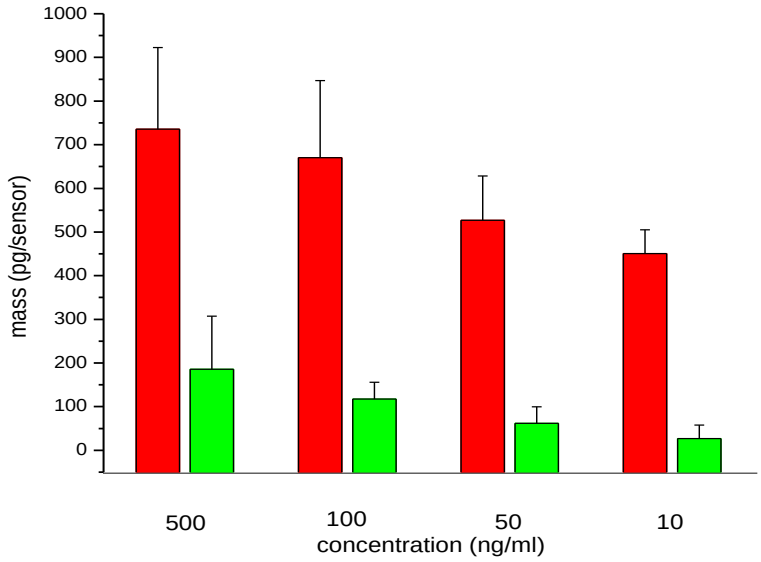

Fig 4.4. Specific (red) and non-specific (green) antibody mass bound at the concentration of 10ng/ml-500ng/ml (n=8)

In this method, CMUTs are able to resolve the mass between specific and non-specific down to 10ng/ml. To a certain extent, bio-detection using CMUTs technology can still optimized to work at much lower protein concentrations which we expect to be in the pg/ml range. The main limitation of CMUTs technology for protein detection is the level of electrical noise that affects the detection at very low amounts of protein concentration.

4.3.3 Quantitative TNFα detection and CMUTs potential for disease diagnostics

In cardiovascular diseases, acute symptoms such as stroke or heart attack can arise in patients with high levels of TNFα. Hence, sensitive and fast detection using CMUTs could benefit patients with cardiovascular disease risk to monitor their condition efficiently, fast and inexpensively.

In the medical diagnostic, a TNFα level of greater than 10 pg/ml in the blood indicated a risk of cardiovascular diseases [21] . In this study, we therefore focused on observing the sensitivity of TNFα detection in comparison to this critical value to evaluate the potential of our technology for cardiovascular diseases diagnostics.

A slightly different immobilization technique was employed by applying BSA to initiate protein functionalization on the CMUTs. The BSA-biotin conjugate was used as the first layer to allow stepavidin to bind onto the surface. After that biotinylated anti-TNFα (binding at Fc domain) was added respectively and the stepavidin/biotin interaction assists immobilization of the antibodies so that the Fab regions of anti TNFα are exposed at the interface. It is noted that a small fraction of biotinylated anti-TNFα can immobilize Fab domains of TNFα on the surface instead of Fc domains.

TNFα at low concentration over the range of 0-400 ng/ml was then applied on anti-TNFα previously coated devices and the calibration curve shows an excellent linear dependency of frequency shift as a function of concentration of TNFα. This quantitative analysis can be used to determine the concentration of TNFα and is a viable method for this protein over the critical range.

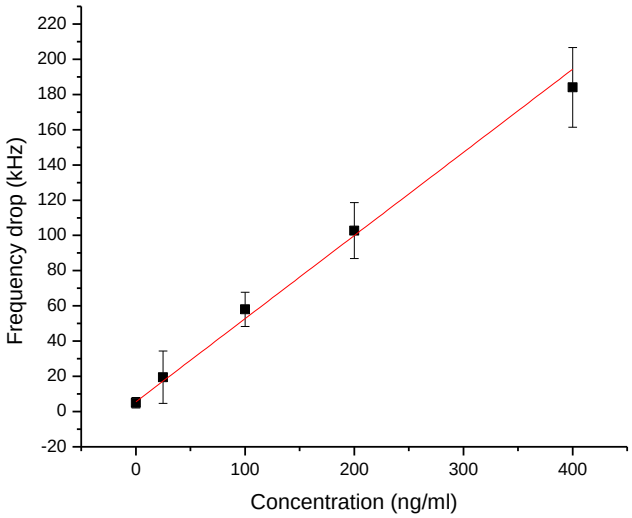

Fig 4.5 Calibration curve of frequency changes in correspond to concentration of TNFα

Although this calibration shows an excellent linearity (R^2 = 0.99) that suggests reliability of detection of TNFα on CMUT devices, it would be interesting to extend the range of concentration to a lower concentration to around 1-10 pg/ml which is the interesting concentration range. At the same time, other protein detection along with TNFα i.e. CRP and IL-6 on the CMUT chips should provide a more conclusive cardiovascular disease diagnostic in the future.

4.4. Conclusions

In this study, we performed different functionalization schemes on um-sized biocompatible CMUTs demonstrating its potential to perform biodetection of any specific protein at high precision and high sensitivity. In contrast to ELISA, antigen capture alone is sufficient for detection, i.e. no labeling and secondary antibodies (for signal and amplification) are required. The antigen is introduced and applied as the final step of the assay onto the sensor chip. This means that the sensor

chips can be pre-fabricated as single-step kits, which is very cost-effective and time saving for research and diagnostic applications.

Furthermore, the size of the substrate is very small and the presented method only requires a minimal volume of 10ul to cover the entire 16-sensor chip without. This contributes to an additional cost reduction by requiring fewer quantities of reagent materials.

In our laboratory, CMUTs are being developed to be fully handheld units relying only on battery power or power via a USB connection from a laptop computer and being operated either as a stand-alone unit or via a computer interface. This will facilitate use for diagnostic applications in medically underserved and hard-to-reach regions or for soldiers in the battle fields avoiding the need to ship samples to a central facility of laboratory for analysis.

With the progress being made, this technology will reach and eventually exceed the limits of ELISA. Although this novel detection method still has a lower sensitivity compared to ELISA, for certain diagnostics applications, an analyte concentration in the range of 10-100 ng/ml is clinically relevant and can be easily performed with this new technology. Additionally, some of the advantages mentioned above such as faster detection time, lower cost and the small amounts of materials required as well as its portability and ability for further miniaturization of this technology make CMUTs an interesting alternative for protein detection in a laboratory or medical setting.

References

1. Lee H J, Park K K, Kupnik M, Oralkan Ö, Khuri-Yakub B T. (2011) Chemical Vapor Detection Using a Capacitive Micromachined Ultrasonic Transducer, *Analytical Chemistry 83*, 9314-9320.http://pubs.acs.org/doi/abs/10.1021/ac201626b
2. Lee H J, Park K K, Cristman P, Oralkan Ö, Kupnik M, Khuri-Yakub B T. (2009) A low-noise oscillator based on a multi-membrane CMUT for high sensitivity resonant chemical sensors, In *22th IEEE MEMS Conference*, pp 761-764, Sorrento, Italy.http://ieeexplore.ieee.org/xpls/abs_all.jsp?arnumber=4805494
3. Park K K, Lee H, Kupnik M, Oralkan Ö, Ramseyer J P, Langc H P, Hegner M, Gerber C, Khuri-Yakub B T. (2011) Capacitive micromachined ultrasonic transducer (CMUT) as a chemical sensor for DMMP detection, *Sensors and Actuators B: Chemical 20*, 1120-1127.http://www.mendeley.com/research/capacitive-micromachined-ultrasonic-transducer-chemical-sensor-5/
4. Wong SH, Watkins RD, Kupnik M, Butts-Pauly K, Khuri-Yakub BT. (2007) Feasibility of MR-Temperature Mapping of Ultrasonic Heating from a CMUT, *IEEE Transactions on Ultrasonics, Ferroelectrics and Frequency Control 55*, 811-818.http://ieeexplore.ieee.org/xpls/abs_all.jsp?arnumber=4494775
5. Khuri-Yakub B T, Oralkan O. (2011) Capacitive micromachined ultrasonic transducers for medical imaging and therapy, *Journal of Micromechanics and Microengineering 21*, 54004-54015.http://iopscience.iop.org/0960-1317/21/5/054004
6. Wong SH, Kupnik M, Watkins RD, Butts-Pauly K, Khuri-Yakub BT. (2010) Capacitive Micromachined Ultrasonic Transducers for Therapeutic Ultrasound Applications, *IEEE*

Transactions on Biomedical Engineering 57, 114-123.http://ieeexplore.ieee.org/xpls/abs_all.jsp?arnumber=5170079&tag=1

7. Snow A, Wohltjen H. (1984) Poly(ethylene maleate)-cyclopentadiene: a model reactive polymer-vapor system for evaluation of a SAW microsensor, *Analytical Chemistry 56*, 1411-1416.http://www.dtic.mil/docs/citations/ADA141531

8. Bruckenstein S, Shay M. (1985) Experimental aspects of use of the quartz crystal microbalance in solution, *Electrochimica Acta 30*, 1295-1300.http://dx.doi.org/10.1016/0013-4686(85)85005-2

9. Battiston F M, Ramseyer J P, Lang H P, Baller M J, Gerber C H, Gimzewski J K, Meyer E, Guntherodt H J. (2001) A Chemical Sensor Based on a microfabricated cantilever array with simultaneous resonance-frequency and bending readout, *Sensors and Actuator B: Chemical 77*, 122-131.http://www.mendeley.com/research/a-chemical-sensor-based-on-a-microfabricated-cantilever-array-with-simultaneous-resonancefrequency-and-bending-readout-1/

10. Wali RP, Wilkinson PR, Eaimkhong S, Hernando-Garciaa J, Sánchez-Rojasd JS, Ababnehe A, Gimzewski JK. (2010) Fourier transform mechanical spectroscopy of micro-fabricated electromechanical resonators: A novel, information-rich pulse method for sensor applications, *Sensors and Actuator B: Chemical 147*, 508-516. http://www.sciencedirect.com/science/article/pii/S0925400510003126

11. Park K K, Lee H J, Yaralioglu G G, Oralkan O, Kupnik M, Quate C F, Khuri-Yakub B T, Braun T, Lang H P, Hegner M, Gerber C, Gimzewski J K. (2007) Capacitive micromachined ultrasonic transducers for chemical detection in nitrogen, *Applied Physics Letter 97*,

094102.http://ieeexplore.ieee.org/xpl/freeabs_all.jsp?arnumber=4831408&abstractAccess=no&userType=inst

12. Zhuang X, Nikoozadeh A, Beasley MA, Yaralioglu GG, Khuri-Yakub BT, Pruitt BL. (2007) Biocompatible coatings for CMUTs in a harsh, aqueous environment, *Jounal of Micromechanics and Microengineering 17*, 994-1001.http://iopscience.iop.org/0960-1317/17/5/020/

13. Ramanaviciene A, Virzonis D, Vanagase G, Ramanavicius A. (2010) Capacitive micromachined ultrasound transducer (cMUT) for immunosensor design, *Analyst 135*, 1531-1534.http://pubs.rsc.org/en/Content/ArticleLanding/2010/AN/c0an00104j

14. Morrison D W G, Dokmeci M R, Demirci U, Khademhosseini A. (2008) Clinical Applications of Micro- and Nanoscale Biosensors, In *BiomedicalNanostructures* (K. E.Gonsalves, C. L. L., C.R.Halberstadt,L.S. Nair, Ed.), JohnWiley&Sons.http://onlinelibrary.wiley.com/doi/10.1002/9780470185834.ch17/summary

15. Ray S, Mehta G, Srivastava S. (2010) Label-free detection techniques for protein microarrays:Prospects, merits and challenges, *Proteomics 10*, 731-748.http://onlinelibrary.wiley.com/doi/10.1002/pmic.200900458/full

16. Thom T, Haase N, Rosamond W, Howard VJ, Rumsfeld J, Manolio T. (2006) Heart disease and stroke statistics—2006 update, *Circulation*, 85-151.http://circ.ahajournals.org/content/113/6/e85.full

17. Tang L, Ren Y, Hong B, Kang K A. (2006) Fluorophore-mediated, fiber-optic, multi-analyte,immunosensing system for rapid diagnosis and prognosis of cardiovascular diseases, *Journal of Biomedical Optics 11*, 021011.http://spie.org/x648.html?product_id=692353

18. Sabatine M S, Morrow D A, de Lemos J, Gibson CM, Murphy SA, Rifai N, McCabe C, Antman EM, Cannon CP, Braunwald E. (2002) Multimarker approach to risk stratification in non-ST elevation acute coronary syndromes: simultaneous assessment of troponin I, c-reactive protein, and b-type natriuretic peptide, *Circulation 105*, 1760-1763.http://www.ncbi.nlm.nih.gov/pubmed/11956114

19. Pai J K, Pischon T, Ma J, Manson J E, Hankinson S E, Joshipura K, Curhan G C, Rifai N, Cannuscio C C, Stampfer M J, Rimm E B. (2004) Inflammatory Markers and the Risk of Coronary Heart Disease in Men and Women, *the New England Journal of Medicine 351*, 2599-2610.http://www.ncbi.nlm.nih.gov/pubmed/15602020

20. Tuomisto K, Jousilahti P, Sundvall J, Pajunen P, Salomaa V. (2006) C-reactive protein, interleukin-6 and tumor necrosis factor alpha as predictors of incident coronary and cardiovascular events and total mortality, *Thromb Haemost 95*, 511-518.http://www.ncbi.nlm.nih.gov/pubmed/16525580

21. Cesari M, Penninx B W, Newman A B, Kritchevsky S B, Nicklas B J, Sutton-Tyrrell K, Tracy R P, Rubin S M, Harris T B, Pahor M. (2003) Inflammatory Markers and Cardiovascular Disease (The Health, Aging and Body Composition Study), *The American Journal of Cardiology 92*, 522-528.http://www.sciencedirect.com/science/article/pii/S0002914903007185

22. Wang Z, Jin G. (2003) Feasibility of protein A for the oriented immobilization of immunoglobulin on silicon surface for a biosensor with imaging ellipsometry, *Journal of biochem and biophysical methods 57*, 203-211.http://www.sciencedirect.com/science/article/pii/S0165022X0300109X

23. Dutra RF, Castro CM, Azevedo CR, Vinhas E, Malagueño E, Melo EH, Lima Filho JL, Kennedy JF. (2000) Immobilization of pneumococcal polysaccharide vaccine on silicon

oxide wafer for an acoustical biosensor, *Biosensors and Bioelectronics 15*, 511-514.http://www.ncbi.nlm.nih.gov/pubmed/11419647

24. Ikeda T, Hata Y, Ninomiya K, Ikura Y, Takeguchi K, Aoyagi S, Hirota R, Kuroda A. (2009) Oriented immobilization of antibodies on a silicon wafer using Si-tagged protein A, *Analytical Biochemistry 385*, 132-137.http://www.ncbi.nlm.nih.gov/pubmed/19017523

25. Scott J. McClellan, Elias I. Franses. (2005) Adsorption of bovine serum albumin at solid/aqueous interfaces, *Colloids and Surfaces A: Physicochem. Eng. Aspects 260*, 265-275.http://dx.doi.org/10.1016/j.colsurfa.2005.03.017

26. L, Cummings. (2010) Characterization of Biomolecular Interactions at the Silicon Photonics Interface, In *2010 NNIN REU Research Accomplishments*, pp 8-9, NNIN REU http://www.nnin.org/doc/2010nninreura/2010nninreuCummingsL.pdf

27. Lee C S, Lee S H, Park S S, Kim Y K, Kim B G. (2003) Protein patterning on silicon-based surface using background hydrophobic thin film, *Biosensors and Bioelectronics 18*, 437-444.http://www.sciencedirect.com/science/article/pii/S0956566302001471

Chapter 5

Application of nanotechnology in stem cells development study: mechanical observation and manipulation

Much of biological research relies on detection of biomolecules such as proteins, DNA, mRNA to study cellular mechanism. In general, instruments for biological research focus on optical visualization especially fluorescent microscopy, which allows selective visualization of specific cells or proteins in the system of interest. It is always beneficial to be able to image and observe these proteins at higher sensitivity with advanced techniques. Nanotechnology offers the capability to observe and monitor objects on a smaller scale in addition to many currently available methods for biological samples, and we believe that it will increase the capability of researchers to study biology at the molecular level; exploring the potential of nanotechnology tools in biological systems may bring new insights and information.

A great example of nanotechnological tools currently adopted widely by biologists is atomic force microscopy (AFM). It is a powerful high resolution instrument with the capability to study proteins and cells. However, AFM requires different sample preparation than a normal microscope because the measurements usually occur on an opened flat surface. In AFM, the sample is probed mechanically by a tip attached on a cantilever. The deflected intensity profile of a laser is then detected as the sample is being scanned (see chapter 2). The AFM can create a surface topography for a sample with small feature (sub-nanometer).

In this chapter, we discuss the potential of interferometric optical profilers as an alternative instrument for biological research, which may lead to improvement on the information and measurement in biology. For example, the use of optical profiler could provide robustness in certain measurements, additional mechanical and physical information such as elasticity, mechanical response and mechanical movement. The system that we focused on was cardiac stem cells from our collaboration in the medical school, UCLA. After modification and the development of novel techniques for this study, we applied force and electricity as stimuli using different techniques derived from the use of nanotechnology. In this chapter, we illustrated the effects of these physical stimuli on the development of stem cells. The results of cellular responses are provided in this chapter along with the future directions.

5.1 Introduction: application of mechanical stimuli in biology and nanotechnology as a platform to study cell biology in details

While nanotechnology has been around for several decades, only a small fraction of researchers have applied these techniques to biological studies. After "single cell force spectroscopy (SCFS)" was developed in our laboratory[1], nanotechnology was proven to reveal information additionally to current conventional methods in biological science. For example, a cell's Young modulus measurement- not available from conventional methods such as optical microscopy- showed us that cancer cells were 70% softer than normal cells[1-3]. According to this work, there seem to be potential new insights that have not been explored in fundamental biology due to limitation of the instruments. Through the application of nanotechnological instruments, new information and techniques may be discovered by unconventional methods. For example, diagnostic of cancer cells can rely on stiffness or young modulus of cells instead of morphology according to the research on SCFS; the use of this idea might lead to a more

accurate and quick process to detect cancers with an automated AFM. Therefore mechanical and physical data in biology may contain additional insights that have not been explored; this is a reason we are interested in mechanical and physical properties of biological systems. Since a single cell is miniature, measurements of its mechanical and physical properties require an instrument that can measure small changes in the system; this is a characteristic of many instruments in nanotechnology. Since most of these instruments have a miniature probe that can be in a contact with a single cell, we believe that the use of nanotechnological instruments will allow us to investigate the cell mechanics efficiently.

In cell environment, changes in physical and chemical properties are regulated by cells. In any case of change, cells have to response certain way depending on the change to maintain the balance and to survive[4]. There is much more research focusing on cellular responses to biochemical changes than the cellular responses to physical changes. This could be because there was not a well-defined technique for mechanical and physical measurement on a cellular level in the past. Hence, we were interested in and focusing on studying the effects of physical or mechanical changes on cells and biological systems using the optical profiling system specially developed for biological samples.

In the prior works, our laboratory has demonstrated the ability to controllably measure and perform single cellular force spectroscopy on a single cell [1-3]. In addition to diagnostic application, force may be used to manipulate biological system and direct the cellular development. This idea was seen and illustrated in many works in biophysics and bioengineering[5, 6]. These research introduce forces through different surface tension, surface stiffness, shear force[7, 8] of the substrate or indentation[9] on cell membranes and observed the

responses of cells to the mechanical forces applied. An example of the cellular responses influenced by force on human fibroblasts is shown in fig 5.1.

In this work, human fibroblasts were placed on 2D collagen matrix and 3D collagen matrix shown in fig 5.1. The shape of fibroblasts grown on two types of substrates appeared to be different. The fibroblast on a 3D matrix projects a dendritic network of extension in collagen matrices while the one on a flat cover slip did not and had different shape in 2D. In addition to geometry, substrate stiffness was also shown to affect cell morphology, cytoskeletal structure, and adhesion [10, 11]. A range of these physical properties can also lead to variety in the cell development[12], especially the differentiation of stem cells [13, 14].

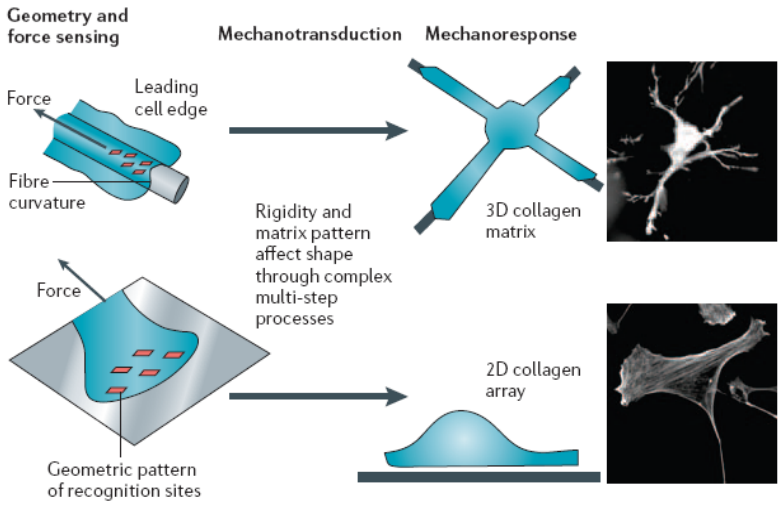

Fig 5.1 Effects of pattern and geometry of substrates on human fibroblasts. Human fibroblasts projected a dendritic network of extensions on 3D collagen matrices but not on collagen-coated coverslips. Three-dimensional surface and geometry has different effect on human fibroblasts than two dimensions.

After many studies, scientists are convinced that mechanical force affects the growth and the development of cells. A well-recognized process suggests that the mechanical properties of the cell's environment are sensed and translated into biochemical signals by cells to trigger

cellular responses [15, 16]; This process occurs in three stages: force and geometry sensing, mechanotransduction and mechanoresponses. In force and geometry sensing, mechanism of force sensing is believed to occur in three possible behaviors. First mechanism is through folding and unfolding of protein caused by forces acting on the proteins (fig 5.2 (A)). Since proteins are folded in as coils, the unraveling of these proteins causes the unexposed functional groups to become exposed to the surroundings. The unraveling of the protein can cause changes of the biochemical environment and trigger cells to response biochemically to these functional groups. This protein unfolding mechanism was observed frequently to affect activities of enzymes and motor proteins[17-19]. Second mechanism is related to the closing and opening of ion channels on cell membranes (fig 5.2 (B)). When these ion channels that regulate chemical flow are affected by force, the biochemistry inside the cells is affected, and hence cellular response occurs to this change. The last mechanism is related to adhesion proteins responsible for cells adhesion such as integrin. The integrin clusters are known to increase in size to maintain cells adhesion in the presence of force [20-22]. As shown in fig 5.2 (C), this type of proteins can be activated to mitigate strong force through “strong receptor-ligand bond” configuration. After the mechanical sensing process, the mechanical signal is converted to a biochemical signal by cells. Then cellular mechanoresponse takes place according to the stimuli.

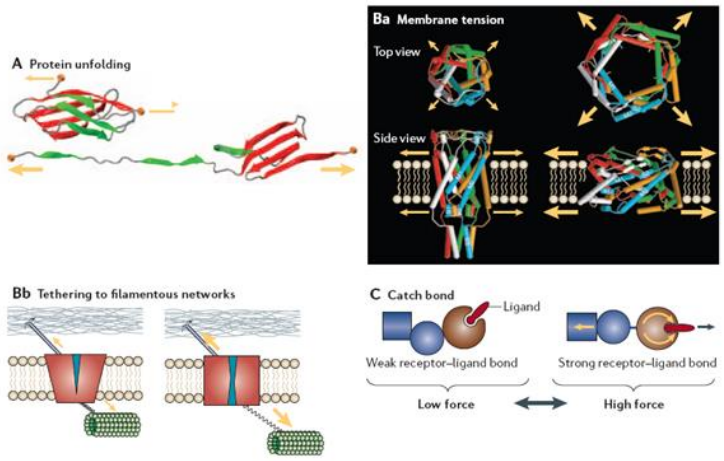

Fig 5.2 Mecahnism of force sensing. (A) force influence on protein unfolding which triggers biochemical signal. (B) stretching of ion channels upon movement of cell membranes by force is sensed and translated (C) adhering protein such as integrin responses to force to hold cells together under force application.

Based on the evidence that illustrates the influence of mechanical force on cells, we believe that it could be a useful parameter to assist and direct the differentiation of stem cells. We focused on the differentiation and the development of embryonic and pluripotent stem cells (PSCs) to become heart cells (mesoderm). Currently, methods to direct and achieve lineage specification towards certain cell types rely on addition of cocktails of chemical inducers into cell culture medium. This process in driving differentiation is, however, inefficient and often time leads to variable in differentiation. We believe that applying mechanical inducer is an interesting approach to guide and direct cellular response of a system such as these stem cells in addition to chemical stimuli. Since physical or mechanical stimuli are sensed and converted into intrinsic biochemical agents by cells, this might be a more successful mean to stimulate and direct cells than adding biochemical agents from the outside of the cells.

In collaboration with Dr. Nakano, Dr. Pyre in the UCLA medical school, we are interested in the development of stem cells on the nanoscopic and microscopic scale. We modified and developed a high-throughput methods called live-cell interferometry(LCI) and mechanical imaging interferometry (MII)[23, 24] for cell mechanical measurements using an interferometric optical profiler. These techniques allowed us to monitor the change of embryonic and pluripotent stem cells after the application of certain inducers (i.e., drugs, stiffness of substrate, external force applied). This study contains 4 different aspects:

a) Force enhanced survival of human pluripotent stem cells (hPSCs) – Unlike many other animals' stem cells, human stem cells grow in colony and experience apoptosis when dissociated. Prior works have implied that force was an important biomechanical signal for mammalian cell proliferation[5, 25].We believed that application of a constant or stationary mechanical force will mimic the natural conditions of compacted cell colonies required for cellular proliferation and enhance survival of the dissociated hPSCs. As expected, chemical dissociation and real-time monitoring of hPSCs revealed 'blebbing' followed by apoptosis. By applying force through micro-magnetic beads, we expect the cells to survive longer.

b) Measuring cardiac rhythms – We examined cellular nanomechanical motion of cardiomyocytes derived from cardiac stem cells after the differentiation through a drug selection process. In collaboration with Dr. Atsushi Nakano, we modified the cell culture process and developed a technique to observe real-time nanomechanical motions. Micro-reflectors were optimized to minimize toxicity to the cells. Monitoring the mechanical motion before and after the differentiation revealed many details of the differentiation and lineage commitment that are not readily measured with conventional characterization methods. In addition, the specific nature

of these signals (e.g., amplitude, frequency) can be used to inform the mechanical stimulation of hPSCs toward directed lineage commitment to cardiomyocytes.

c) Force directed differentiation of stem cells – A device that provides control of an applied magnetic field (time and magnitude) was designed and fabricated. This apparatus designed to operate either in an incubator or while integrated into a real-time measurement system, will allow us to apply controlled mechanical force to live hPSCs. This is essential to direct stem cells to mature and differentiate towards mesoderm such as heart cells. Preliminary work involved monitoring OCT4-EGFP levels under conditions of applied static mechanical force to assess the effects of force on the differentiation. This green fluorescent protein was the key indication for pluripotency of stem cells. The absence of this protein suggested that cells already differentiated. By following the intensity, we established a curve which can be used to understand the kinetics of the differentiation in the presence of force.

d) Electrical pulse directed differentiation of stem cells – previous works showed that electrical stimulation of animal stem cells leads to expression of cardiac genes. We believe that electrical pulse is another potential stimulus to direct the stem cells differentiation towards cardiomyocytes. We repeated similar experiments done on animal stem cells on human stem cells. We initially fabricated a platform to apply biphasic pulse in a controlled environment. The preliminary results suggested a relevance of electrical excitation to cardiac gene expressions in qPCR. However, more results are needed to confirm this finding.

In all these four aspects of the research, we illustrated engineering capability to address the limitations that biologists may encounter in their research. Collaboration in both aspects is a great philosophy to advance in this field. Currently, synchronization in beating of differentiated

embryonic stem cells (ESC) was observed. We were to first to visually confirm that neo-natal cardiomyocytes started to beat individually before they synchronize using our customized interferometer. The electrical stimulus was shown to be effective to assist cardiac stem cells to differentiate into cardiomyocytes. We also observed a kinetic curve for hPSC differentiation. However, more repetitions are required to differentiate the curve for analysis for force effect on hPSC differentiation. In summary, this chapter provides insight to the techniques that were applied successfully to study the differentiation of stem cells. In the future, the author is confidence that the techniques would gain attention and be revisited for research in this field.

5.2 Materials and techniques

5.2.1 Stem cells

Stem cells have been gaining much interest over the last 5-10 years because of their ability to renew and differentiate into mature cells. Therapeutic involving stem cells are proposed and believed to be an alternative for the future. Although the stem cell therapy is theoretically feasible, the differentiation and the growth of stem cells are complex and hard to control. The use of biochemical and chemical stimuli to direct stem cells has failed to drive the differentiation towards certain lineage commitment. A more innovative method with higher efficiency is on the search and highly desired. As mentioned earlier, we are interested in using mechanical stimuli such as force and electrical pulse to direct the differentiation of stem cells because they have illustrated potential to induce the cells to respond to them. We think that they would be a promising inducer for to direct the differentiation of stem cells more successfully. After some investigation, the system that could benefit from the physical inducers is cardiac muscles. This is

because the cardiac muscles involve in mechanical motions during contraction and relaxation cycles; They should be the system that responds best to physical inducers such as force. We predicted that mechanical force may play a great role in the differentiation of cardiac stem cells. In addition to force, electrical pulse has been used to activate heart failure in a clinical practic, and detection of pulse is commonly used to detect heart movement. We also hypothesized that electrical pulse would be another inducer to have a great effect on the differentiation of cardiac stem cells, and assist the stem cells to become more mature cardiomyocytes.

5.2.1 (a) human pluripotent stem cells

Human pluripotent stem cells derived from hESCs culture provided by Dr. Sean Sherman through collaboration with Dr. April Pyre. According to his preparation [26], hESCs (HSF1 or H9)- with Oct4 expression- were grown on gelatin-coated plates with mitomycin C-treated MEFs at passage 3 in hESC medium consists of Dulbecco's modified Eagle's medium/Ham's F-12 medium with 20% knockout serum, non-essential amino acid, and 200 mM L-glutamine, plus 2-mercaptoethanol solution and 4 ng/ml basic fibroblast growth factor. All the cells provided were grown on feeders. hESCs were routinely passaged every 4-6 days using collagenase at 1:2 or 1:3 depending on cell density. For our experiment involving interferometric optical profiler, the cells were grown on a silicon dice instead of a normal glass culture dish. After tested the toxicity with silicon and gold coated beads, the cell responded well and grew normally. We selected the cell density to be around 100,000 single cells in a 3.5 mm culture dish, where silicon dice can be placed at the bottom. After gelatin and MEFs were plated, hESCs were plated on the silicon dice 24 hours later. This silicon dice was then placed later at the bottom of the culture dish. The cells were kept to grow for two days before experiments started.

5.2.1 (b) mouse embryonic stem cells

Mouse stem cells were provided by Armin Arshi in Dr. Atsushi Nakano's laboratory through our collaboration.

(i) ES cell culture and differentiation.

Undifferentiated wild type mouse E14Tg2a (ATCC) cells and *Nkx2-5*$^{neoR/+}$ mouse embryonic stem cells (ES) were maintained on Mitomycin-treated mouse embryonic fibroblast feeder cells in the media (see [27]and [28] for full details). Then, formation of embryoid bodies took place and lasted for 5-7 days. After that the cells were then suspended and differentiated in hanging drops and became larger embryoid bodies (EBs). This is known as day zero during the course of differentiation. After the EBs became large enough inside hanging drops (fig 5.3), they were transferred and plated on culture dish. However, cells used for experiment involving the interferometric optical profiler were plated on a 2x2 silicon dice instead. The cells were kept at 37 °C, 5% CO_2, and media was exchanged every two days. On day 10, the cells were partially differentiated, the drug selection process started by adding G418 neomycin antibiotic (600 μg/mL), which kills the cells that did not have cardiac expression, into the media. And hence the sample were purified and left with beating cardiomyocytes that differentiated from the stem cells. The time of this process was summarized in fig 5.3.

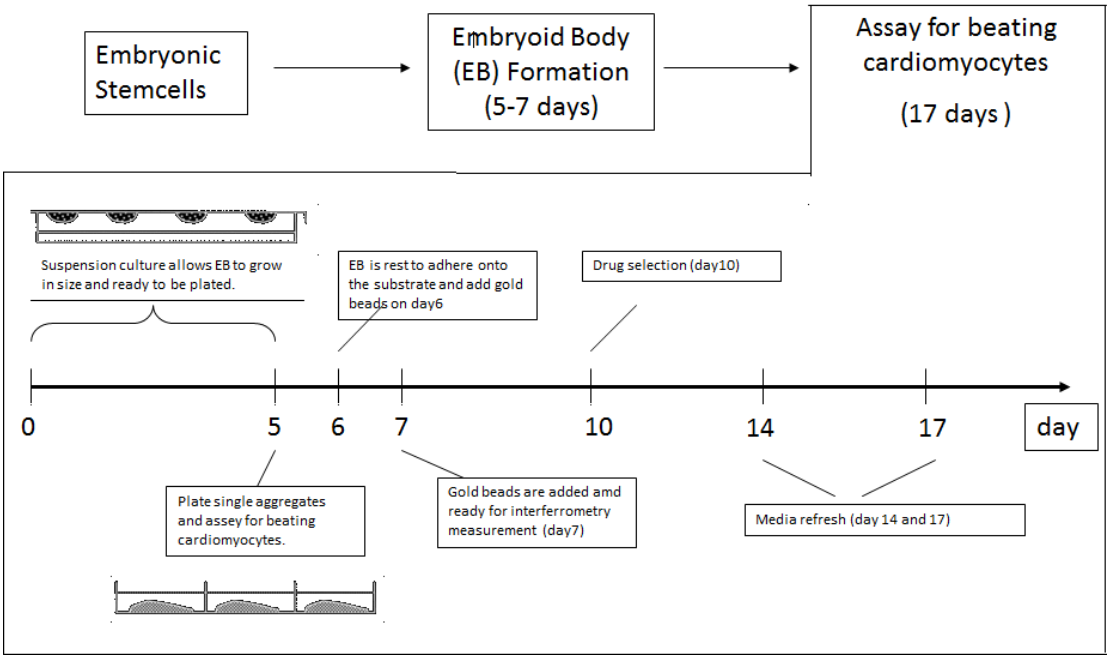

Fig 5.3 Schematic and timeline of differentiation of mouse cardiac stem cells to cardiomyocytes.

*(ii) Preparation of neonatal cardiomyocytes***.**

Neonatal hearts were dissected, washed in a Hank's balanced salt solution (HBSS), and bathed in 0.5 mg/mL trypsin-HBSS overnight at 4ºC for pre-digestion as previously described [29]. Non-adherent cardiomyocytes were then plated onto a silicon dice coated with 10 µg/mL fibronectin at 75% confluency prior to co-culture with ES-derived cardiomyocytes (for full details see [28]). The samples were kept in an incubator at 37 °C, 5% CO_2 and were taken out for interometric measurements. Media exchange was done every two days during the experiment.

5.2.2 Live Cell Interferometry (LCI) and Mechanical Imaging Interferometry (MII)

Interferometry is a powerful instrumental method for measuring displacement, surface topography, and changes in refractive index by observing the interference pattern of coherent light due to the difference in path length. Originally used in astronomy, the technique has been widely deployed in optical profilometry of Microelectromechanical systems (MEMS)[30], thin films, hard drive. Interferometric measurements are relatively quick (~1-2s) and provide sub-nanometer accuracy in displacement measurements [31]. The interferometric optical profilometer enables wide-field imaging of samples while retaining nanoscale resolution in the vertical direction (see chapter 2). Recent operational demonstrations in liquid environments have thrust this emerging technique into the forefront of high-throughput, non-contact methods for structural and mechanical characterization in fields ranging from physics and engineering to the chemical and biological sciences.

Efforts toward obtaining insight into fundamental biomechanical phenomena at the cellular and organismal level are gaining more attention as changes in cell morphology, motion and mechanical rigidity[32] have been related to strain, changes in environment and shift in disease states [31],[1, 3]. And some biomechanical property were utilized as a key index to therapeutic responses [33] . Additionally, cellular mechanical measurements may help us understand the development of many biological systems such as the development of embryonic stem cells to become cardiomyocytes. In past decades, many established techniques for cellular mechanics such as AFM [34] and optical particle tracking [35] were developed to explore cell mechanics. However, they required a highly complicated setup and are limited to single cell measurements, rendering them less attractive in clinical studies. To address these limitations, modification of an imaging interferometeric optical profiler has recently enabled high-throughput

optical phase-shift interferometry and fluorescence microscopy for real-time 3D imaging of live-cells. This technique is known as Live Cell Interferometry (LCI).

In addition to a normal interferometric optical profiler, reference mirror and fluid cells with matching glass cover were integrated into the system for measurement in liquid (fig 5.5). By measuring changes in optical path length distribution across many points within the cell simultaneously, LCI can determine the redistribution of cellular structures and profile of biological sample clearly and spontaneously. Other than high-throughput imaging, Live-Cell Interferometry also offer other advantages over AFM and optical particle tracking such as real-time rapid response in measurement[36], higher accuracy[36, 37], simplification in sample preparation and less cell disturbance.

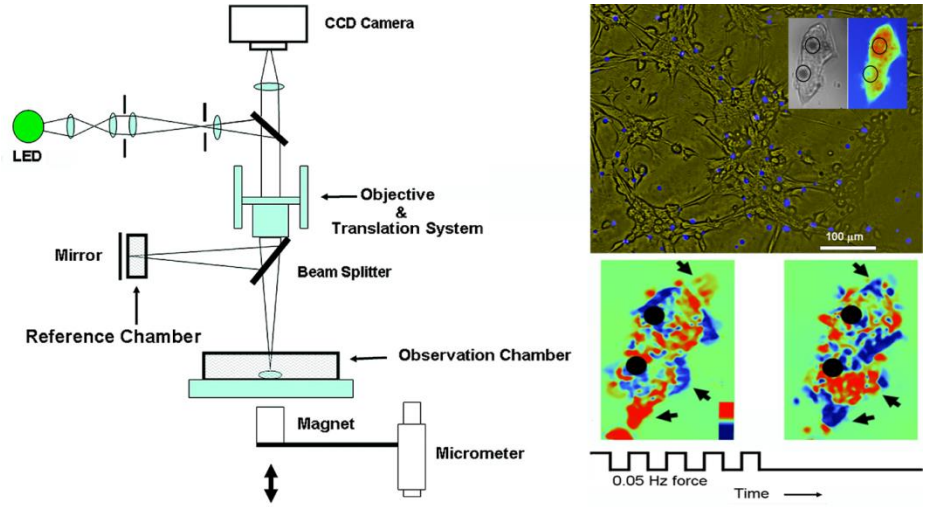

Fig 5.4 Intensity and overlaid interferometric images of live NIH 3T3 fibroblasts acquired at 10× magnification (upper right) showing the simultaneous detection of magnetic microreflectors and a single cell with two magnetic microspheres on the cell surface (inset) [32]. Differential LCI comparison of cell material

distributions after t=200s of cyclically applied force and at t=200 s after cessation of force. Arrows denote regions of material redistribution within the cell [31]

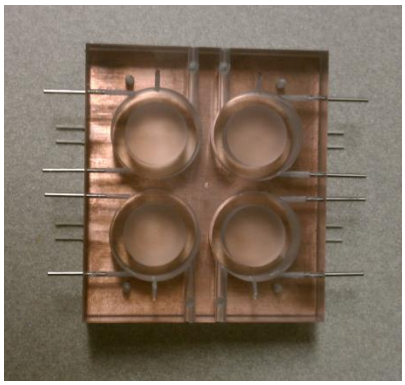

Fig 5.5 Observation chamber and built-in fluid cells to host samples. The fluid cells are usually connected to a pump that cycle media with 5% carbon dioxide infused within to accommodate live cells. This setup allows live cells to survive inside the chamber up to many weeks.

Modification of the interferometric optical profiler has enabled the mechanical observation of biomaterials including cells, tissues and small organisms through Mechanical Imaging Interferometry (MII)[36]. The MII method uses a combination of optical phase-shift interferometry, fluorescence microscopy, and quantitative force spectroscopy to directly monitor the individual cellular response to chemical or mechanical stimuli in a massively parallel fashion. In this mode, magnetic microreflectors are placed on the sample (i.e., on the cell membrane) to enhance reflection of light from the profiler and help improve the resolution of mechanical vertical displacement or change in cell thickness. This technique allows us to directly monitor the natural contractile motion of cells and organisms when they respond to an inducer or a change in their environment. MII can capture these responses accurately and rapidly while offering a series of real-time 3D images over periods of time ranging from minutes to weeks.

In the MII method, surface adherent magnetic micro-reflectors can also be used to deliver controlled mechanical forces to the sample using an external magnetic field. Real-time detection of the position and displacement of individual magnetic micro-reflectors over a wide field of views provides indentation profiles similar to those acquired by force-spectroscopy using the atomic force microscopy (AFM), thereby enabling the parallel, quantitative determination of modulus and viscoelasticity, as well as observation of cell dynamics such as force-induced cytoskeletal remodeling. By this approach, both static and dynamic stimuli can be used to mechanically stimulate the cells over a wide range of forces (20pN-20nN) and frequencies (1Hz-100kHz). Examples of this method include mechanical indentation on Matrigel and polyacrylamide gel films can be used to estimate the Young's modulus of the Matrigel film[38] and polyacrylamide gel, NIH3T3 Fibroblast [36]

5.2.3 Application of force through magnetic beads

Micro magnetic microspheres (UMC4N) were obtained from COMPEL-Bangs Laboratories, Inc. These beads are nickel beads with diameter of 8 um. Before the experiments, they were coated with gold by a sputterer (see chapter 2) to reduce toxicity and increase the biocompability with cell samples. The optimum thickness of a gold layer for this application was determined to be around 100nm. After completing the toxicity test of the beads on stem cell samples – both human hPSC and mouse ESC, the force induced by these beads were calibrated on a cantilever array. First a cantilever was dip-coated into the bead dispersion (fig 5.6a). The beads should be attached and stick onto the cantilever. It was crucial that only one cantilever in

the array was coated, and there was a clean and uncoated cantilever next to the coated cantilever for reference imaging (fig 5.6b).

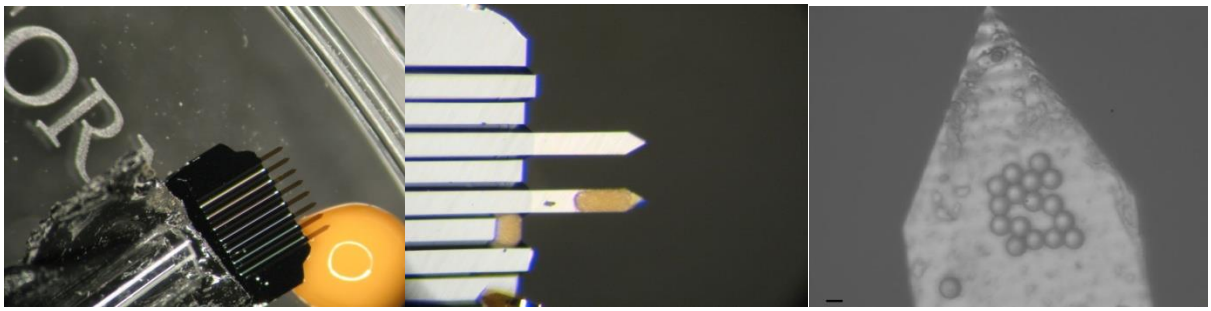

(a) (b) (c)

Fig 5.6 coating of nickle micro magnetic beads on microcantilevers for force calibration

For the calibration purposes a monolayer of beads were required because the beads had to be visually countable under the optical profiler (fig 5.6c). However, this could be hard to achieve since the dip-coating technique resulted into mutilple beads layers on a cantilever. The excess beads were washed off carefully with ethanol to achieved a monolayer of the magnetic beads as show in fig 5.6c.

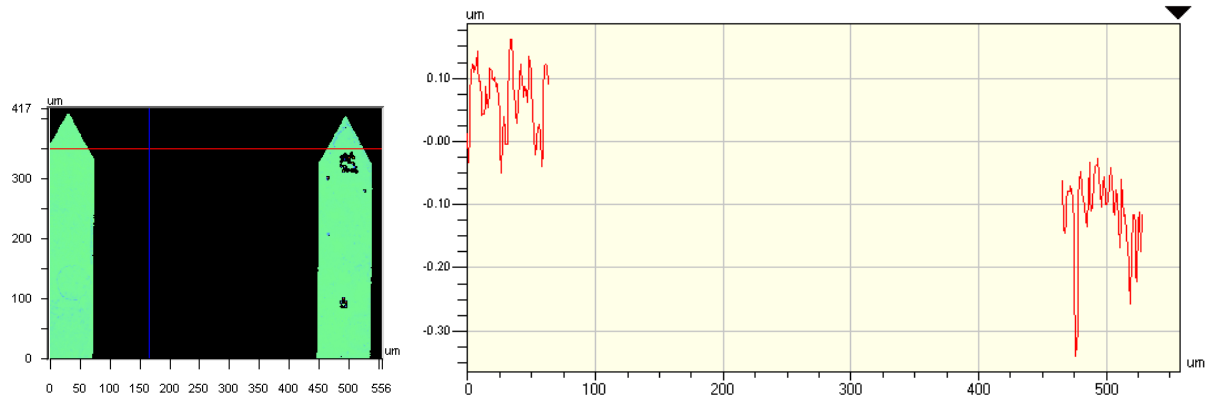

Fig 5.7 height profile of a cantilever with magnetic beads coated with respect to the adjacent non-coated cantilever. Left picture shows the lay out of the two catilever. Right picture shows the profile and actual measurement of the two cantilevers under optical profiler.

Next the cantilever with bead and the adjacent clean cantilever were viewed together under the optical profiler. After placing the cantilever arrays under the optical profiler, a height profile (fig 5.7) was recorded subsequently as a magnet was moved closer to the cantilever. During this process, the cantilever with magnetic beads was bent by magnetic force while the clean cantilever stayed unbent (fig 5.8). The difference in height profile between the bent and unbent was quantified and used to calculate the force induced on the cantilever.

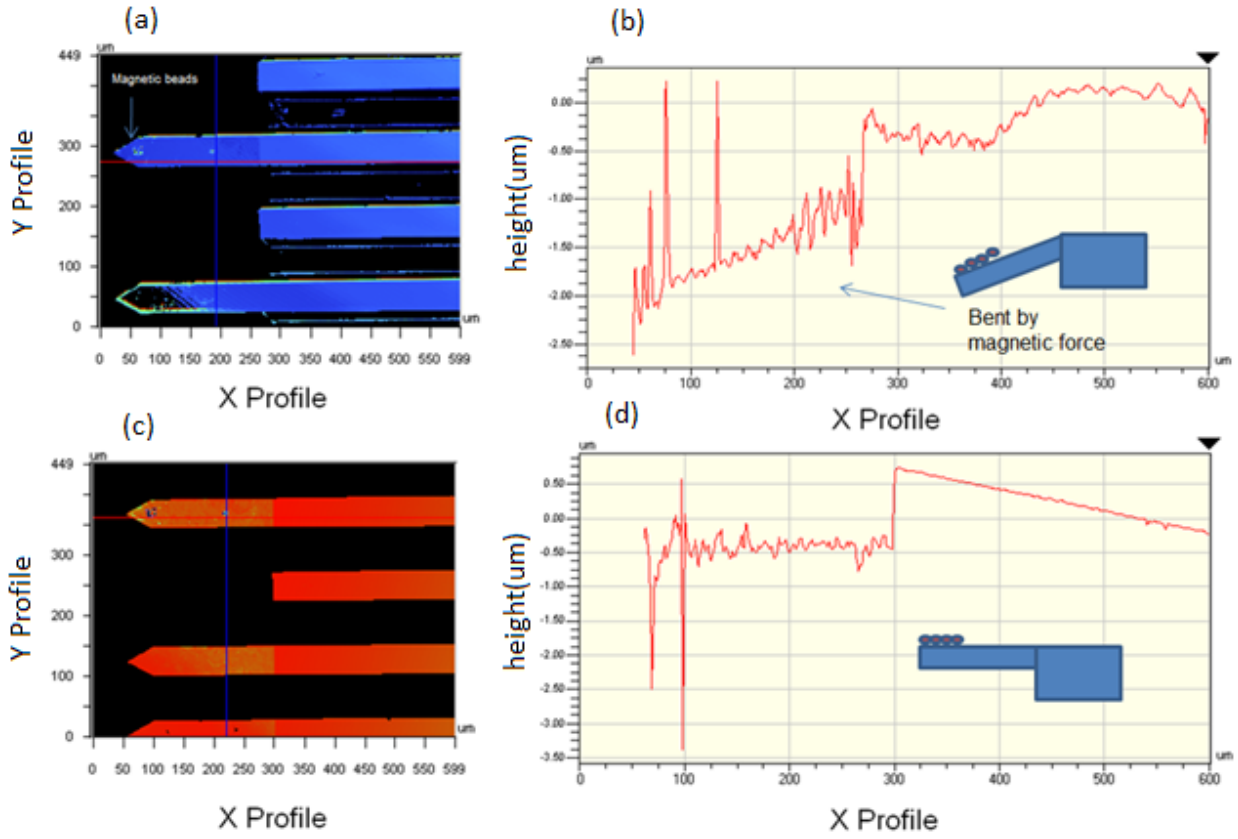

Fig 5.8 Bending of cantilever with magnetic beads in the presence of magnetic field. The optical profiler displayed X and Y profile of cantilever arrays with beads coated in the presence of a magnet (a) and without the magnetic field (c). (b) shows the height profile along the x-direction (red horizon line) of the coated cantilever and illustrate bending of the cantilever when there is magnetic field. (d) shows the height profile along the x-direction (red horizon line) of the coated cantilever and illustrate that the cantilever was not bent when the magnet was removed.

The force approximation was done simply by using newton's law (cantilever's spring contant = 0.07 N/m). The calibration curve from these measurement is shown in fig 5.9. This gives us a good sense on the amount of force applied on the sample controlled by spatial separation between the beads and the magnet. In this case, we determined the force that can be applied per one bead to be within a range of 0.05-9.09nN

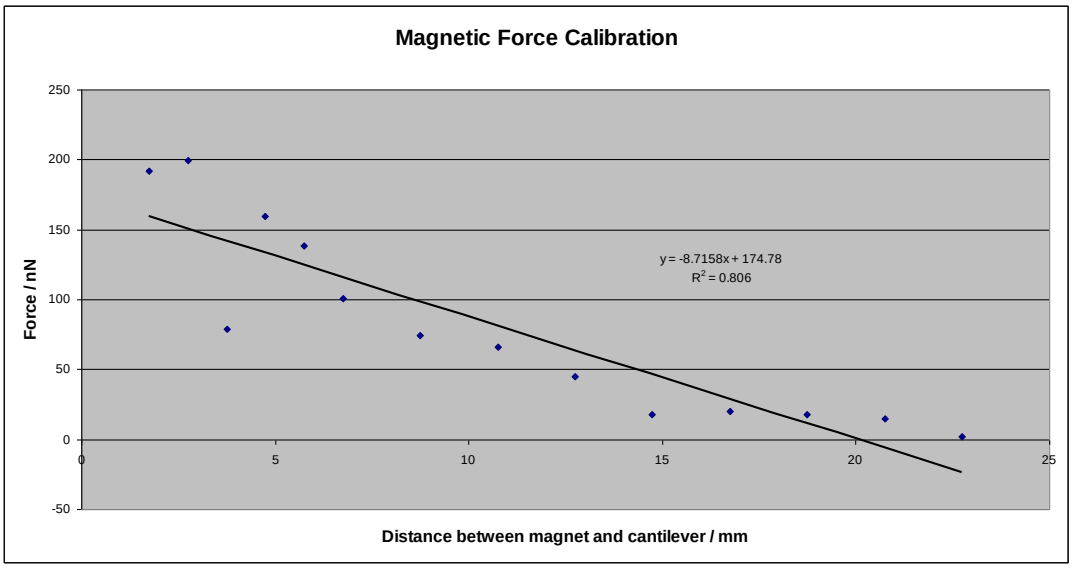

Fig 5.9 force calibration curve from magnetic beads and magnet.

After the calibration of force was completed, we focused on manipulation of force pattern to mimic a heartbeat. Since we hypothesized that force could influence the differentiation of stem cells to become heart cells, a force pattern similar to a heartbeat was more interesting to be applied to the cells. To achieve the desired dynamic force, an alternate magnetic field was manipulated with a device built to control the frequency and period of the magnetic field (fig 5.10). By inserting a magnetic shielding material, mu-metal, between the magnet and the beads,

magnetic force was minimized. For our experiment, we designed a mu-metal disc with a gap to rotate in between the magnet and the beads (fig 5.10 right). When the hole on the mu-metal disc was aligned with the magnet, the magnetic field from the magnet can exert a force on the beads. However it was blocked otherwise. By controlling the spinning rate through the voltage supplied to the motor, we can essentially control the force pattern with the desired frequency (fig 5.11).

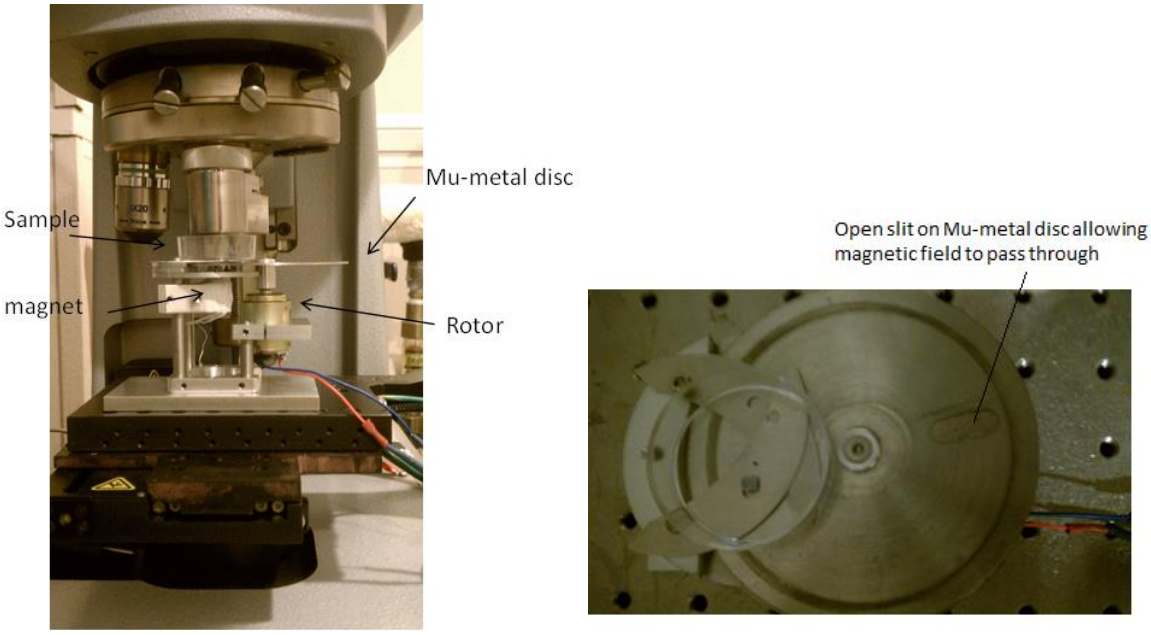

Fig 5.10 apparatus designed for magnetic field manipulation. Left is a side view of the equipment. Right is the top view of the equipment.

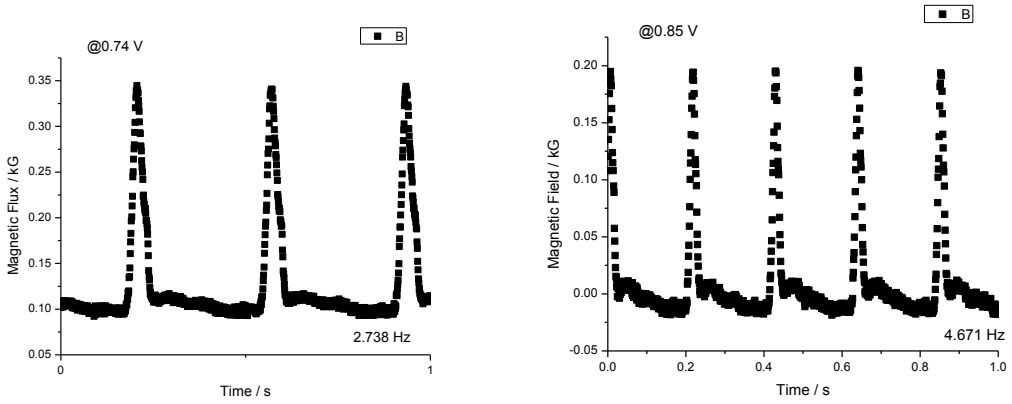

Fig 5.11 Magnetic field observed on a Tesla meter through the device in fig 5.10. Frequency of the field varies with the voltage supplied on the motor to rotate the mu-metal disc. The frequency of the field can be adjusted, and is preferred to be similar to a heartbeat (1Hz)

5.2.4 Measurement of pluripotency through florescent microscopy

Fluorescent microscopy has been used extensively in biological research. The hPSC cells we received express OCT4-green fluorescent proteins (GFP) which can be used as an indicator of cells' pluripotency. We designed our experiment by observing the green fluorescent intensity level from the cells as an indication for pluripotency. When combining this information over time as force is being applied, green fluorescent intensity monitoring can help us understand whether forces affect the differentiation of these cells.

To measure the green fluorescent protein, we used "Zeiss LSM5 Confocal Fluorescence Microscope" equipped with a filter for 448nm wavelength allowing us to observe green fluorescent protein. It has an advanced analysis program to collect and identify the GFP intensity allowing user to select the region of interest on the sample, as shown in fig 5.12. For our analysis, a selected region of the sample was imaged twice. The first image was done on the

microscope without the flurescent filter. And the second image, which was the fluorescent images of each sample, was taken with a green fluorescent filter. These two pictures of the same region were viewed along each other for comparison and helped us to identify accurately the position of hPSCs. This was to assure that the intensity observed corresponds to the pluripotency from these cells and was not random noise background.

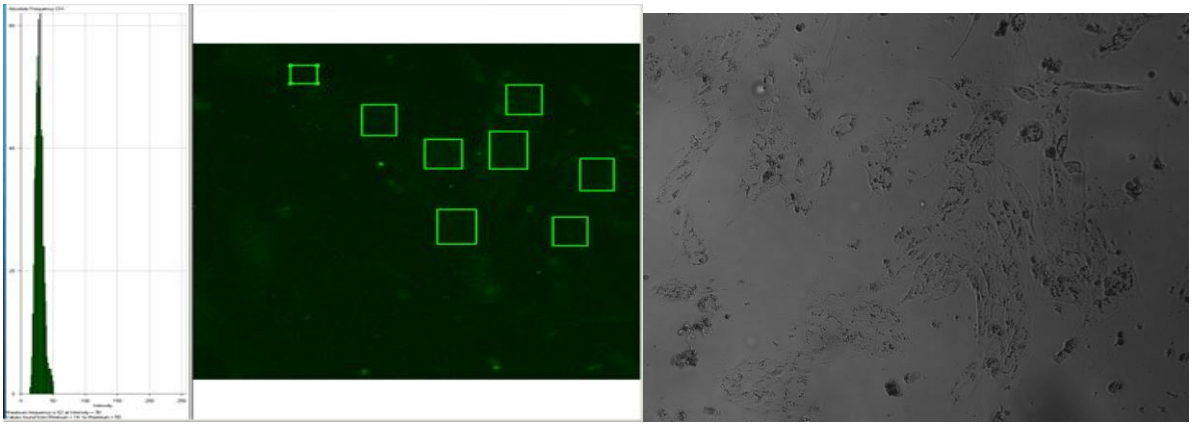

Fig 5.12 Determination of green fluorescent protein intensity. A normal picture of hPSCs (right) is viewed along to fluorescent picuture (left) to assure the presence of cells.

Usually for a sample of hPSC, 10-20 images were taken. In each image, we collected intensity from 10 regions by specifying a region of interest. As shown in fig 5.12, after the 10 regions were specified, the program computed an intensity histrogram shown on the left of fig 5.12. We then collected this information anded perform gaussian curve fitting for the value of intensity and standard deviation.

5.2.5 Fabrication of electrical pulsing platform

To stimulate and apply electrical pulses to stem cells, we fabricated a chip with platinum electrodes (fig 5.13). The substrates that we deposit platinum layers to create the chips on were both silicon and glass. However for visualization purposes, glass substrate were more preferred

because it allowed observers to see the development of cardiac stem cells (e.g., beating) through a microscope. The fabrication process started with growing a 500 nm oxide layer of thermal oxide in wet conditions at 1100 °C. Then the wafers were treated with Hexamethyldisilazane (HMDS) to promote adhesion, and coated with 2µm thickness of a negative resist nLOF 2020 on a SVG 8800 track coater. The resist was later developed in MF 26A and water.

Once the substrate was prepared and ready for electrode deposition, a 50 nm Chromium wetting layer was deposited at 0.5 nm/s, followed by a 150nm layer of platinum, deposited at 0.5nm/s in a CHA mark 40 deposition chamber. The lift off process was completed by submerging the wafers in AZ300T stripper. After the lift off, we obtained a chip with 12 electrodes. This chip is capable of running 4 individual experiments separately after being separated into 4 different wells using material such as SU8 or PDMS to create boundaries thick enough to maintain the stem cells.

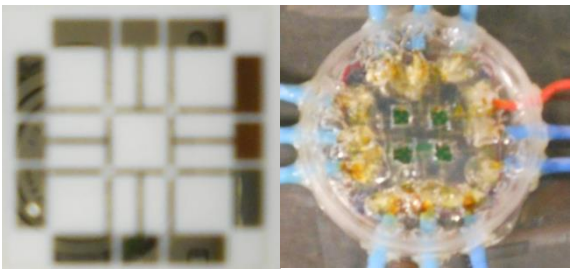

Fig 5.13 A chip for electrical pulsing: platinum electrodes on a glass substrate (left). A wired chip placed inside a 3.5mm culture dish, coated with PDMS to create 4 wells ready to host stem cells (right).

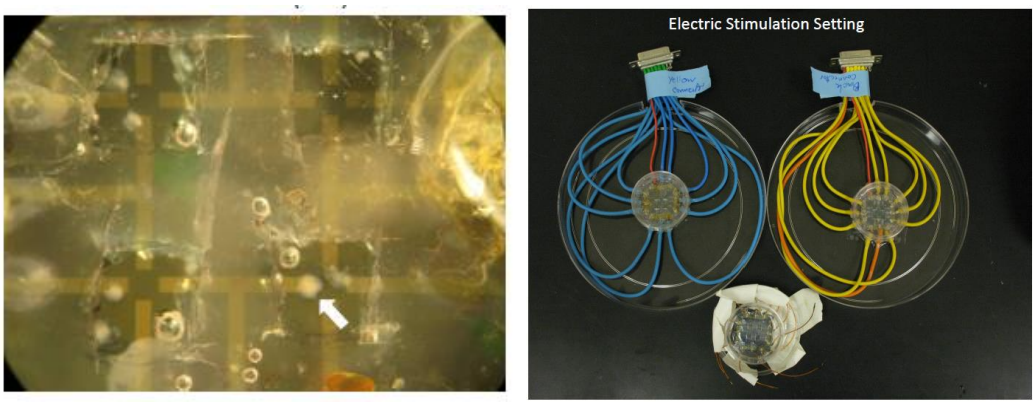

Fig 5.14 closed up of a chip with EB showing four individual wells (left). Pulsing platform and equipments ready for plug-in (right)

These chips were later wired, connected to a 15-pin socket and plugged into a SWU and multiplexer to provide the desired current to each well as input on the LabVIEW program. On the LabView program, we designed to apply bi-phasic pulse (see fig 5.16) into each well on a chip. This is to balance the charge applied to the cells and avoid an accumulation of charge that can interfere with the cells' growth. As the SWU switch was sorting current into each well, it continuously increased voltage until the observed current reached the target current (i.e., 10 and 15 µA). The voltage limit was set to be just below 0.9V to prevent the hydrolysis of water, which can cause cells' death. The LabView program controlled the switch and the circuit to apply a desired pulse, according to the input parameters, into each well in turn until all four wells were pulsed. We performed pulsing on stem cells using 3 chips (total of 12 wells) with one chip designated to hold the controls.

5.3 Experimental procedures

The experimental procedures for all four aspects (refer to section 5.1) in this study are discussed and explained in this section separately.

5.3.1 Force enhanced survival of human pluripotent stem cells (hPSCs)

In this part, we focused on a survival of hPSCs after being dissociated from a colony. It is interesting that human stem cells experience apoptosis (cell death) when dissociated into individual cells. Many believe that the physical contact and compacted force with other cells may be required for them to grow properly. We then seek to investigate the impact and the effect of force by initially dissociating the hPSCs using ethylenediaminetetraacetic acid (EDTA) to remove calcium ions, which are necessary for adhesion proteins. The cells were plated on a 2x2 cm^2 silicon substrate and placed in a fluid cells designed for LCI measurement (fig 5.5). This was to enhance visualization and reflection required by LCI. By applying 2 mM of EDTA in media solution, the dissociation of cells was observed, followed by apoptosis. LCI has high enough resolution for observer to observe "blebbling" of cells occurred during the apoptosis. We planned to study the effect of magnetic force provided through the magnetic beads by applying anti-hPSCs coated magnetic beads onto the cells. These beads should coat on the cell membranes evenly and provide magnetic force acting on hPSCs in the presence of a magnet. By applying force during the dissociation of a hPSC colony, we might be able to prove that the cells survive longer when force is applied to mimic the compacted condition in a colony. This can be achieved from looking at the thickness and separation of cells as a function of time using the LCI technique.

5.3.2 Measuring cardiac rhythms

Using MII significantly improved the quality of cariomyocyte images and let us observes small beating more easily than using conventional techniques normally used to observe cellular motion such as M-mode echocardiogram; This means motions which are not detectable by M-mode echocardiogram can be observed with MII technique. MII also provide high contrast of images during the measurement, and hence microscopic and nanoscopic motions that may happen at an early stage of the development were detected. It is advantageous to be able to monitor the initiation of the motions.

The preparation of cells for MII experiment started from obtaining embryonic stem cells from mice. Then from these cells, embryoid bodies were formed and placed in hanging drops for five days for them to grow (see 5.2.1(a)). Subsequently, neonatal cardiomyocytes were acquired from a young heart. They were prepared and plated on a fibroblast-coated silicon substrate. After that the stem cells were plated on top of the neonatal cardiomyocytes before addition of gold coated magnetic beads. The cells were kept for a day before an observation with the MII technique occurred. To ensure that the cells were in the best condition, they were kept in an incubator at 37 °C with 5% CO_2 all the time. The measurement was limited to 15 minutes in the flow cells, and the conditions during the measurements were best kept to be similar to the conditions in the incubator.

During the measurement, MII technique was used to view vertical motions of the cells by observing the changes and contrast in the intensity of the cells as they moved. The gold beads attached on the cell membrane provided higher contrast since they were much more reflective than the cells; hence, it is a good reference point to extract a data from in our analysis. The data

was then processed through the MATLAB algorithm created for MII analysis. A graph representing the vertical motions as a function of time was created. Frequency and amplitude of the motions can be estimated from this graph and analysis if necessary. The synchronization of beating neonatal cardiomyocytes and mESCs were later interpreted.

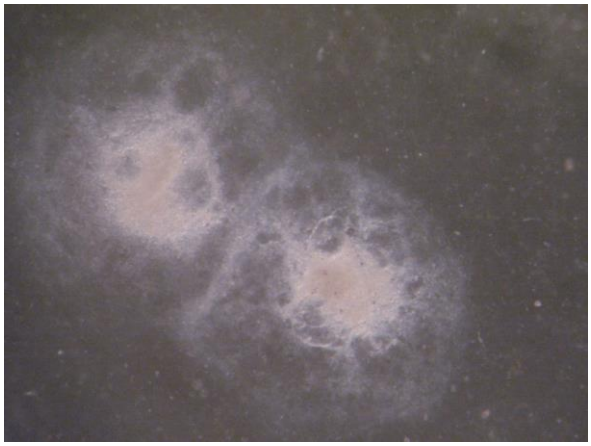

Fig 5.15 mouse stem cell colony with gold coated magnetic beads

5.3.3 Force directed differentiation of stem cells

A two-week experiment on hPSCs was performed after the cells were plated for 2 days. During this time, the cells were kept in an incubator to maintain optimal conditions. The cells were only taken outside the incubator for OCT4 fluorescent measurement for less than 15 minutes at a time. For measurement on each image, the green fluorescent intensity was normalized with the intensity collected from a "blank" sample containing only feeder cells. The samples were separated into four groups. The first two were controls, and the other two were

added with 5uM and 15uM of growth factor protein SB431542 (SB) to drive the differentiation of the cells towards mesoderm. After measurement of OCT4-green fluorescent intensity (GFP), a curve of GFP intensity over time was created. The decay of GFP intensity indicated a characteristic and kinetic of the differentiation, which is unique for development of certain cell types (i.e., ectoderm, mesoderm).

After establishing a standard curve for differentiation, the experiment was repeated again with force application. The cells were separated into three sets: control, hPSCs with gold coated magnetic beads (no magnet), and hPSCs with gold coated magnetic beads on top of a magnet. The last set represented a set of cells under the influence of magnetic force through the attraction between the beads and the magnet. The distance between the cells and the magnet was roughly 1.5 cms. The cells were monitored with the same fluorescent microscope to determine GFP intensity. For the set with the presence of a magnet, only a selected region of cells (~1x1cm^2) was marked and kept under the influence of the magnet. Similarly, a graph of GFP intensity in the time domain was created for this experiment for further interpretation.

5.3.4 Electrical pulse directed differentiation of stem cells

For this experiment, human embryonic stem cells were made into embryoid bodies and later plated on the chip with electrodes fabricated in (see section 5.2.4). One chip has four individual wells, and each one contains five embryoid bodies in it. Currently, we run experiments with three chips being pulsed. One of the chips was solely kept as a control. The pulse used was designed to be bi-phasic with the frequency of 1Hz to counteract and cancel charge applied on the sample to maintain the neutral charge condition.

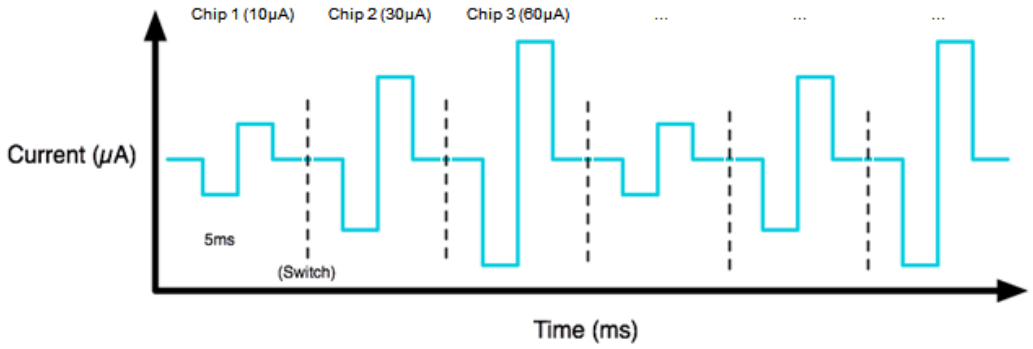

Fig.5.16 an example of bi-phasic pulse applied to the cells.

Cells on two chips were pulsed galvanostatically with the current of 10 μA on one chip and 15μA on the other. Each chip was pulsed for 20 ms at a time in turn throughout the entire experiment. During pulsing, the cells were kept at 37 °C and 5% CO_2 in an incubator for four days. The media was exchanged every two days to ensure the best condition for cells to grow. In addition to pulsing, we designed an algorithm to read any change in voltage, which may cause by cell movements, in the sample every two hours. This function will hopefully help to identify any development that cannot be visualized yet. After the termination of experiment, the cells were collected and analyzed by a quantitative polymerase chain (qPCR) machine to detect a gene expression profile of the cells. For this experiment, we were interested in three cardiac genes: Alpha-myosin heavy chain (MHCa), beta-myosin heavy chain (MHCb) and Troponin T type 2 (tnnt2). MHCa and MHCb represent the gene found in mature and immature cardiomyocytes respectively. Tnnt2 is a cardiac gene involve in muscle contraction. After the gene expression profile was determined, we compared the results with respect to the data of the control and interpreted the observation.

5.4 Results and discussions

The results of the experiments described in section 5.3.1 to 5.3.4 are discussed in this section.

5.4.1 Force enhanced survival of human pluripotent stem cells (hPSCs) using LCI

After observing and imaging hPSCs with LCI developed in our laboratory, the structure and shape of hPSC cells were visualized and seen clearly with high contrast under an optical profiler equipped with LCI technique.

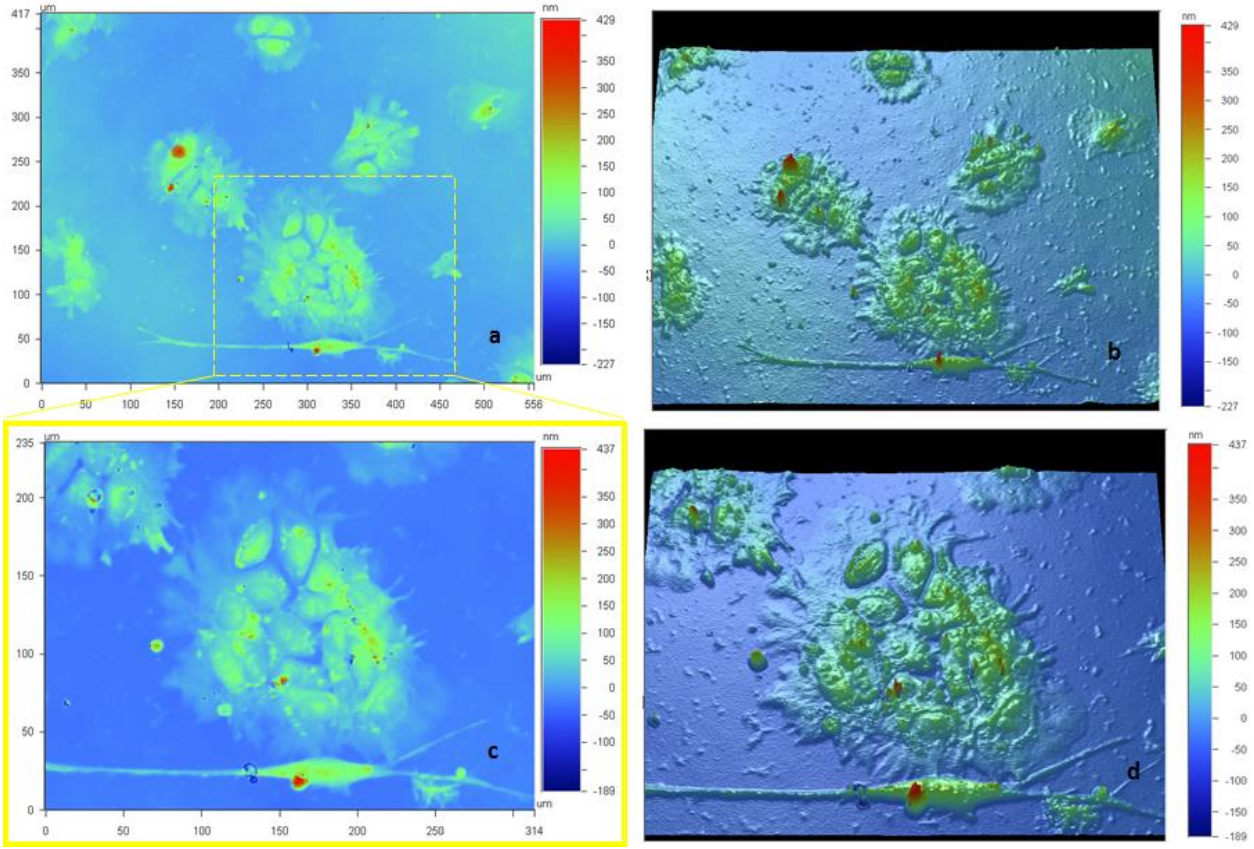

Fig 5.17 LCI images of hPSCs. a) broad view 2D images. b) 3D constructed image of (a). c) a zoom in of a colony of hPSCs to illustrate high contrast from this technique. As shown in this picture, boundary of cells and their nuclei were observed clearly. d) 3D constructed image of (c).

After optimizing the conditions and parameters on LCI for hPSCs, we dissociated a cell colony with EDTA under the optical profiler. With LCI technique, cellular structures were revealed very clearly (fig 5.18) in detail. In fig 5.18a, a colony of hPSCs was initially observed with LCI before dissociation in fig 5.18b. Before dissociation, normal healthy cells were relatively flat and had expanses as expected. After dissociation, the cells bulged up and increased their height. Then they separated from each other. In this case, LCI provided a detailed height profile such as height of the same cells over time (fig 5.18d). Since the height could be used to indicate the degree of dissociation, the information in fig 5.18d may help to identify the kinetics of the dissociation.

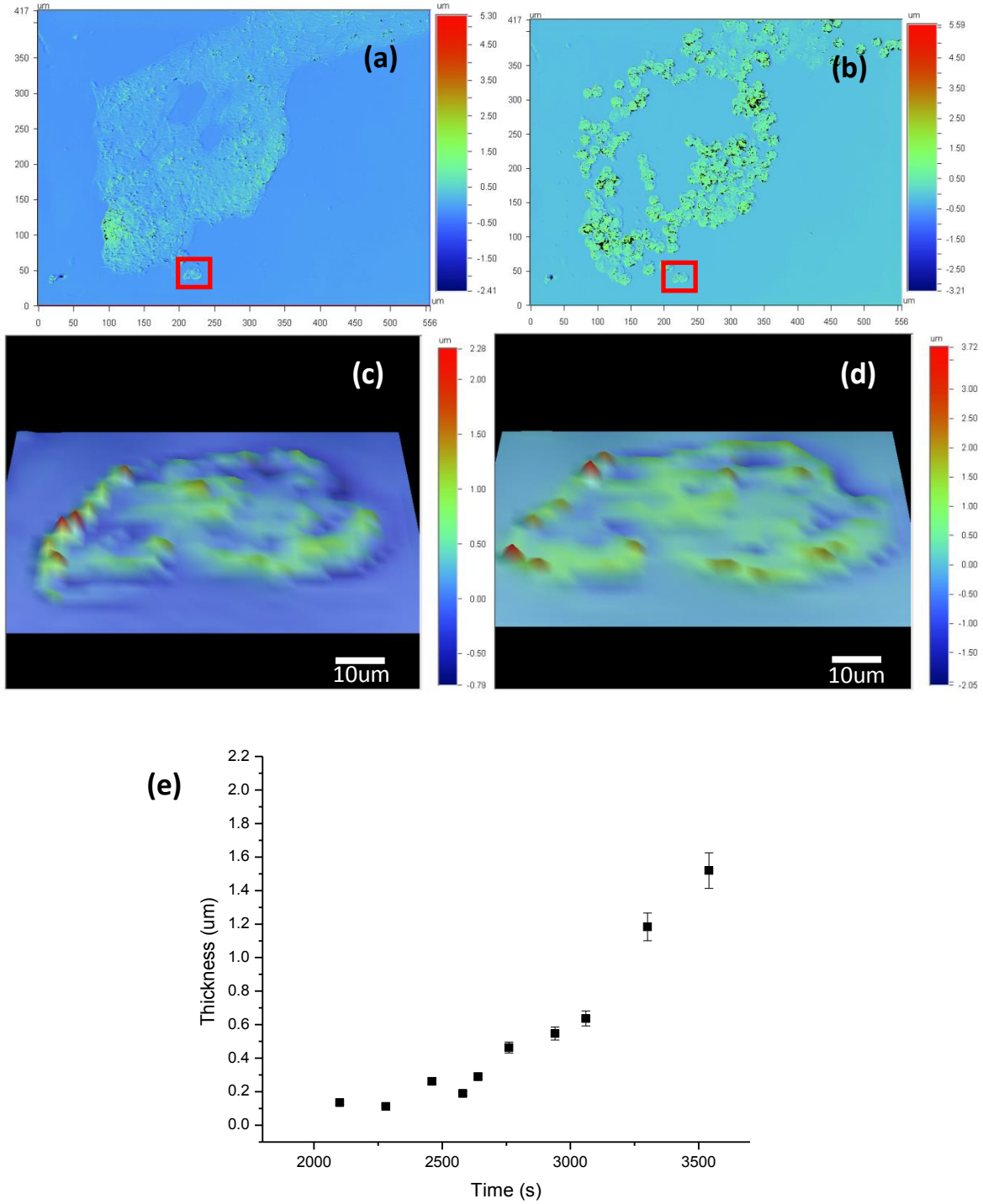

Fig 5.18 Illustration of apoptosis of pluripotent human stem cells using LCI (a) broad view of pluripotent human stem cells before and (b) after treated with Ethylenediaminetetraacetic acid (EDTA). EDTA removes Ca^{2+} and caused

From this type of measurement, character or kinetic of the dissociation can be established. For example, certain constants can be extracted with appropriate curve fitting. In turn, once we apply magnetic beads and magnet in the system to introduce force, a cell thickness vs time with different character (e.g., slope, fitted constant) is expected. There is also a potential that the cells may not dissociate in the presence of EDTA and force provided that the right conditions are applied. However, interpretation from the thickness in time domain should reveal the impact of force on proliferation of hPSCs.

5.4.2 Measuring cardiac rhythms

There is a theory stating that when one cardiac stem cell starts to beat, it influences the surrounding cells in the same colony to differentiate and beat together, similarly to a chain reaction; consequently, the whole colony would eventually beat together in synchrony with the same frequency. This model emphasizes that the cells usually start beating individually; they are not beating in synchrony at the beginning. However, after some time all the cells that are in the same colony are synchronized. This theory also implies that the adjacent movement should have a great influence on the movement of the differentiated stem cells

MII was used for this part of the study to measure cellular motion over a long period of time. In our experiment (see 5.3.2), we were interested in confirming the idea above experimentally. In particular, the effect and influence of substrate used in the cell culture on the differentiation of stem cells was our focus. Many works performed experiments using stationary substrates with different stiffness (e.g., PDMS), but only few research experimented with moving substrates. Since the development of cardiomyocytes from cardiac stem cells involves the

initiation of the motion, we hypothesized that a dynamic substrate would influence the stem cells to move along with it; hence the differentiation can be initiated more efficiently by inducing motion on the cells. We applied MII to track the vertical motion of already beating embryoid bodies before and after being plated on beating neonatoal cardiomyocytes. This was to show if the motion of neonatal cardiomyocytes had an influence on an embryoid bodies plated on top or adjacent to them. After digital recording was done, we selected two regions of interest: one covered a neonatal cardiomyocyte and the other covered an adjacent embryoid body (fig 5.19). Then, the images and videos recorded by MII technique were processed with the MATLAB algorithm to generate a motion profile as a function of time (see fig 5.20 and fig 5.21) based on the regions selected.

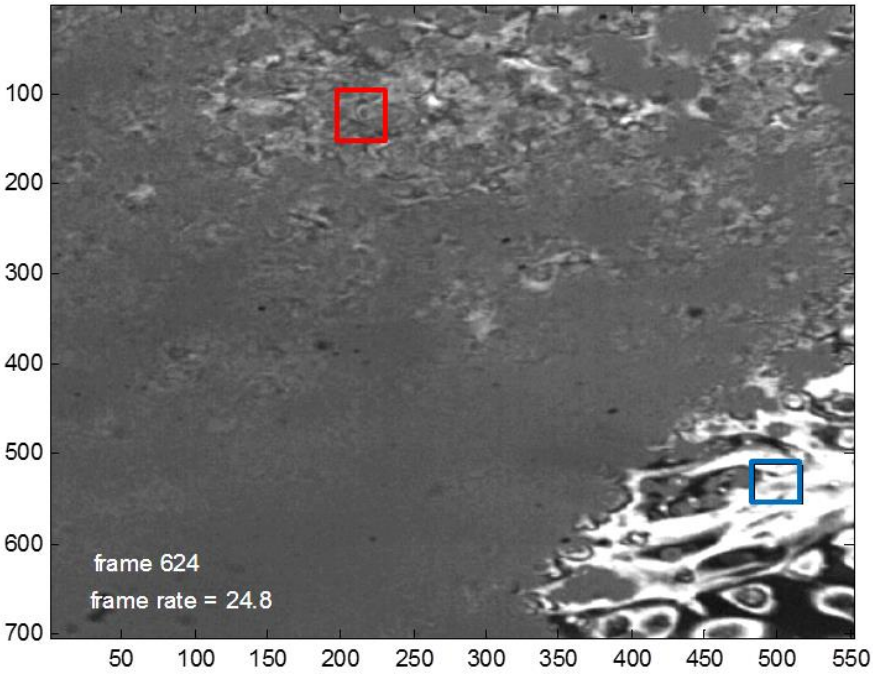

Fig 5.19 Embryoid body of mESCs plated on top of cardiomyocytes. Two selected regions were chosen to represent the movement of an embryoid body (EB) (red) and an adjacent cardiomyocyte (blue)

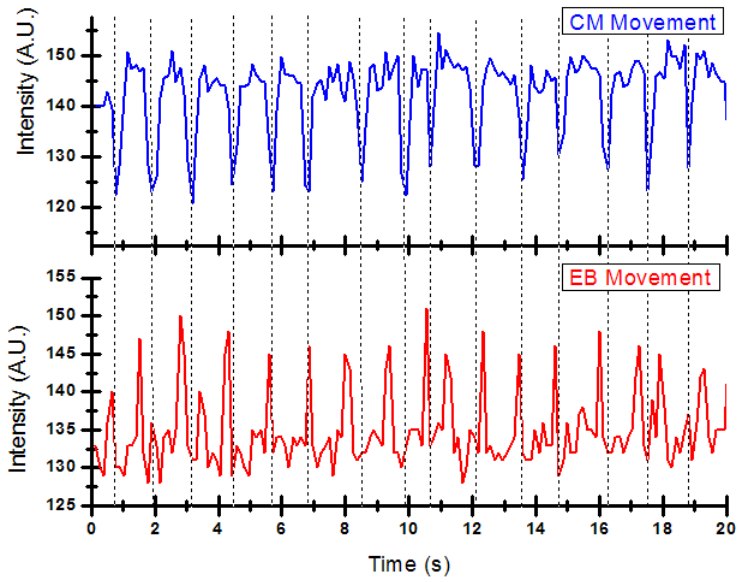

Fig 5.20 Beating of an embryoid body (EB) (red) and an adjacent neonatal cardiomyocyte (blue) at early stage before synchronization

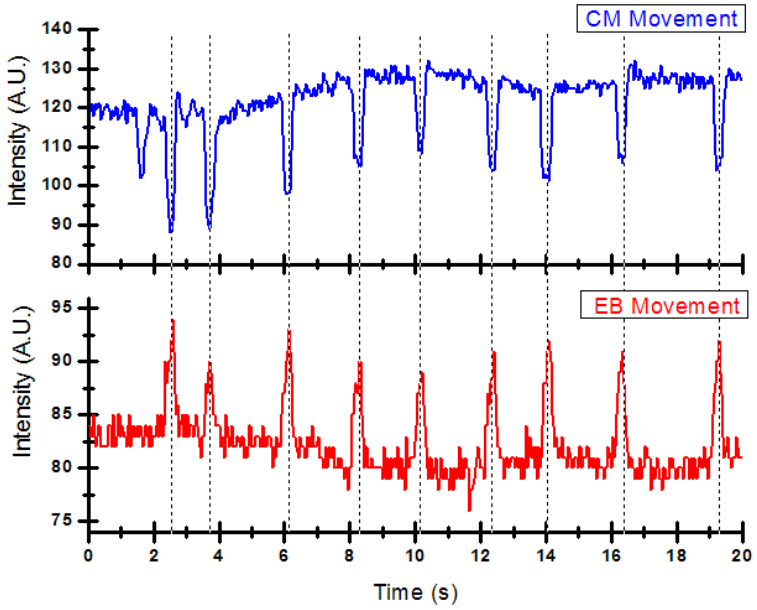

Fig 5.21 Beating of an embryoid body (EB) (red) and an adjacent cardiomyocyte (blue) several day after plating. Both of them became synchronized and beating together.

On the first day after the embryoid bodies were plated on neonatal cardiomyocytes, the beating of the embryoid body and the neonatal cardiomyocyte selected was shown in fig 5.20. As we can see that the beating between the embryoid body and the cardiomyocytes was not synchronized. The influence of neonatal cardiomyocytes on embryoid body was illustrated in fig 5.21, which represents the signal taken two days after. As we can see that the beating of the embryoid body matches perfectly to the motion of the neonatal cardiomyocytes. This finding confirms the idea that dynamic substrate would influence the embryoid body to move with it at the same frequency. Based on our results, we have modified and create a system capable to investigate the differentiation in detail. In the future, it will be interesting to understand the mechanism or the kinetics of the adaptation of stem cells to the external motion applied on it. Also with this platform, a natural motion of embryoid bodies during the differentiation can be recorded and use to create a pattern of force suitable to use to direct the differentiation.

5.4.3 Force directed differentiation of stem cells

In this part of the study, human pluripotent stem cells (hPSCs) with OCT4-green fluorescent protein (GFP) expression were used. We were interested in using this green protein as a key parameter since it represents the pluripotency of the hPSCs. We calibrated a fluorescent microscope for the GFP measurement by setting up a filter corresponding to the green wavelength (λ=488nm) to observe this protein. By comparing two pictures of a sample using white light and green filter, pluripotent cells were seen and identified. For example, fibroblast or other artifacts (red boxes) in the sample were seen only by a normal microscope but not fluorescent mode as we can see in fig 5.22.

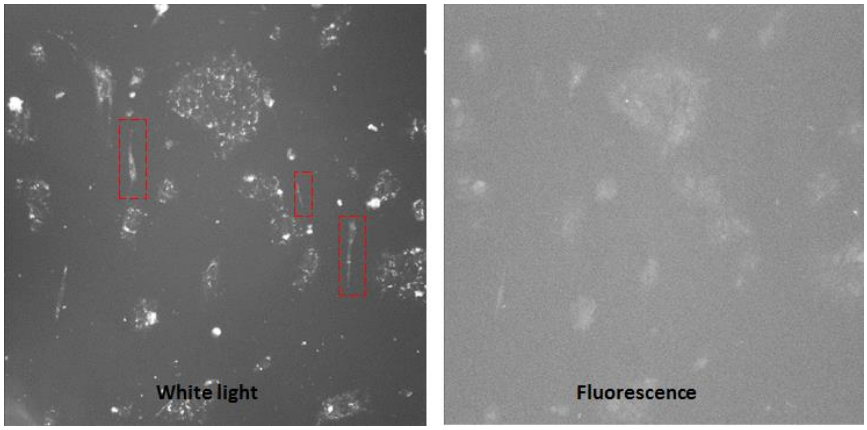

Fig 5.22 hPSCs under optical(left) and fluorescent(right) microscope

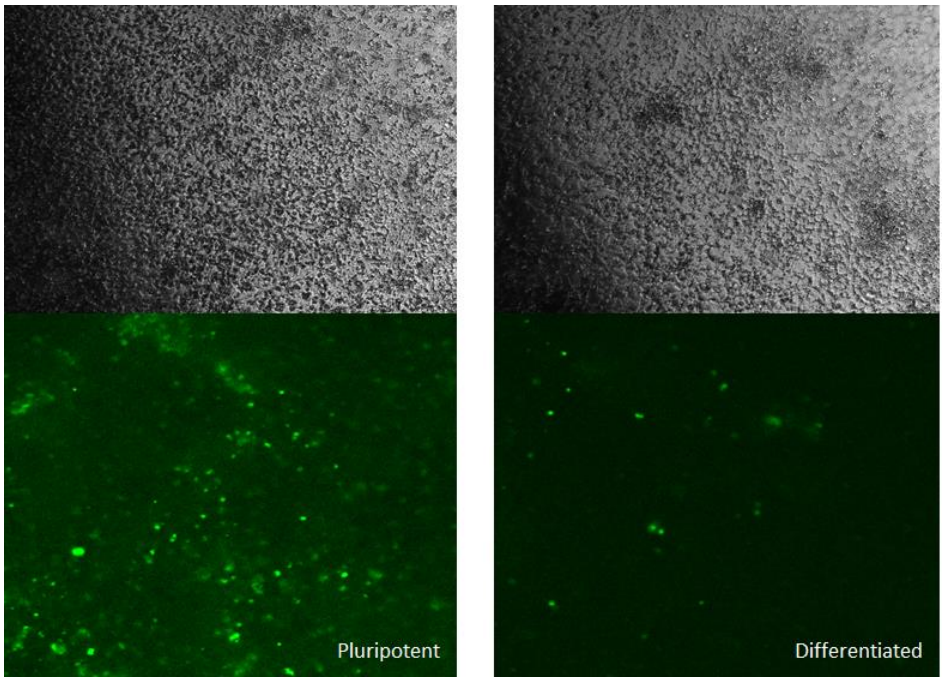

Fig 5.23 Oct4-GFP image a hPSCs sample when they were pluripotent(left) and differentiated cells (right)

In addition, we verified the reliability of the green protein as a marker for pluripotency by observing an hPSCs sample at different time point. First measurement was performed two days after the cells were plated (fig 5.23 left) while the other measurement for the image on the right was done two weeks after. This means that the latter measurement should reveal the fluorescent image of cells that were already differentiated and lost their pluripotency while the first

measurement illustrated the pluripotent cells under fluorescent microscope. As we can see in fig 5.23, the early image has higher intensity of GFP than the latter measurement as expected. This means that OCT4-GFP can be reliably used as a pluripotent marker for our finding and suitable for our instruments.

The kinetics of pluripotency, which implies the kinetic of the differentiation, is still a relatively new concept, and information on this topic is still limited. Nicolas Plachta and his group studied the kinetic of OCT4 proteins, and performed a measurement using fluorescent intensity of this green protein as an indication to study the development process of embryo[39].

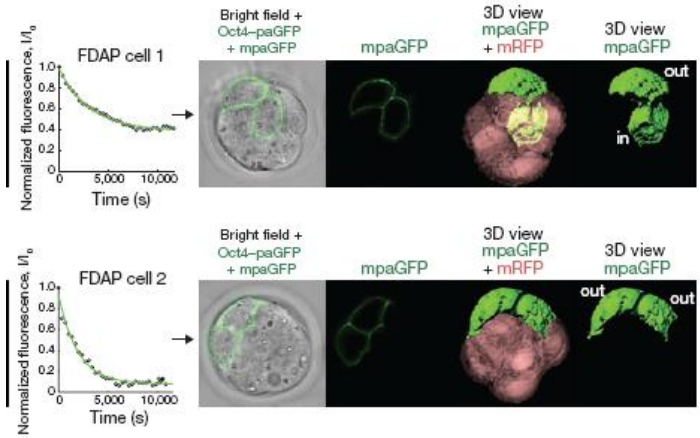

Fig 5.24 development of embryo into ectoderm (bottom) in comparison to endoderm and mesoderm (top). The Oct4 intensity decay faster in the case of ectoderm while it decays slower for development of endoderm and mesoderm.

In their work, fast decay of OCT4 intensity (fast kinetics) was found in the development of ectoderm, where slow decay of OCT4 intensity (slow kinetics) was found in the development of embryo towards endoderm and mesoderm. These results imply that different type of cells or organ develops or differentiates from stem cells at a different rate. Based on this work, we performed similar experiment by establishing a curve of OCT4-GFP intensity of the samples in

the time domain. Since we were using different equipment from this work, it was necessary to create a reference curve to represent a standard intensity profile in the development of mesoderm. Once this curve was established, we can compare other curves to the reference to verify if the development in the sample is towards mesoderm. To create the reference curve, we applied SB small molecules known to direct the differentiation of hPSCs towards mesoderm in a cell culture, and the GFP intensity of the cells were monitored for 2 weeks to create the reference curve (fig 5.25). According to this graph, the GFP intensity of the samples with SB decreases significantly faster than the controls. The rate of the decay depends on the concentration of SB small molecule; the higher concentration of SB was shown to drive the differentiation of the sample faster (the cells lost their pluripotency quicker in fig 5.25).

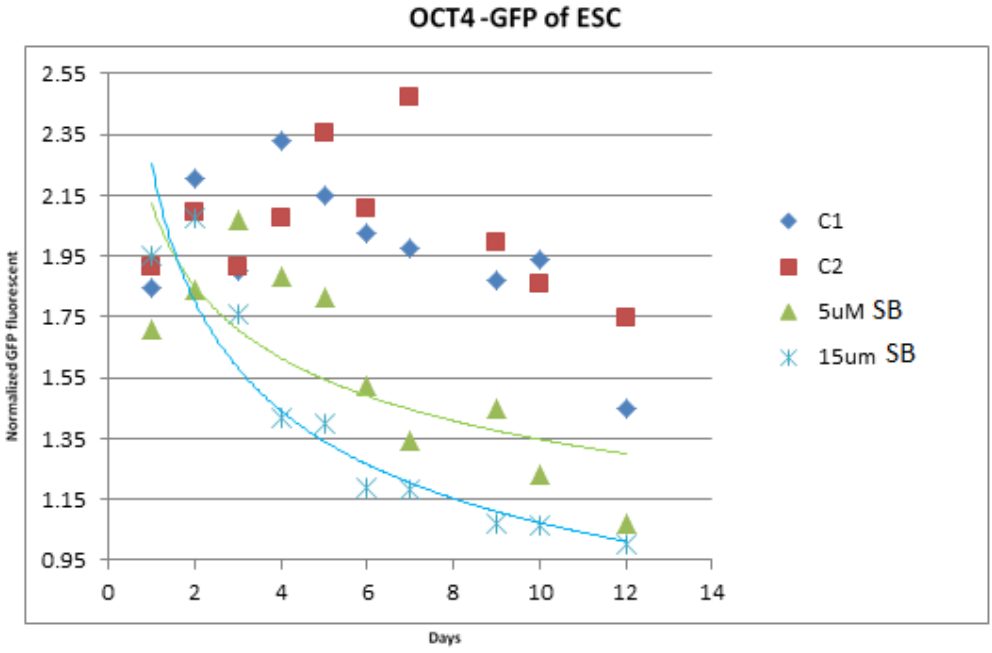

Fig 5.25 Standard curve for the differentiation of hPSCs towards mesoderm (induced by SB). The samples with SB molecule differentiated faster than control (red, dark blue). The higher concentration of SB tended to drive the differentiation faster as shown in sharper drop in pluripotency with 15µM addition of SB (pale blue) compared to 5µM (green).

After establishing a standard curve similarly to fig 5.24 [39], some parameters such as the rate of the intensity decay (in term of exponential constant) can be extracted and used as an index when comparing other samples to the reference. In the next stage, we obtained the intensity profile of samples to test the effect of force on the differentiation of stem cells by comparing the GFP intensity profile with the controls. We placed cell samples into three groups: control, hPSC with beads (no magnet) and hPSC with force (beads+magnet). After two weeks of monitoring, the GFP intensity was collected and shown in fig 5.26.

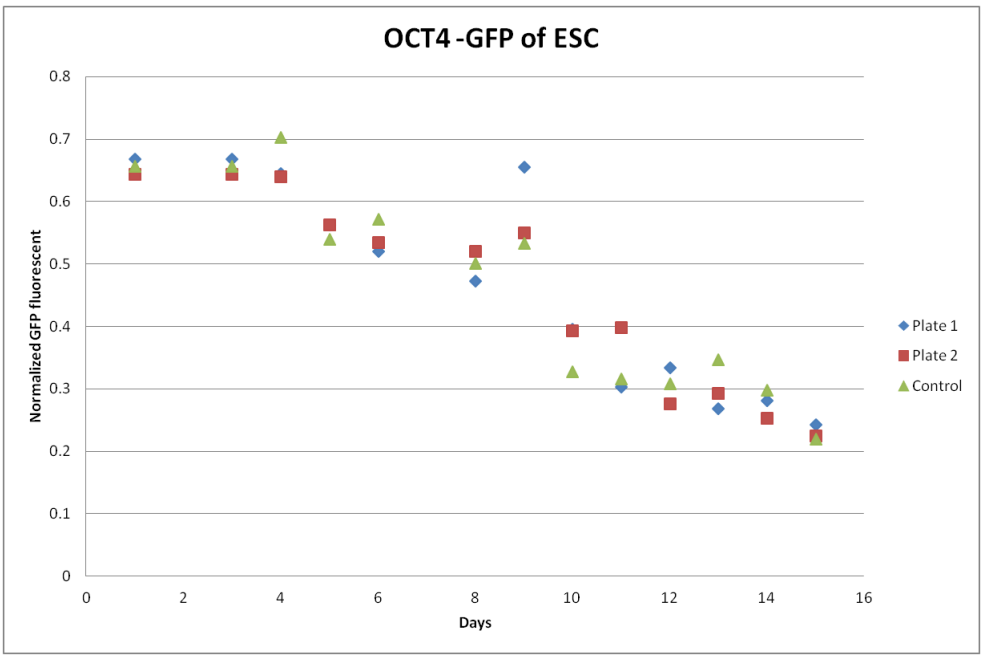

Fig 5.26. Oct4-GFP intensity of hPSCs. A control hPSCs sample (green), hPSCs with beads(blue) and hPSCs with force (red) were measured for GFP intensity over time. Effect of force on the differentiation was not illustrated in this graph

In fig 5.26, the curves of the three samples were relatively similar, and there was no significant distinction between each other. For further analysis, fitting the curves for exponent constant may provide further quantitative relationship between the samples. However, more repetitions and data points are recommended for future experiments. It could also be because of

the amount and the pattern of the force used did not create an impact on the differentiation. For example, since beating is dynamic process, applying static force- in our case- may not induce the movement of the cells. This is a reason we performed the cardiac rhythm tracking using MII in section 5.3.3 and 5.4.3 because we may observe a natural pattern that can be used to direct the differentiation. To learn and realize the signal of the motion from the nature would help us narrow to the right force pattern or amount required. Regardless of the result, this type of interpretation and setup would be useful for further kinetic study using the intensity of OCT4-GFP protein.

5.4.4 Electrical pulse directed differentiation of stem cells

In addition to force as a physical stimulus, we explored the effect of electric pulse on the development of stem cells. Many researches have published their work explaining the effect of electrical pulse on many animal stem cells. We explored this effect mainly on human embryonic stem cells (hESCs) using the current of 10 and 15 μA. After being plated on the specially made platform for pulsing experiment, the cells were kept in the optimum condition within an incubator. After pulsing period was terminated, we collected the cells for qPCR, and the results were shown in fig 5.27.

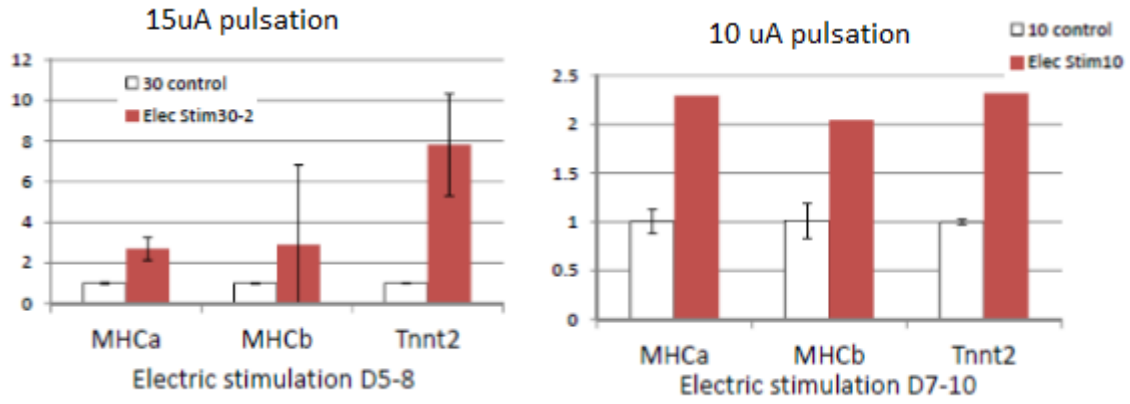

Fig 5.27 qPCR of cardiac gene expressions: MHCa, MHCb and Tnnt2 of the hESCs after 4 days pulsation of 15uA(left) and 10uA(right) current with respect to controls.

During the pulsing, we had cells in three different chips. The first chip was pulsed with 10 µA. The second chip was then pulsed with 15uA. And the last chip was designated to hold the controls. The qPCR results in term of cardiac gene expression of pulsed cells with respect to the controls were shown in fig 5.27. From the results, the cells that were excited by electrical pulses expressed more cardiac genes than the controls. We are hence confident that with more repetition for accuracy, the effect of electrical pulse on hESCs can be determined. Although there was a positive result in term of gene expression, noticeable beating was not observed in this experiment. In the future, there are many parameter such as current value, pulsing time, pulse shape that need to be optimized for the best and conclusive results.

5.5 Conclusions

We have modified and engineered systems useful for advance stem cells studies. There were strong preliminary results suggested the effect of mechanical and physical stimuli such as motion, force and electricity on the development of cardiomyocytes. By using the novel techniques, we also illustrated the benefits and the improvements on data and images. Many

experiments such as electrical pulse stimulation, OCT4 kinetics study should be pursued and repeated for more accurate results to reach an exclusive conclusion on the effect of force and electricity.

Applications of many nanotechnology techniques were seen throughout this chapter, and we believe that biology will continue to benefit from nanotechnology since there seem to be many untapped insight and results waiting to be explored. Collaboration between biologist, physicians, engineers and nanotechnologists would lead to many novel interesting platforms, and the application of nanotechnology would provide an access to more results to understand biological system greater in the future.

References

1. S.E. Cross, Y.S.J., J. Rao, J.K. Gimzewski, *Nanomechanical analysis of cells from cancer patients.* Nature Nanotechnology, 2007. **2**: p. 780.
2. S. Cross, Y.S.J., J.Tondre, R.Wong, J.Y. Rao, J.K. Gimzewski, *AFM-based analysis of human metastatic cancer cells.* Nanotechnology, 2008. **19**: p. 384003.
3. J.Reed, B.M., B.PIttenger, S.Magonov, J.Troke, M.A.Teitell,J.K.Gimzewski, *Single molecule transcription profiling with AFM.* Nanotechnology, 2007. **18**.
4. Y.Shiu, *Mechanical Forces on Cells*, in *Tissue Engineering and Artificial Organs*, J.D.Bronzino, Editor. 2006, Taylor & Francis Group, LLC. p. 33-1.
5. V. Vogel, M.S., *Local force and geometry sensing regulate cell functions.* Nature Reviews: Molecular Cell Biology, 2006. **7**: p. 265-275.
6. F.Grinnell, C.H.H., E.Tamariz,D.J.Lee,G.Skuta, *Dendritic fibroblasts in three-dimensional collagen matrices.* Cell Molecular Biological, 2003. **14(**2): p. 384-395.
7. M.L Smith, D.E.G., W. C Little, K. E Kubow, R. A. Eguiluz, S. Luna-Morris, V. Vogel, *Force-Induced Unfolding of Fibronectin in the Extracellular Matrix of Living Cells.* Plos Biology, 2007. **5**(10): p. 2243-2254.
8. P.Hell, H.P.S., *Lateral shear forces applied to cells with single elastic micropillars to influence focal adhesion dynamics.* Journal of Physics: Condensed Matter, 2010. **22**: p. 19418.
9. M.Liu, K.T., M.Post, *Mechanical force-induced signal transduction in lung cells.* American Journal of Physiology - Lung Cellular and Molecular Physiology, 1999. **277**: p. L667-L683.
10. T.Yeung,P.C.G., L.A.Flanagan,B.Marg,M.Ortiz,M.Funaki,N.Zahir,W.Ming,V.Weaver,P.A.Janmey, *Effects of substrate stifness on cell morphology,cytoskeletal structure, and adhesion.* Cell Motilility Cytoskeleton, 2005. **60**(1): p. 24-34.

11. M.Benjamin, B.H., *Mechanical influences on cells, tissues and organs - 'Mechanical Morphogenesis'.* European Journal of Morphology, 2003. **41**(1): p. 3-7.

12. N. D. Evans, C.M., E. Gentleman, V. LaPointe, S. N. Patankar, M. Kallivretaki, X. Chen, C.J. Roberts, M.M. Stevens, *Substrate Stiffness Affects Early Differentiation Events in Embryonic Stem Cells* European Cells and Materials, 2009. **18**: p. 1-14.

13. A.J.Engler, S.S., H.L.Swwney,D.E.Discher, *Matrix Elasticity Directs Stem Cell Lineage Specification.* Cells, 2006. **126**: p. 677-689.

14. R. J. McMurray, N.G., P. M. Tsimbouri, K. V. Burgess,L. E. McNamara, R. T., K. Murawski, E. Kingham,R. O. C. Oreffo,M.J. Dalby, *Nanoscale surfaces for the long-term maintenance of mesenchymal stem cell phenotype and multipotency.* Nature Materials, 2011. **10**: p. 637-644.

15. V.Vogel, *Mechanotransduction Involving Multimodular Proteins: Converting Force into Biochemical Signals.* Annual Review of Biophysics and Biomolecular Structure., 2006. **35**: p. 459-488.

16. B.D.Hoffman, J.C.C., *Cell Mechanics: Dissecting the Physical Responses of Cells to Force.* The Annual Review of Biomedical Engineering, 2009. **11**: p. 259-88.

17. S.Khan, M.P.S., *Force effects on biochemical kinetics.* Annual Review of Biochemistry, 1997. **66**: p. 785-805.

18. C.Bustamante, *Of torques, forces, and protein machines.* Protein Science, 2004. **13**: p. 3061-3065.

19. T.J.Purcell, H.L.S., J.A.Spudich, *A force-dependent state controls the coordination of processive myosin.* PNAS, 2005. **102**: p. 13873-13878.

20. D.Riveline, *Focal contacts as mechanosensors:externally applied local mechanical force induces growth of focal contacts by an mDia1-dependent and ROCK-independent mechanism.* Journal of Cell Biology, 2001. **153**: p. 1175-1186.

21. A. D. Bershadsky, C.B., L. Carramusa, Y. Zilberman, B. Gilquin, S. Khochbin, A. Alexandrova, A. B. Verkhovsky, T. Shemesh, M. M Kozlov, *Assembly and mechanosensory function of focal adhesions:experiments and models.* European Journal of Cell Biology, 2005. **85**(3-4): p. 165-173.

22. B.Wehrle-Haller, B.I., *The inner lives of focal adhesions.* Trend in Cell Biology, 2002. **12**: p. 382-389.

23. J. Reed, J.J.T., J. Schmit, S. Han, M. A. Teitell, J. K. Gimzewski, *Live Cell Interferometry Reveals Cellular Dynamism During Force Propagation.* ACS Nano, 2008. **2**(5): p. 841-846.

24. J. Reed, W.J.W., O. N. Petzold, J. K. Gimzewski, *In Situ Mechanical Interferometry of Matrigel Films.* Langmuir, 2009. **25**: p. 36-39.

25. M.Ohgushi, M.M., M. Eiraku, K. Murakami, T. Aramaki,A. Nishiyama, K. Muguruma, T.Nakano, H.Suga, M. Ueno, T. Ishizaki,H. Suemori, S. Narumiya, H.Niwa, Y. Sasa, *Molecular Pathway and Cell State Responsible for Dissociation-Induced Apoptosis in Human Pluripotent Stem Cells.* Cell Stem Cell, 2010. **7**: p. 225-239.

26. Sherman, S.P., *Identification and characterization of regulators of survival in human pluripotent stem cells*, in *Molecular Biology*. 2012, University of California, Los Angeles: Los Angeles. p. 118.

27. Y.Nakashima, K.O., Y.Yoshida, T.Kojima, T.Kita, M.Tanaka, T.Kimura, *The search for Nkx2-5-regulated genes using purified embryonic stem cell-derived cardiomyocytes with Nkx2-5 gene targeting.* Biochem Biophys Res Commun, 2009. **390**(3): p. 821-6.

28. Diaz Perez, S.V., et al., *Derivation of new human embryonic stem cell lines reveals rapid epigenetic progression in vitro that can be prevented by chemical modification of chromatin.* Hum Mol Genet, 2012. **21**(4): p. 751-64.

29. H.Nakano, E.W., M.Hoshijima,MSasaki,S.Minamisawa,K.R.Chien,A.Nakano, *Cardiac origin of smooth muscle cells in the inflow tract.* J Mol Cell Cardiol, 2011. **50**(2): p. 337-45.

30. J Schmit, J.R., E Novak and JK Gimzewski, *Performance advances in interferometric optical profilers for imaging and testing* Journal of Optics A : Pure Application Optics, 2008. **10**.

31. J.Reed , J.T., J.Schmit , S.Han , M.A.Teitell , J.K.Gimzewski, *Live Cell Interferometry Reveals Cellular Dynamism During Force Propagation.* ACS.Nano, 2008. **2**: p. 841-846.

32. J.Reed, M.F., J.J.Troke, J.Schmit, S.Han, M.A.Teitell, J.K.Gimzewski, *Imaging interferometry for investigation of mechanics of multiple cells in a large field of view.* Biomed, 2008.

33. J. Reed, J.C., T. A Zangle, S. Kalim, J. S Hong, S. E Pefley, X. Zheng, J. K Gimzewski, M.A Teitell, *Rapid, Massively Parallel Single-Cell Drug Response Measurements via Live Cell Interferometry*. Biophysical Journal, 2011. **101**: p. 1025-1031.

34. R.E. Mahaffy, S.P., E. Gerde, J. Kas, C.K. Shih, *Quantitative analysis of the viscoelastic properties of thin regions of fibroblasts using atomic force microscopy.* Journal of Biophys, 2004. **86**: p. 1777-1793.

35. D Weihs, T.M., MA Teitell, *Bio-microrheology: a frontier in microrheology.* Journal of Biophysics, 2006. **91**: p. 4296-4305.

36. J.Reed, M.F., J.J.Troke, J.Schmit, S.Han, M.A.Teitell, J.K.Gimzewski, *High throughput cell nanomechanics with mechanical imaging interferometry.* Nanotechnology, 2008. **19**(23): p. 1-16.

37. S. M. Mijailovich, M.K.M.Z., B. Fabry, J. J. Fredberg and *A finite element model of cell deformation during magnetic bead twisting.* Journal of Applied Physiology, 2002. **93**(4): p. 1429-1436.

38. J.Reed, W.J.W., O.N. Petzold, J.K.Gimzewski, *In Situ Mechanical Interferometry of Matrigel Films.* Langmuir, 2009. **25**: p. 36-39.

39. N. Plachta, T.B., S. Pease, S. E. Fraser, P. Pantazis, *Oct4 kinetics predict cell lineage patterning in the early mammalian embryo.* Nature Cell Biology, 2010. **13**(2): p. 117-123.